

Initial Solubility Measurements of Bitumen Cuts in Supercritical Carbon Dioxide

by

Edmund Herman Yu

A thesis submitted in partial fulfillment of the requirements for the degree of

Master of Science

in

Environmental Engineering

Department of Civil and Environmental Engineering
University of Alberta

© Edmund Herman Yu, 2021

ABSTRACT

Initial solubilities for whole bitumen and bitumen cuts of light gas oil (LGO), heavy gas oil (HGO), and vacuum residue (resid) were measured in supercritical carbon dioxide (SC-CO₂) and SC-CO₂ modified with 5 or 15 mol% toluene. The initial solubility measurements were performed on a bench-scale batch supercritical fluid extraction (SFE) system at 333 K and 24 MPa (SC-CO₂ density of 0.78 g/mL). LGO had the highest average initial solubility in SC-CO₂ at 8.7×10^{-2} g/g, followed by whole bitumen at 1.3×10^{-2} g/g, HGO at 1.1×10^{-2} g/g, and resid at 5.9×10^{-4} g/g. When SC-CO₂ was modified with 5 mol% toluene, HGO had the highest average initial solubility at 4.5×10^{-2} g/g, followed by whole bitumen at 3.5×10^{-2} g/g, and resid at 5.6×10^{-2} g/g; the initial solubility for LGO could not be reliably measured. When SC-CO₂ was modified with 15 mol% toluene, whole bitumen measured the highest average initial solubility at 1.1×10^{-1} g/g, followed by resid at 2.4×10^{-2} g/g. The initial solubility of LGO was not measured at the 15 mol% toluene condition and the initial solubility for HGO could not be reliably measured. HTSD analysis of the extracts from the initial solubility measurements indicated that heavier hydrocarbons were dissolved in the SC-CO₂ with the addition of toluene as a modifier.

ACKNOWLEDGEMENTS

First and foremost, I would like to take this opportunity to sincerely thank my supervisor - Dr. Selma Guigard. Selma, thank you for giving me the chance to be a part of your research group which provided me with the opportunity to work on such an interesting and challenging research topic. The mentorship, kindness, patience, motivation, and positivity that you have shown towards me throughout the completion of this research project will always be cherished and remembered. I would also like to thank Dr. Warren Stiver who has generously provided me with his tremendous support and insightful knowledge throughout the completion of this research project, despite being so far away in Guelph, Ontario.

Next, I would like to thank all of the wonderful technicians from the Department of Civil and Environmental Engineering, especially to our SFE research group's technician, Eleisha Underwood. Eleisha, your knowledge, expertise, kindness, witty humour, and friendship made the completion of this research project a lot less daunting and a lot more enjoyable. A really big thank you to the rest of the SFE research group, including: Dr. Christianne Street and Dr. Maedeh Roodpeyma – for providing me with their support and sharing their insightful knowledge and experimental experiences with me. Thank you to our summer students, Natalia Shiu and Aryou Manousi for their assistance in the lab.

I would also like extend my gratitude to Syncrude Canada Ltd. and specifically their employees, Dr. Jennifer McMillan, Dr. Sujit Bhattacharya, and Justin Weber for the financial support, analytical services, and expertise that were provided for making this research project possible.

To my friends who also went through graduate studies at the same time as me – Heidi Cossey and Kelvin Chan. Thank you for the sincere advice, words of encouragement, companionship, and most importantly, the laughter that you have shared with me throughout this journey.

And lastly, to my family – I would not be where I am today without your unconditional love and support. Mom and dad, thank you for all of the sacrifices that you have made for me over the years and for always believing in me even when I fail to believe in myself. Anthony and Rose, thank you for all of the life advices that you have shared with me and for always supporting me in everything that I do.

TABLE OF CONTENTS

CHAPTER 1: INTRODUCTION.....	1
1.1 Problem Scenario	1
1.2 Research Objectives.....	4
1.3 Thesis Organization	5
CHAPTER 2: LITERATURE REVIEW	7
2.1 Oil Sands in Alberta.....	7
2.2 Recovery Methods for Bitumen.....	10
2.2.1 In-situ Bitumen Recovery Methods	11
2.2.2 Ex-situ Surface Mining and the Hot Water Extraction Recovery Process	17
2.3 Supercritical Fluids	21
2.3.1 Overview of the Supercritical State	22
2.3.2 Supercritical Carbon Dioxide	24
2.3.3 Common Applications for Supercritical Fluids	25
2.3.4 Initial Solubility in Supercritical Fluids.....	26
2.4 Summary.....	32
CHAPTER 3: MATERIALS AND METHODS	34
3.1 Summary of Experiments	34
3.2 Materials	35
3.2.1 Samples	35
3.2.1.1 Whole Bitumen	35
3.2.1.2 Light Gas Oil, Heavy Gas Oil, and Vacuum Residue.....	35
3.2.2 Chemicals.....	37
3.3 Supercritical Carbon Dioxide Extraction Apparatus	37

3.3.1 Extraction Vessel, MagneDrive® Mixer, and Helical Impeller	42
3.3.2 Toluene (Modifier) Addition	45
3.3.3 LabVIEW™ Data Collection.....	46
3.4 Procedure for Initial Solubility Measurement Experiments	47
3.4.1 Procedures for Initial Solubility Experiments with SC-CO ₂ Only	48
3.4.2 Procedure for Initial Solubility Experiments with SC-CO ₂ and Toluene	50
3.4.3 Samples	51
3.5 High Temperature Simulated Distillation.....	51
3.6 Calculating Initial Solubility.....	52
CHAPTER 4: RESULTS AND DISCUSSION	54
4.1 Initial Solubility Measurements for Whole Bitumen and Bitumen Cuts	54
4.1.1 Initial Solubility Measurements for Whole Bitumen with SC-CO ₂ only	54
4.1.2 Initial Solubility Measurements for Whole Bitumen with Toluene Added to SC-CO ₂	57
4.1.3 Initial Solubility Measurements for Bitumen Cuts with SC-CO ₂ only.....	60
4.1.4 Initial Solubility Measurements for Bitumen Cuts with Toluene Added to SC-CO ₂ ..	65
4.2 Compositional Analysis for Whole Bitumen and Bitumen Cuts	71
4.2.1 Compositional Analysis of Samples from Whole Bitumen with SC-CO ₂ only.....	73
4.2.2 Compositional Analysis of Samples from Whole Bitumen with Toluene Added to SC-CO ₂	77
4.2.3 Compositional Analysis of Samples from Bitumen Cuts with SC-CO ₂ only	86
4.2.4 Compositional Analysis of Samples from Bitumen Cuts with Toluene Added to SC-CO ₂	97
CHAPTER 5: CONCLUSIONS AND RECOMMENDATIONS.....	119
5.1 Conclusions.....	119
5.2 Recommendations.....	120
REFERENCES.....	121

APPENDIX A: PROPERTIES OF THE FEED MATERIAL	143
APPENDIX B: LabVIEW™ DATA RECORDINGS	145
APPENDIX C: INITIAL SOLUBILITY MEASUREMENT PROCEDURE.....	147
APPENDIX D: HYDROCARBON COLLECTION DATA.....	164
APPENDIX E: HIGH TEMPERATURE SIMULATED DISTILLATION	167

LIST OF TABLES

Table 1. A comparison of properties between Athabasca bitumen with synthetic and conventional crude oils.	9
Table 2. Properties of gas, liquid, and SCF.	24
Table 3. Critical temperatures and pressures of various compounds.....	24
Table 4. Solubilities (weight fraction) of three Cold Lake bitumen cuts and bitumen with SC-CO ₂ at 16 MPa and temperatures of 323 and 373 K.....	27
Table 5. Extraction efficiencies of various feed streams for SC-CO ₂ when applied with different concentrations of modifiers.....	31
Table 6. Summary of the experiments conducted at 24 MPa and 333 K using SC-CO ₂	34
Table 7. Summary of the chemicals used in experiments.....	37
Table 8. List of components, their suppliers, and pressure ratings (if applicable) used for the SFE system.	41
Table 9. Volumes and flow rates of toluene added at various concentrations for whole bitumen, light gas oil, heavy gas oil, and resid samples.	51
Table 10. Initial solubilities of whole bitumen with SC-CO ₂ modified with toluene (0, 5, and 15 mol%) at 24 MPa and 333 K.....	55
Table 11. Initial solubilities of LGO, HGO, and resid with SC-CO ₂ modified with toluene (0, 5, and 15 mol%) at 24 MPa and 333 K.....	62
Table 12. Recovery mass percentages for whole bitumen, LGO, HGO, and resid starting materials at various distillation temperature ranges.....	73
Table 13. Recovery mass percentages of hydrocarbons at various distillation temperature ranges from extract, <i>vessel residue</i> , and <i>time zero</i> samples collected in Run 3 (whole bitumen in SC-CO ₂ only).	76
Table 14. Recovery mass percentages of hydrocarbons at various distillation temperature ranges from extract, <i>vessel residue</i> , and <i>time zero</i> samples collected from Run 6 (whole bitumen in SC-CO ₂ modified with 5 mol% toluene).	80

Table 15. Recovery mass percentages of hydrocarbons at various distillation temperature ranges from extract, <i>vessel residue</i> , and <i>time zero</i> samples collected from Run 11 (whole bitumen in SC-CO ₂ modified with 15 mol% toluene).	85
Table 16. Recovery mass percentages of hydrocarbons at various distillation temperature ranges from extract, <i>vessel residue</i> , and <i>time zero</i> samples collected from Run 13 (LGO in SC-CO ₂ only).	89
Table 17. Recovery mass percentages of hydrocarbons at various distillation temperature ranges from extract, <i>vessel residue</i> , and <i>time zero</i> samples collected from Run 20 (HGO in SC-CO ₂ only).	93
Table 18. Recovery mass percentages of hydrocarbons at various distillation temperature ranges from the <i>vessel residue</i> and <i>time zero</i> samples collected in Run 31 (Resid in SC-CO ₂ only).....	97
Table 19. Recovery mass percentage of hydrocarbons at various distillation temperature ranges from extract, <i>vessel residue</i> , and <i>time zero</i> samples collected from Run 16 (LGO in SC-CO ₂ modified with 5 mol% toluene).	100
Table 20. Recovery mass percentages of hydrocarbons at various distillation temperature ranges from extract, <i>vessel residue</i> , and <i>time zero</i> samples collected from Run 23 (HGO in SC-CO ₂ modified with 5 mol% toluene).	105
Table 21. Recovery mass percentages of hydrocarbons at various distillation temperature ranges from extract, <i>vessel residue</i> , and <i>time zero</i> samples collected from Run 26 (HGO in SC-CO ₂ modified with 15 mol% toluene).	109
Table 22. Recovery mass percentages of hydrocarbons at various distillation temperature ranges from extract, <i>vessel residue</i> , and <i>time zero</i> samples collected from Run 34 (Resid in SC-CO ₂ modified with 5 mol% toluene).	113
Table 23. Recovery mass percentages of hydrocarbons at various distillation temperature ranges from <i>extract</i> , <i>vessel residue</i> , and <i>time zero</i> samples collected from Run 35 (Resid in SC-CO ₂ modified with 15 mol% toluene).	116

LIST OF FIGURES

Figure 1. Untreated oil sands particle formed of bitumen surrounded by water film and sand.....	8
Figure 2. A typical CSS process showing the steaming, soaking, and production phases.	12
Figure 3. A typical SAGD process.	14
Figure 4. Phase diagram of carbon dioxide depicting the solid, liquid, gas, and supercritical phase regions.....	23
Figure 5. Schematic of laboratory-scale SFE system used for initial solubility measurements. ..	40
Figure 6. Cross-sectional display of the 300 mL extraction vessel.	42
Figure 7. Overhead view of the stainless-steel vessel and a part of the MagneDrive assembly. .	43
Figure 8. The stainless-steel extraction vessel sleeve (left) and the detached stainless-steel helical impeller (right).....	43
Figure 9. Stainless steel helical impeller attached to the driveshaft of the MagneDrive®, SC-CO ₂ inlet tubing, and thermistor temperature probe.....	44
Figure 10. The SFE system.....	45
Figure 11. Front view of the chemical modifier setup for the SFE system.	46
Figure 12. A screenshot of the LabVIEW™ software, displaying pressure, temperature, and flow rates during an experiment.....	47
Figure 13. HTSD curves for whole bitumen, LGO, HGO, and resid starting materials.....	72
Figure 14. Visual comparison of extracts, starting materials, and vessel residue from initial solubility experiments for whole bitumen with SC-CO ₂ only: (a) Run 1, (b) Run 2, and (c) Run 3.	74
Figure 15. HTSD curves for samples from Run 3 (whole bitumen in SC-CO ₂ only).	75
Figure 16. Visual comparison of extracts, starting materials, and vessel residue from initial solubility experiments for whole bitumen with SC-CO ₂ added with 5 mol% toluene: (a) Run 4, (b) Run 5, (c) Run 6, and (d) Run 7.....	78
Figure 17. HTSD curves for samples from Run 6 (whole bitumen in SC-CO ₂ at 333 K, 24 MPa with 5 mol% toluene addition).....	80

Figure 18. Visual comparison of extracts, starting materials, and vessel residue from initial solubility experiments for whole bitumen with SC-CO ₂ added with 15 mol% toluene: (a) Run 8, (b) Run 9, (c) Run 10, and (d) Run 11.	82
Figure 19. HTSD curves for samples from Run 11 (whole bitumen in SC-CO ₂ at 333 K, 24 MPa with 15 mol% toluene addition).....	84
Figure 20. Visual comparison of extracts, starting materials, and vessel residue from initial solubility experiments for LGO with SC-CO ₂ only: (a) Run 12, (b) Run 13, and (c) Run 14.	87
Figure 21. HTSD curves for samples from Run 13 (LGO in SC-CO ₂ at 333 K, 24 MPa with no toluene addition).	89
Figure 22. Visual comparison of extracts, starting materials, and vessel residue from initial solubility experiments for HGO with SC-CO ₂ with no toluene added: (a) Run 19, (b) Run 20, and (c) Run 21.	91
Figure 23. HTSD curves for samples from Run 20 (HGO in SC-CO ₂ at 333 K, 24 MPa with no toluene addition).	92
Figure 24. Visual comparison of extracts, starting materials, and vessel residue from initial solubility experiments for resid with SC-CO ₂ with no toluene addition: (a) Run 29, (b) Run 30, and (c) Run 31.....	95
Figure 25. HTSD curves for the vessel residue and time zero samples from Run 31 (resid in SC-CO ₂ at 333 K, 24 MPa with no toluene addition).....	96
Figure 26. Visual comparison of extracts, starting materials, and vessel residue from initial solubility experiments for LGO with SC-CO ₂ added with 5 mol% toluene: (a) Run 15, (b) Run 16, (c) Run 17, and (d) Run 18.	99
Figure 27. HTSD curves for samples from Run 16 (LGO in SC-CO ₂ at 333 K, 24 MPa with 5 mol% toluene addition).....	100
Figure 28. Visual comparison of extracts, starting materials, and vessel residue from initial solubility experiments for HGO with SC-CO ₂ added with 5 mol% toluene: (a) Run 22, (b) Run 23, (c) Run 24, and (d) Run 25.	103
Figure 29. HTSD curves for samples from Run 23 (HGO in SC-CO ₂ at 333 K, 24 MPa with 5 mol% toluene addition).....	104

Figure 30. Visual comparison of extracts, starting materials, and vessel residue from initial solubility experiments for HGO with SC-CO ₂ added with 15 mol% toluene: (a) Run 26, (b) Run 27, (c) Run 28.	107
Figure 31. HTSD curve for samples from Run 26 (HGO in SC-CO ₂ at 333 K, 24 MPa with 15 mol% toluene addition).....	108
Figure 32. Visual comparison of extracts, starting materials, and vessel residue from initial solubility experiments for resid with SC-CO ₂ added with 5 mol% toluene: (a) Run 32, (b) Run 33, and (c) Run 34.....	111
Figure 33. HTSD curves for samples from Run 34 (resid in SC-CO ₂ at 333 K, 24 MPa with 5 mol% toluene addition).....	112
Figure 34. Visual comparison of extracts, starting materials, and vessel residue from initial solubility experiments for resid with SC-CO ₂ added with 15 mol% toluene: (a) Run 35, (b) Run 36, and (c) Run 37.....	114
Figure 35. HTSD curves for samples from Run 35 (resid in SC-CO ₂ at 333 K, 24 MPa with 15 mol% toluene addition).....	116

LIST OF ABBREVIATIONS

ACS	American Chemical Society
API	American Petroleum Institute
ASTM	American Society for Testing and Materials
CNOOC	China National Offshore Oil Corporation
c/o	Carry-over
CSS	Cyclic steam stimulation
dep	Depressurization
Dilbit	Diluted bitumen
FID	Flame ionization detector
GC	Gas chromatograph
HGO	Heavy gas oil
Hi-P	High pressure
HPLC	High performance (high pressure) liquid chromatography
HTSD	High temperature simulated distillation
ISC	In-situ combustion
LGO	Light gas oil
NFT	Naphthenic froth treatment
NREF	Natural Resources Engineering Facility
OD	Outer diameter
PAH	Polycyclic aromatic hydrocarbons
PCB	Polychlorinated biphenyls
PFT	Paraffinic froth treatment
Resid	Vacuum residue
SAGD	Steam assisted gravity drainage
SARA	Saturates, aromatics, resins, asphaltenes
SC-CO ₂	Supercritical carbon dioxide
SCF	Supercritical fluid
SCO	Synthetic crude oil
SFE	Supercritical fluid extraction

THAI	Toe-to-heel air injection
VAPEX	Vapour extraction

LIST OF SYMBOLS AND UNITS

atm	Standard atmosphere
B_2	Temperature independent model inputs
Bd	Baud
bpd	Barrels per day
cm ²	Squared centimeters
cP	Centipoise
cSt	Centistoke
°	Degree
°C	Degrees Celsius
°F	Degrees Fahrenheit
ft	Foot
g	Gram
H/C	Hydrogen to carbon ratio
Hz	Hertz
in	Inch
k	Association number constant
K	Kelvins
kg	Kilograms
km ²	Squared kilometers
kPa	Kilopascal
L	Liter
μL	Microlitre
lb	Pound
m	Meter
m ³	Cubic meter
mg	Milligram
mL	Milliliter
mm	Millimetre
mol	Mole

MPa	Megapascal
Pa	Pascal
ρ	Density of SCF (kg/m ³)
ρ_f	Specific density
ppm	Parts per million
psi	Pound per square inch
psig	Pound per square inch gauge
RPM	Rotations per minute
s	Second
wt%	Weight percent

CHAPTER 1: INTRODUCTION

1.1 Problem Scenario

Over the decades, the industrialized world has become largely dependent on the use of oil and its by-products to generate energy for powering the expanding industrial sectors, fueling the transportation of people and goods, and generating petrochemicals that are used in the manufacturing of cosmetic goods, medical supplies, textiles, electronics, and many other essential products (CAPP 2020; UKOG 2020). Despite the varied success in researching and developing more environmentally sustainable forms of energy and material alternatives in the hopes of lowering the global reliance on oil and its products, the consumption of crude oil has continuously increased over the years: from 67 million barrels per day (bpd) in 1990, 77 million bpd in 2000, 91 million bpd in 2014, and a projected 104 million bpd by the year 2030 (Clemente 2015; IEA 2011). Crude oil can be largely differentiated between its conventional and unconventional forms. In its natural liquid state with lower concentrations of impurities, conventional crude has been predominantly favoured for production over the years because it is generally easier and less expensive to be extracted, pumped, transported, and refined compared to unconventional crudes (Government of British Columbia 2019; PSAC 2019). As a result in sustaining the ever-growing market demand for crude oil, the once abundant reserves of conventional crude have largely dwindled over the decades (Government of Canada 2020). Decreasing global supplies of conventional crude has become a new reality that is faced by industry producers in the midst of growing market demands. Due to this, obtaining oil from unconventional crude reserves, that were once considered to be too expensive and technologically unfeasible, has gained more interest (Gordon 2012; USGS 2003).

Canada has an abundance of hydrocarbon resources, most of which are found as unconventional crude oil reserves in Alberta (Government of Alberta 2017). Unconventional crude, such as extra heavy oil and bitumen, exhibit higher viscosities and densities than conventional crude, making the ability to pump or have the unconventional oil flow so that it can be recovered through traditional means of drilled production wells is much more difficult (Government of British Columbia 2019; Gordon 2012; USGS 2003). Furthermore, unconventional crudes (bitumen for example), naturally contain higher concentrations of

heteroatomic and metal impurities, and thus require more complex upgrading before it can be produced into a more marketable synthetic crude oil (Government of British Columbia 2019; Færgestad 2016; IEA 2011).

More viscous and denser unconventional oil can be recovered by one of two methods, depending on the depth at which it is found in the formation. These two methods are: in-situ or ex-situ recovery approaches (Government of Alberta 2017). With recovering unconventional crude oil from oil sands formations that are more than 75 m deep, an in-situ approach is used. Unconventional crude found in oil sands formations that are less than 75 m below the ground surface is typically recovered by an ex-situ approach through surface mining (Government of Alberta 2017).

In-situ applications typically involve a combination of thermal and chemical recovery methods to extract bitumen. Common thermal in-situ techniques such as the cyclic steam stimulation and steam-assisted gravity drainage processes use heated water or steam to effectively reduce the viscosity of the crude oil to levels favouring recovery (Færgestad 2016; Chalaturnyk et al. 2002; NEB 2000). Likewise, chemical recovery methods utilizing vaporized solvents have also been developed and can effectively dislodge and isolate the heavy crude oil components from complex matrices (Færgestad 2016; Upreti et al. 2007). These in-situ recovery methods often utilize large volumes of water and chemicals, require extensive surface facilities for water heating and steam generation, and require additional effort to effectively separate and treat the water-bitumen mixture following its recovery (Ikebe et al. 2010; Upreti et al 2007; Chalaturnyk et al. 2002).

The ex-situ application of surface mining the oil sands ore followed by the hot water extraction of the bitumen components from this ore produces substantially more waste streams in the forms of wastewater tailings due to the large amounts of water utilized during the production process (NRCAN 2019b; Kasperski and Mikula 2011). The tailings contain bitumen, hydrocarbons, naphthenic acids, phenols, arsenic, cadmium, chromium, lead, and other heavy metals, and their release into the environment can result in detrimental consequences to the health and well-being of the surrounding natural ecosystems (Pembina Institute 2017). In the interim, these waste tailings are temporarily deposited into man-made ponds for storage. Over time, the residual bitumen found in these tailings will either rise up onto the surface of the ponds or persist to be entrapped within the tailings material (Romaniuk et al. 2015). Currently, research

focusing on dewatering the tailings and recycling the process water to be reused in the bitumen extraction process are being explored (Quinlan and Tam 2015).

Although capable of extracting and removing bitumen from different geological formations, the current in-situ and ex-situ recovery methods use large volumes of water for heating, steam generation, separation, and dilution, and they are energy intensive and costly, from the standpoint of dealing with the produced waste streams (Færgestad 2016; Kasperski and Mikula 2011). Furthermore, the size and toxicity of the tailings ponds generated poses substantial risks to the surrounding wildlife and to the natural environment (Færgestad 2016; Cabrera 2008; Allen 2008; Chalaturnyk et al. 2002).

With the environmental and operational challenges faced by the current extraction methods of producing bitumen from oil sands, there is interest in the research and implementation of more environmentally sustainable extraction alternatives that use less water, are less energy intensive, and that can treat or avoid the production of bitumen-containing waste streams. Supercritical fluid extraction (SFE) has been suggested as a viable alternative. Fundamentally, SFE utilizes a supercritical fluid (SCF) to extract and separate compounds from various matrices – such as extracting bitumen from oil sands (Rose et al. 2000; Deo et al. 1992). The supercritical state is achieved when the selected fluid is pressurized and heated beyond a critical pressure and temperature (also known as its critical point); this allows for the phase transitioning of the fluid's thermodynamic properties to converge into a singular uniform state of matter (Brunner 2005; McHugh and Krukoniš 1994). In its supercritical state, the SCF exhibits densities of a liquid, viscosities of a gas, and diffusivities between that of a liquid and a gas (Płotka-Wasyłka et al. 2017; Herrero et al. 2006; Akgerman 1997). These properties can significantly enhance the SCF's mass transport, dissolution, and solvating capabilities (Płotka-Wasyłka et al. 2017; Knox 2005; Manivannan and Sawan 1998; Akgerman 1997). Small changes to the operating pressures and temperatures of the SCF can influence its ability to extract and solubilize different compounds (Płotka-Wasyłka et al. 2017; Herrero et al. 2006; Knox 2005).

The commercialization of SFE was first developed for the food processing industry for the decaffeination of coffee and tea, and for the extraction of flavours, fragrances, and essential oils for uses in foods and cosmetic (Sun and Temelli 2006; Brunner 2005; Chandra and Nair 1997; Palmer and Ting 1995). The use of SFE for pharmaceutical applications were also developed for drug delivery processes and for the production of drug powders (García-Casa et al.

2018; Kumar et al. 2014; Tom et al. 1993). Further development of the SFE application for the treatment of soil matrices contaminated with heavy metals, pesticides, hydrocarbons, and other chemical pollutants were also demonstrated (Saldaña et al. 2005; Lin et al. 1995; Laitinen et al. 1994). In recent years, the SFE of hydrocarbons from oil sands and process waste streams has also been demonstrated at the laboratory scale, although further research, study, and development is still required to fully commercialize its application (Cossey et al. 2019; La and Guigard 2015; Li et al. 2015; Rudyk and Spirov 2014).

Although many substances can be conveniently brought to the supercritical state of behaviour upon achieving their respective critical pressures and temperatures, the selection of an appropriate SCF for an intended application is dependent on several factors, including toxicity, reactivity, technical feasibility, environmental sustainability, and cost (Płotka-Wasyłka et al. 2017). Supercritical carbon dioxide (SC-CO₂) has been primarily preferred in many SFE applications due to its non-flammable, non-toxic, chemically inert, inexpensive, and easily attainable characteristics (Khaw et al. 2017; Gupta and Shim 2007; Herrero et al. 2006). Modifiers such as toluene are chemical additives that can be added to the SC-CO₂ to enhance its solubility and extraction with solutes (Płotka-Wasyłka et al. 2017; Phelps et al. 1996).

1.2 Research Objectives

To further develop the SFE of bitumen from process waste streams using SC-CO₂, modelling applications are applied in compliment with the experimental program to simulate and forecast the configurations required for the design and operation of a full-scale SFE processing unit. Characteristic properties such as the initial solubility, equilibrium behaviour, and mass transfer dynamics of the bitumen – CO₂ interaction are inputted into the model. However, the compositional complexity of bitumen creates substantial challenges for this modelling effort, as it would be unrealistic and tedious to model the bitumen material on a compound-by-compound approach. Therefore, approximating the bitumen's complex composition would be required. To do so, a pseudo component approach is applied. Through characterizing bitumen into pseudo components, this divides the bitumen into a finite number of individual hydrocarbon segments, or bitumen cuts. Analysis, such as measuring the initial solubilities of these bitumen cuts in SC-CO₂ can then be performed and utilized for modelling purposes. Modelling through pseudo components can provide a more accurate approximation than analyzing the bitumen feed as a

whole, while altogether, it is less tedious and less inconceivable than building a model that is based on a compound-by-compound analysis of the bitumen feed.

Therefore, the main goal of this research is to measure the initial solubilities for three different bitumen cuts in SC-CO₂ so that these solubility measurements can be utilized for modelling purposes. Specifically, the objectives of this research are the following:

1. Measure the initial solubilities for whole bitumen, LGO, HGO, and resid without the addition of modifier, using a bench-scale SFE system at a SC-CO₂ density of 0.78 g/mL (at a pressure and temperature of 24 MPa and 333 K, respectively).
2. Measure the initial solubilities for whole bitumen, LGO, HGO, and resid with the addition of 5 and 15 mol% toluene added as a modifier, using a bench-scale SFE system at a SC-CO₂ density of 0.78 g/mL (at a pressure and temperature of 24 MPa and 333 K, respectively).
3. Examine the quality (composition) of the collected hydrocarbons from the initial solubility experiments with whole bitumen, LGO, HGO, and resid samples using high temperature simulated distillation (HTSD).

The measured initial solubility values will be used as a part of a larger effort in developing a model that can predict the solubilities of bitumen in SC-CO₂ with and without modifiers. The solubilities of bitumen in SC-CO₂ can directly affect the rate, yield, design, and economy of a SFE process with goals to extract residual bitumen from oil sands process waste streams on a much larger continuous scale.

1.3 Thesis Organization

This thesis is divided into five main chapters. Chapter 1 briefly describes the motivation for pursuing this research work and the main objectives of this thesis. The literature review in Chapter 2 characterizes and examines the different physical and chemical properties of bitumen found in Alberta's oil sands, the conventional in-situ and ex-situ applications that are currently used for extracting bitumen, the traditional applications that are utilized for upgrading bitumen, the environmental and technical disadvantages that are associated to these applications, and some of the emerging technologies that have been recently developed aiming to address these downfalls. The literature review will also examine SFE and its application to extract bitumen from surface mined oil sands. Chapter 3 outlines the materials and methods that are used to

perform this research study. Chapter 4 details the results from the experiments performed for whole bitumen and the bitumen cuts of LGO, HGO, and resid with SC-CO₂ at conditions with and without toluene added as a modifier. Chapter 4 will also include the analytical HTSD results characterizing the qualitative composition of the hydrocarbons collected. The potential sources of error identified during this research study will also be discussed. Lastly, Chapter 5 will provide a summary of the main conclusions drawn from the results obtained from this research study, while recommendations for future work in improving the approximation of the initial solubility for a bitumen feed will be suggested.

CHAPTER 2: LITERATURE REVIEW

This chapter details the background information relating to Alberta's oil sands bitumen. Discussions of their geological deposits, compositional characteristics and properties, the current in-situ and ex-situ bitumen extraction methods utilized, the problems and issues faced by these current extraction applications, and the emerging bitumen extraction technologies that are being developed will be examined. Specifically, this chapter will focus on the research and developmental efforts of utilizing supercritical fluid extraction as a more viable method to recover bitumen from oil sands and process waste streams.

2.1 Oil Sands in Alberta

Alberta is home to the world's third largest crude oil reserve, behind Saudi Arabia and Venezuela (Government of Alberta 2017). A majority of Alberta's crude oil supply is unconventional and the crude oil is entrapped within sandy matrices contained with various mixtures of quartz sand, clay, water, bitumen, and other mineral materials (NRCAN 2019a; CAPP 2018). In fact, approximately 83.4% of the total crude oil produced in Alberta as of April 2019 came solely from unconventional oil (Government of Alberta 2019b). Altogether, an estimated 165.4 billion barrels of crude oil is deposited in Alberta's oil sands and encompasses 140,000 to 142,000 km² of the province's landmass (Government of Alberta 2017).

Alberta's oil sands formations are predominantly located in three main regions: Peace River, Cold Lake, and Athabasca (Gordon 2012). Of the total 140,000 km² of oil sands deposits in Alberta, approximately 12% (29,000 km²) is located in the Peace River region, 13% (18,000 km²) in the Cold Lake area, and 66% (93,000 km²) is situated in the Athabasca region (Government of Alberta 2017). While these oil sands formations are located deep below layers of muskeg, glacial tills, sandstone, and shale sediments, their depositional thickness (ranging between 50 to 825 m) and their bitumen content (that can range up to 19 wt% of bitumen) varies (Government of Alberta 2019c; Chalaturnyk et al. 2002).

Located in the northeastern regions of Alberta, the Athabasca formation is the largest and the most accessible bitumen deposit of the three deposits (Zhou et al. 2008). Found mainly in the McMurray Formation of the Lower Cretaceous Mannville Group, the Athabasca bitumen

reserves are deposited at depths ranging between 0 to 500 m below ground surface (Zhou et al. 2008). While a small fraction of Alberta's oil sands reserve is shallow and can be surface mined, a large majority of the bitumen reserves found in the Peace River and Cold Lake deposits are deeply embedded at depths of 550 to 700 m and 985 to 1970 m below ground surface, respectively (Government of Alberta 2017; Zhou et al. 2008). To effectively recover bitumen from these formations in Alberta, in-situ techniques are commonly utilized.

Characteristically, the Athabasca oil sands consist as a mixture formed predominantly of bitumen (ranging between 0 to 19 wt%; average of 12 wt%), water (3 to 6 wt%), and mineral contents such as quartz, silt, and clay (84 to 86 wt%) (Gordon 2012; Chalaturnyk et al. 2002). As shown in Figure 1, the oil sand mixture fundamentally consists of sand particles that are individually encased by a water-film layer (Government of Alberta 2019a). The void spaces created between the sand-water complexes are effectively filled with bitumen (Government of Alberta 2019d).

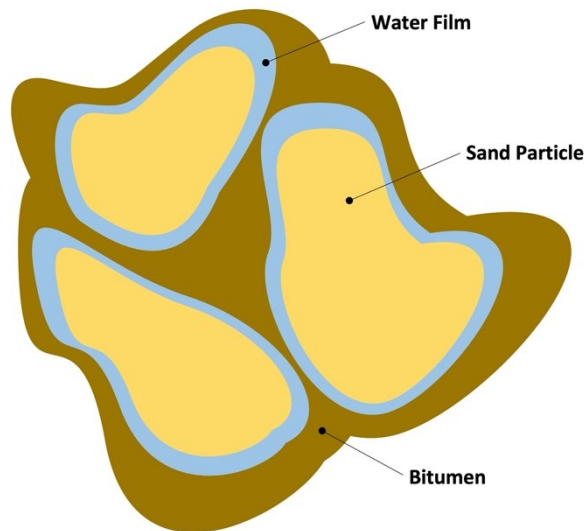


Figure 1. Untreated oil sands particle formed of bitumen surrounded by water film and sand (adapted from Government of Alberta 2019a).

A comparison between the properties of Athabasca bitumen, synthetic crude oil, and conventional crude oil is provided in Table 1.

Table 1. A comparison of properties between Athabasca bitumen with synthetic and conventional crude oils (adapted from Yoon et al. 2009; Hyndman and Luhning 1991).

Properties	Athabasca Bitumen	Synthetic Crude Oil	Conventional Crude Oil
API (°)	8	32	41
Viscosity (cSt at 40°C)	3000	3.0	2.9
H/C Ratio	1.50	n/a	n/a
Sulfur (wt%)	4.78	0.08	0.2
Nitrogen (wt%)	1.63	0.03	0.04
Oxygen (wt%)	1.81	n/a	n/a
Nickel (ppm)	68.50	<1	<1
Vanadium (ppm)	174.00	<1	<1
Asphaltenes (wt%)	15.59	n/a	n/a
Saturate Aromatics (wt%)	67.97	n/a	n/a
Resin (wt%)	16.44	n/a	n/a

Compositionally, bitumen can be fractionated into four major categories of compounds in terms of solubility and polarity; these categories include saturates (S), aromatics (A), resins (R), and asphaltenes (A) (He et al. 2013; Speight 2006). Saturates are mainly formed from linear or branched non-polar hydrocarbon sequences that can also contain aliphatic cyclic paraffins (Santos et al. 2014). Aromatics are formed from aromatic structural rings that are joined with a series of aliphatic chains (Santos et al. 2014). Saturates and aromatics contain the highest hydrogen to carbon (H/C) ratio while maintaining low molecular masses (Yoon et al. 2009).

Heteroatomic contents are components found in the crude oil that are neither carbon nor hydrogen. Heteroatoms such as sulfur, nitrogen, oxygen, and other various heavy metals like vanadium and nickel are commonly found at higher concentrations in the asphaltene and resin fractions of the bitumen (Yoon et al. 2009; Gray 2001). Asphaltenes in bitumen are characterized as an aromatic-polar compound formed from various combinations of carbon, hydrogen, oxygen, nitrogen, sulfur, nickel, and vanadium (Abu-Khader and Speight 2007). Resulting from a more complicated chemical composition, the molecular weights of asphaltenes are resultantly heavier (Santos et al. 2014; Abu-Khader and Speight 2007). Even with a lower H/C ratio of 1.18, asphaltenes still makes up 15.6 wt% of the overall composition found in Athabasca bitumen, and is a main contributor to the elevated viscosities exhibited by bitumen (Abu-Khader and Speight

2007; Yoon et al. 2009). Furthermore, the concentration of asphaltene and resin found in crude oil proportionally corresponds to the oil's sulfur content but is inversely proportional to the oil's API gravity measurement (Koots and Speight 1975). As a result of these characteristics, unconventional crudes such as bitumen will need to undergo a series of distillation and upgrading procedures to eliminate the different chemical impurities found in the oil before it can be sent for refining (Hyndman and Luhning 1991). However, the large presence of heteroatoms and metal contents in bitumen can significantly impede and undermine the performance of the catalysts used by the upgrading applications (Yoon et al. 2009; Abu-Khader and Speight 2007).

2.2 Recovery Methods for Bitumen

Hindered by its high viscosity characteristics, the production of heavy crude oils such as bitumen is substantially more difficult to extract, pump, and transport in its natural state by traditional methods (Santos et al. 2014; Færgestad 2016). The recovery of bitumen from Alberta's oil sands is currently accomplished by either one of the two available methods: surface mining (ex-situ) or combinations of the in-situ methods (Government of Alberta 2017). Of the total 142,200 km² of oil sands area found in the Athabasca, Cold Lake, and Peace River regions, only 3% are surface minable (Government of Alberta 2017; Gordon 2012). The remaining 97% are solely recoverable through in-situ methods (Government of Alberta 2017).

For bitumen reserves that are geologically located at shallower depths, the ex-situ production approach in the form of surface mining and hot water extraction is commonly utilized (Government of Alberta 2017; Færgestad 2016; Clark and Pasternack 1932). Alternatively, deeper heavy oil deposits are commonly accessed by the in-situ approach involving thermal methods that lowers the viscosity of the bitumen; this allows the bitumen to flow and be collected by extraction wells more easily (Government of Alberta 2017; Færgestad 2016). The cyclic steam stimulation process, the steam-assisted gravity drainage method, vapour extraction, and the toe-to-heel air injection approach are in-situ methods that are commonly employed (Færgestad 2016; Upreti et al. 2007; Xia and Greaves 2006; Xia et al. 2002). Examples from both the in-situ and the ex-situ approaches will be further explored in the following sections.

2.2.1 In-situ Bitumen Recovery Methods

While only 3% of Alberta's total oil sands deposits can be effectively recovered by the surface mining approach, the remaining 97% of Alberta's bitumen reserves are situated at depths where the application of surface mining becomes technologically impractical and economically unfeasible to be effectively utilized (Government of Alberta 2017). As a result, the deeper deposits are alternatively recovered by in-situ methods that typically involves a combination of on-site thermal induction and/or chemical stimulation techniques to render the highly viscous crude oils into a less viscous state (Færgestad 2016; NEB 2000). By reducing the bitumen's high viscosity, recovery of the deeply deposited crudes can be more easily collected and pumped by extraction wells (Government of Alberta 2017). In-situ recovery methods of the cyclic steam stimulation process, the steam-assisted gravity drainage method, the toe-to-heel air injection technique, and vapour extraction will be extensively examined below.

Cyclic steam stimulation (CSS) is a commonly applied in-situ bitumen recovery technique that is engineered based on the underlying relationship between heat and viscosity behaviours of heavy oils (NEB 2000). The current iteration of the CSS technique has been largely unchanged since its initial development by Imperial Oil back in 1958 (NEB 2000). Operated as a multi-stage, single well system, the CSS process can be sub-divided into three major operational stages: steaming, soaking, and production (Færgestad 2016; NEB 2000). Steam generated by large on-site heating boilers are injected at temperatures of 300°C and pressures of 11,000 kPa into a vertically drilled wellbore that is localized at a targeted bitumen deposit over the span of several weeks (NEB 2000; Vittoratos et al. 1990). During this time, the escalated temperature of the steam sufficiently lowers the high viscosities of the bitumen deposit to favourable levels that eases extractions (Færgestad 2016; NEB 2000). Furthermore, the high injection pressure of the steam supply can effectively generate hydraulic fissures into surrounding obstructive geological formations to form a less disruptive well path allowing for enhanced recovery (Færgestad 2016; NEB 2000). As the steam injection condenses and soaks into the targeted reservoirs, the bitumen deposits are interacted with the heated moisture to become less viscous in behaviour (Gray 2015). At this point, bitumen and water can be pumped up the wellbore to be retrieved (NEB 2000). Production from the bitumen reservoir is continually maintained until the injected steam can no longer contribute the necessary thermal capacities to effectively lower the oil viscosity at levels that are extractable by wellbores (NEB 2000). As this

occurs, productions are ceased as another steam injection cycle is repeated again (Færgestad 2016).

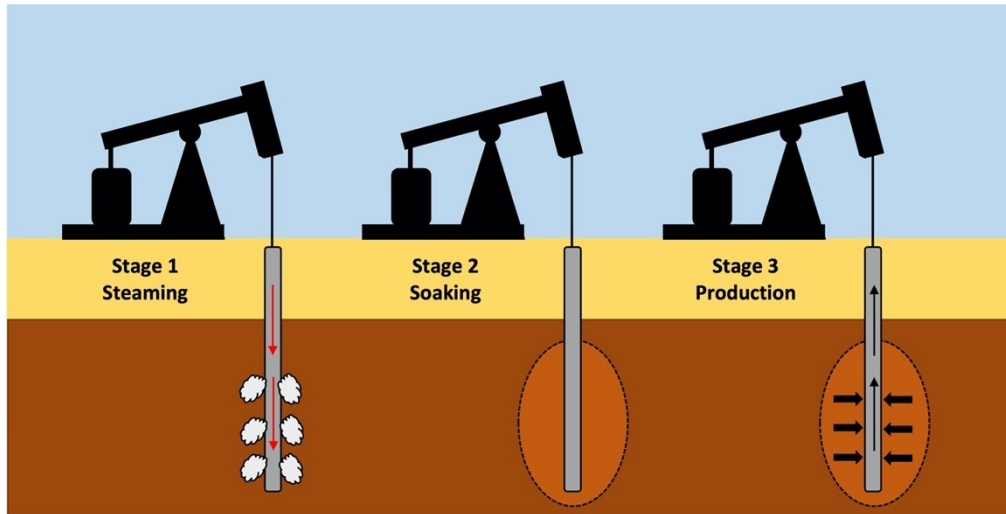


Figure 2. A typical CSS process showing the steaming, soaking, and production phases (adapted from NEB 2000).

The extracted bitumen and water mixture retrieved from the CSS process must undergo additional separation (Færgestad 2016). A diluent is introduced into the oil-water mixture to further decrease the viscosity of the bitumen components (Gray 2015). Surfactants are also added to separate the water from the bitumen (Banerjee 2012). The mixture is then channeled into a free-water knockout drum, allowing for large amounts of free water to be separated from the bitumen (Gray 2015). Any water remaining in the bitumen is then evaporated by heating the bitumen inside a desalter unit at temperatures ranging between 100 to 150°C (Gray 2015). The water is directed to a series of treatment stages first involving skim tanks, induced gas flotation vessels, and oil removal filters to further remove any bitumen content from the retrieved produced water (Husky Energy 2011). The produced water then undergoes lime softening, filtration, and weak acid cation exchange before it can be reused for steam generation in the CSS process (Husky Energy 2011; Heins and Peterson 2003).

CSS is most commonly applied to deep bitumen deposits encased by thicker capping shales that can withstand high steam injecting pressures (Holly et al. 2016). Although the CSS method is characterized as a quick and rather simple bitumen recovery technique, its oil recovery factor of 12 to 20% is much less than other in-situ processes (Alvarez and Han 2013). Based on

data gathered from 2014, the CSS technique was utilized to produce approximately 11% (or 251,666 out of 2,203,433 bpd) of the crude oil in Alberta (Holly et al. 2016). Specifically, of the 251,666 bpd produced in 2014, 247,656 bpd was from the Cold Lake deposits, 4,010 bpd was from the Peace River reserves, while the Athabasca and other bitumen deposits did not use CSS at all (Holly et al. 2016).

Similarly targeted for the recovery of deeply situated bitumen deposits, the in-situ steam-assisted gravity drainage (SAGD) method was first conceptualized by Dr. Roger Butler and Imperial Oil in the mid-1970s (Government of Alberta 2019a; NEB 2000). Drawing from similar technological fundamentals as the CSS approach, the SAGD uses steam injection into the targeted heavy oil reserves to reduce the viscosity of the bitumen to aid in well production (Færgestad 2016; Upreti et al. 2007). However, the SAGD process does not use alternating steam and production cycles as with the CSS method. SAGD uses parallelly-twinning, horizontally situated wells (Færgestad 2016). The paired wells situated between 2 to 10 m apart, can allow for continuous bitumen production unlike CSS (Nasr and Ayodele 2005; NEB 2000).

By twinning the horizontally stacked wells in the targeted reservoir, steam can be continuously injected through the upper well, causing vertical and horizontal expansion within the oil formation to occur into creating a steam chamber (Færgestad 2016; NEB 2000). Containing the highly viscous bitumen deposits, the steam chamber is heated to 200°C and effectively lowers the bitumen's viscosity (NEB 2000). The less viscous bitumen combined with the cooled steam moisture is then mobilized by gravity and flows to the lower production well (Færgestad 2016; Chow et al. 2008; NEB 2000). Following its collection, the bitumen-water mixture is retrieved and the water is separated from the bitumen so that the water can be recycled for steam again (Ikebe et al. 2010). Ultimately, the steam injection and bitumen recovery process in SAGD can happen continuously without having to switch between them like in CSS (Holly et al. 2016).

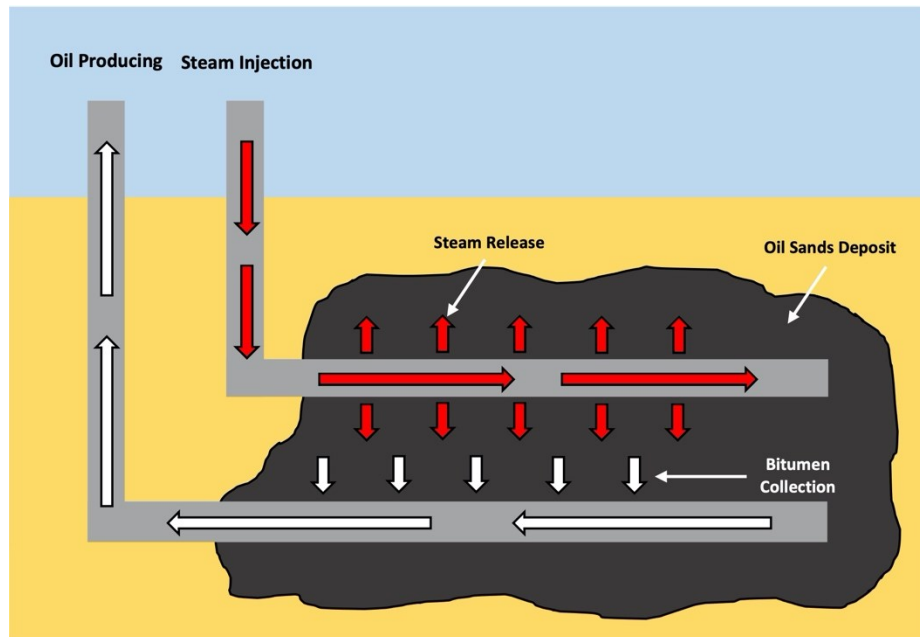


Figure 3. A typical SAGD process (adapted from NEB 2000).

Compared to CSS, the implementation of SAGD has proven to be a more advantageous approach due to its continuous steaming and bitumen recovery. Resultantly, bitumen recovery percentages ranging between 50 to 70% can be achieved by the SAGD method (Færgestad 2016; Holly et al. 2016; Alvarez and Han 2013; NEB 2000). However, the continuous heating and boiling of the process water to produce the steam required for the bitumen recovery process is energy intensive and can result in substantially high operational costs (Færgestad 2016). Despite this disadvantage, SAGD was applied to produce approximately 31% (686,324 out of 2,203,433 bpd) of Alberta's crude oil in 2014, second to that of surface mining (Holly et al. 2016). From the 31% of the crude oil produced by SAGD in Alberta, 201,627 bpd was produced from the Athabasca oil sands region, 19,592 bpd from the Cold Lake area, 459,162 bpd from the Conklin deposits, 4,285 bpd from the Peace River reserves, and 1,658 bpd from the Wabiskaw reservoirs (Holly et al. 2016).

Prior to the use of steam injection as a heating media for recovering deeply deposited viscous crude oils, the thermally enhanced oil recovery method of in-situ combustion (ISC) was commonly employed (Kulkarni and Rao 2004). Conventionally, the ISC method utilizes a pair of vertical injection and producing wells that are spaced hundreds of meters apart (Yao et al. 2018; Xia and Greaves 2006; Xia et al. 2003). On one end, the vertical air injection well combusts a small amount of deposited crude oil creating an ignition zone within the reservoir, known as fire

flooding (Schlumberger 2019a; Schlumberger 2019b; Kulkarni and Rao 2004). The small-scale ignitions created intends to increase the surrounding temperature of the reservoir area to promote reduced viscosities of the entrapped crude oil (Schlumberger 2019a; Kulkarni and Rao 2004; Xia et al. 2003). As the ignition zone propagates and further expands, larger volumes of heavy crude oil will become less viscous, ultimately allowing its flow into the adjacent vertical production well (Xia et al. 2003). Unfortunately, issues of gravity segregation between the density differences of the injected gas and oil can result in air breakthrough (Aristizábal and Vargas 2005). Additionally, the large distances between the vertical injection and production wells can result in increased oil saturation at the production site (Xia et al. 2003). Emulsion formation and challenges in maintaining high temperatures within the extraction site are also disadvantages of ISC (Xia et al. 2003). Resulting from its poor condition controls and technological downfalls, the utilization of the ISC method was gradually phased-out by the oil producing industry (Xia et al. 2003).

In attempts to address the major technical downfalls of the ISC process, the toe-to-heel air injection (THAI) method was alternatively developed (Kulkarni and Rao 2004; Xia et al. 2003). While adopting similar mechanisms as that of ISC, the THAI recovery method further incorporates both a vertical injection well and a horizontally oriented production well situated on the same horizontal axis with the toe of the production well in close proximity to the injection site (Schlumberger 2019c; Xia and Greaves 2006). Unlike the ISC configuration, the smaller distance between the injection and production wells allows the combustion front initiated at the injection point to travel from the “toe” of the production well to its “heel” (Xia and Greaves 2006; Xia et al. 2003; Xia and Greaves 2002). Similar to the ISC technique, a combustion front is initiated at the vertical injection well as heavy coke residues are continually burned to produce the necessary heat to reduce the viscosity of the entrapped heavy oil content to promote for enhanced oil mobility (Xia et al. 2003). The cooler downstream regions of the reservoir contained with the more viscous crude content will force the less viscous crude oil directly downwards to be collected by the horizontal production well (Xia et al. 2003). By doing so, a vertically oriented combustion zone is strictly maintained to effectively control the occurrence of gas overriding (Xia et al. 2003). Additionally, a high air flux can be continuously preserved during the occurrence of the THAI process to maintain high temperatures at the production site (Xia et al. 2003). Although testing of the THAI process has shown that it can significantly lower

the produced oil's viscosity level from 48,000 to 50 MPa·s and it can recover 80% of the oil in place in a laboratory setting, its application at the commercial scale has yet to be successfully demonstrated (Morgan 2016; Xia and Greaves 2006).

Although the application of thermal-based in-situ oil recovery methods are viewed as suitable techniques to recover the deeply deposited bitumen reserves that cannot be conventionally mined, there are still disadvantages with these processes (Upreti et al. 2007; Singhal et al. 1996). For applications such as CSS and SAGD, large volumes of water are required to be heated into steam for deep injections into the depths of the bitumen reservoirs (Upreti et al. 2007). In fact, a 3:1 water to oil ratio is commonly required for steam generation in such processes (Singhal et al. 1996). Steam generation from the large volumes of water requires significant energy and results in costly operational expenses to do so (Færgestad 2016). Other thermally induced in-situ processes can also encounter issues related to heat loss within its targeted treatment area, making this type of application highly inefficient and ineffective for use for prolonged periods of time (Upreti et al. 2007). Due to these disadvantages, alternative applications, such as the use of chemical additives, to more effectively reduce the viscosity of bitumen have been further examined and researched.

Vapour extraction (VAPEX) is a chemical-based in-situ bitumen recovery process (Upreti et al. 2007). Similar to the SAGD approach, a set of parallelly-twinning, horizontally stacked wells are utilized to lower the targeted oil reserve's viscosity while simultaneously collecting the mobilized heavy oils (Færgestad 2016; Mokrys and Butler 1993). Unlike SAGD, heated steam injections are not applied into the reservoir from the upper well; but instead, injections of vaporized solvents (e.g. propane, butane) are injected (Moussa 2019; Færgestad 2016; Upreti et al. 2007). The injected solvent vapour expands within the reservoir to create a vapour chamber and dilutes the bitumen content to effectively lower the oil's viscosity (Upreti et al. 2007). The diluted oil can then be more easily mobilized into collection by the lower production well (Færgestad 2016). The components to the oil-solvent mixture can then be separated through a pressure drop in a flash tank; with a 90% recovery rate, the recovered solvent material can then be reused for dilution again (El-Haj et al. 2009; Upreti et al. 2007).

Benefitting from its solvent-based nature, the capital and operational costs of VAPEX is typically lower than that of its thermal based counterparts due to the lack of surface facilities required for steam generation and process water treatment (Upreti et al. 2007). Additionally, less

energy is consumed by VAPEX from its lack of heating requirements needed for its recovery process (Færgestad 2016). In fact, for an equivalent oil production rate, VAPEX uses 3% of the total energy required for the SAGD process (Upreti et al. 2007). Despite its advantages, concerns of asphaltene precipitation resulting from alterations of pressure and temperature conditions of the collection site can occur at VAPEX production wellbores; this causes drastic reductions in oil recovery rates (Upreti et al. 2007; Haghghat and Maini 2010). In the mid-2000s, the VAPEX technology was widely researched and further developed on the pilot-scale levels by CNOOC International at their Plover Lake facilities, Imperial Oil at its Cold Lake developments, Encana Corporation at their Foster Creek project, and Suncor Energy at their Fort McMurray operations (Upreti et al. 2007). However, the full commercialization of the VAPEX process has not yet been successfully accomplished (Alberta Innovates 2017; Jaremko 2017).

2.2.2 Ex-situ Surface Mining and the Hot Water Extraction Recovery Process

Near-surface oil sand reserves situated at shallower geological depths of less than 50 to 75 m are feasibly excavated by open-pit mining operations (Chow et al. 2008; Chalaturnyk et al. 2002; NEB 2000). Oil sand deposits are predominantly topped by 4 to 5 geological layers of topsoil, muskeg/peatland, overburden, oil sands ore, and limestone (Oil Sands Magazine 2019a). The preliminary step to surface mining involves the harvesting and removal of the vegetation from the topsoil layer. The removal of vegetation from the topsoil surface exposes the muskeg layer that needs to be cleared (Oil Sands Magazine 2019a). Dewatering of the submerged water table throughout the operational life of the mine is essential to stabilize the excavation site from seepage caused by heavy rain or seasonal snow melts (Oil Sands Magazine 2019a). The muskeg and overburden layers can then be removed to expose the oil sands ore that are mined. The excavated oil sands ore are carted off-site to a processing/recovery facility that allows for the bitumen contents to be separated from its encasing sandy organic materials (Færgestad 2016). Conventionally applied in Alberta, the mined oil sands undergo a series of bitumen isolating processes that are largely derived from the original hot water extraction method developed by Dr. Karl Clark in 1929 (University of Alberta 2005; NEB 2000). Based on Clark's hot water extraction method, the currently used application is largely improved to better accommodate for larger-scale extraction applications, improve operability, increase recoverability of bitumen, and greatly reduce energy consumption (Hyndman and Luhning 1991). Due to such improvements, a

bitumen recovery rate of over 90% from the mined oil sands ore is normally achieved (Chow et al. 2008).

The excavated oil sands ore are initially crushed and deposited into a slurry mixture of hot water (heated to 85°C), steam, and supplements of caustic additives (NaOH) during the preliminary conditioning process (Chalaturnyk et al. 2002; NEB 2000; Mossop 1980). The primary intention of the conditioning phase is to structurally disassemble the oil-sandy composition, which ultimately isolates the unwanted mineral and organic impurities from the bitumen content (Chow et al. 2008; Chalaturnyk et al. 2002). The caustic additives applied at this stage can beneficially modify the asphaltic acids found in bitumen to be more water soluble, while enacting as surfactants to minimize the surface and interfacial tensions of the medium; such applications offered by the caustic additives can aid in the disassembly of the oil sands' structure while promoting the recoverability of bitumen (Chalaturnyk et al. 2002). When the slurry is transported to the separation cells, a velocity, temperature, and residence time of 3.5 m/s, 41 – 53°C, and 7 – 12 minutes, respectively, is ideally maintained to further promote the separation of bitumen from the oil sands (Chow et al. 2008).

Following the conditioning process, the aerated slurry is then channeled into a large cone-bottomed primary separation vessel, where gradual temperature increases allow the slurry content to exhibit densities similar to water (Chow et al. 2008). Due to this shift in density, air is added to the processed slurry to further encourage bitumen floatation during its separation phase. Additionally, water is added at a 1:4 water to bitumen ratio at this step (Chow et al. 2008). This allows for the aerated bitumen froth to rise onto the upper surface of the vessel to be skimmed off and carried away for froth processing. The heavier sands and mineral materials are settled out at the bottom of the vessel to be collected for additional treatments to retrieve any remaining bitumen contents that can be potentially recovered (NEB 2000; Starr and Bulmer 1979). Un-aerated oil sand slurries found beneath the skimmed froth layer from the primary vessel, known as middlings, are transported to a secondary separation vessel for additional flotation treatment to further retrieve any residual bitumen that can be recovered (Oil Sands Magazine 2019b; Chalaturnyk et al. 2002).

The bitumen froth skimmed from the primary separation vessel is approximately 25 wt% water and 10 wt% solids (Chow et al. 2008). At an initial extraction temperature of 60°C, the bitumen froth exhibits viscosity of approximately 5,000 cP. To reduce its viscosity and density

for better separation, the froth is further heated and a diluent solvent, such as naphtha, is added at a 1:1 ratio (Starr and Bulmer 1979; Chow et al. 2008). Paraffinic froth treatment (PFT) is a less-applied separation process that utilizes paraffinic solvents instead of naphtha-based diluents like in the more conventional naphthenic froth treatment (NFT) approach (Rao and Liu 2013). The PFT method can yield less contaminants in the extracted bitumen and is less energy intensive compared to the NFT technique (Rao and Liu 2013). Unfortunately, the PFT approach utilizes more paraffinic solvent to equivalently recover a similar amount of bitumen as compared to the NFT process (Rao and Liu 2013). Furthermore, paraffinic solvents do not effectively dissolve asphaltenes, causing asphaltenes to be precipitated and discharged into the froth tailings (Rao and Liu 2013).

The combination of bitumen froth and diluent then enters into a high-speed centrifuge where remaining water and solid contents are further removed (Chow et al. 2008; NEB 2000; Starr and Bulmer 1979). Following its use, the diluent is recovered to be reused in the process, while the extracted bitumen from the centrifuging process is delivered to be distilled and upgraded (NEB 2000). The remaining sand and organic materials will be discarded into the tailings capturing ponds (Rao and Liu 2013; NEB 2000).

2.2.2.1 Process Waste Streams

While other in-situ bitumen recovery techniques have been widely developed over the last decades, surface mining of the oil sands ore in Alberta still remains as a prevalent technique that is largely performed for shallower reserves (Kasperski and Mikula 2011). Despite its advantages, the ex-situ approach of surface mining generates substantial concerns regarding to the environmental impacts created on the excavated land, as well as the production and management of the vast amounts of wastewater tailings created as a result (NRCAN 2019b; Kasperski and Mikula 2011). As of 2015, 1.18 trillion litres of waste tailings have been generated in Alberta from oil sands mining (Pembina Institute 2017). The tailings contain concentrations of bitumen, hydrocarbons, naphthenic acids, phenols, arsenic, cadmium, chromium, lead, and other heavy metals. Release of these tailings into the environment without being properly treated can result in detrimental consequences to the health, well-being, and safety of the surrounding natural ecosystems (Pembina Institute 2017). Therefore, the generated

waste tailings are temporarily stored in man-made containment ponds, known as tailings ponds (AER 2019; Oil Sands Magazine 2019b; Kasperski and Mikula 2011).

2.2.2.2 Remediation and Reclamation of Tailings Ponds

Over the years, research funded by the oil sands industry has been focused on developing ways to more effectively remediate and reclaim tailings ponds. Suncor Energy Inc. (Abusaid et al. 2011) implemented the use of a petroleum coke cap to help accelerate the dewatering of the tailings, which would normally take centuries to do so naturally. In this process, a petroleum coke cap is spread onto the surface of the tailings pond in winter when the pond is frozen over. When the pond begins to thaw in the following spring season, the coke cap remains afloat on the pond surface (Abusaid et al. 2011). Provided by the structural integrity of the coke cap to act as a platform on the pond surface, heavy machineries were able to drive across the pond so that vertical drains can be installed into the tailings pond to help discharge water from the pond at a faster rate. After a few years when the deposits in the pond have settled enough, the area can then be effectively reclaimed.

The addition of CO₂ as a dewatering method was also explored by Canadian Natural Resources Ltd. at their Horizon facility (COSIA n.d.a). Research found that when CO₂ is added to the process waste stream prior to its discharge into a tailings pond, the added CO₂ was able to reduce the pH of the tailings and effectively consolidate the solid contents in the waste stream. By doing so, this allowed the solids to settle at a much faster rate and helped further accelerate the dewatering process in the tailings (Zhu et al. 2011; COSIA n.d.a). The released water could then be reused by other oil sands process applications.

Centrifugation is a common separation process that has been commercially used by Syncrude Canada and Shell Canada at its facilities to treat tailings (COSIA n.d.b). During this process, coagulant and/or flocculant agents are first added to the tailings material before being placed into a centrifuge. From the centrifuge, the tailings become dewatered and leaves behind a solid cake material (Kasperski and Mikula 2011). The removed water content from the tailings can then be recollected and reused by the oil sands extraction process again.

2.2.2.3 Recovery of Residual Bitumen in Waste Streams

One of the biggest environmental concerns related to the use of tailings ponds is the presence of residual bitumen and naphthenic acids that are present in these process waste streams. Naphthenic acids are produced from oil sands bitumen during the caustic/hot water process (Scott et al. 2005). Along with the other contaminants found in the process waste stream, its release into the natural environment can be extremely hazardous to animals and aquatic organisms (Allen 2008; Quagraine et al. 2005). While centrifugation has been explored as a viable method to recover residual bitumen from tailings, this process is still performed primarily with the intention to dewater tailings instead (Kasperski and Mikula 2011).

Chemical applications have also been explored as possible methods to recover residual bitumen from process waste streams. Romaniuk et al. (2015) studied the application of adding lime (CaO) to tailings and determined that the added CaO helped increase the tailing's pH. The increased pH can effectively disrupt the bitumen-clay complex in the tailings, allowing the residual bitumen content to be released and driven up to the tailings surface. Air flotation can then be used to further remove the bitumen.

2.3 Supercritical Fluids

Although the current methods of extracting, upgrading, and processing bitumen from oil sands have been developed as functional applications, environmental factors relating to the impacts of the tailing wastes produced, reclamation of the operation areas, and water usage are still major concerns faced by the conventional application of producing bitumen from oil sands. Due to these less-desirable attributes, a more environmentally sustainable and cost-effective way of producing bitumen is largely sought after to be developed and utilized instead.

In recent years, supercritical fluid extraction (SFE) has emerged as a potential candidate to fulfill such demands (Li et al. 2015; Yan et al. 2015). Although SFE have more prominently been industrialized within the food, pharmaceutical, and cleaning sectors, more recent research and developments into its application for heavy crude oil and bitumen extraction from oil sands have been largely demonstrated with relative success (La and Guigard 2015; Yan et al. 2015). Fundamentally, the SFE technology is applied as a solvent-induced extraction method utilizing a supercritical fluid (SCF) as its extracting solvent (McHugh and Krukoniš 1994). The following sections will provide a more extensive understanding of what SFE entails and how its application

is currently researched and developed so that it can be applied and utilized for the extraction of bitumen on a larger commercial scale.

2.3.1 Overview of the Supercritical State

By heating and pressurizing a pure substance beyond a distinguishing critical temperature and pressure, also known as the critical point, the fluid is transitioned into its supercritical state as shown in Figure 4 (McHugh and Krukoniš 1994). As its critical temperature and pressure is effectively approached and surpassed, gradual phase transitioning of the fluid's thermodynamic properties simultaneously occur to allow for the convergence of its liquid and gaseous phases into a singular supercritical fluid state (Płotka-Wasyłka et al. 2017; Brunner 2005; Knox 2005; McHugh and Krukoniš 1994). At this supercritical state, the fluid possesses liquid-like densities and gas-like diffusivities and viscosities as shown in Table 2 (Płotka-Wasyłka et al. 2017; Brunner 2005; McHugh and Krukoniš 1994). Furthermore, the combination of its gas-like viscosity and near zero surface tension enables SCFs to more easily penetrate and dissolve into a wider range of matrices (Akgerman 1997; Raynie 1997). The combination of these properties enables SCFs to exhibit enhanced mass transport, dissolution, and solvating abilities (Płotka-Wasyłka et al. 2017; Herrero et al. 2006; Knox 2005; Manivannan and Sawan 1998). As a result of these preferential characteristics, development and research for using SCFs as a solvent to selectively extract and dissolve specific compounds from various types of matrices have been largely fostered over the years – an example would be the extraction of bitumen from oil sands and process waste streams (Cossey 2018; Płotka-Wasyłka et al. 2017; La and Guigard 2015).

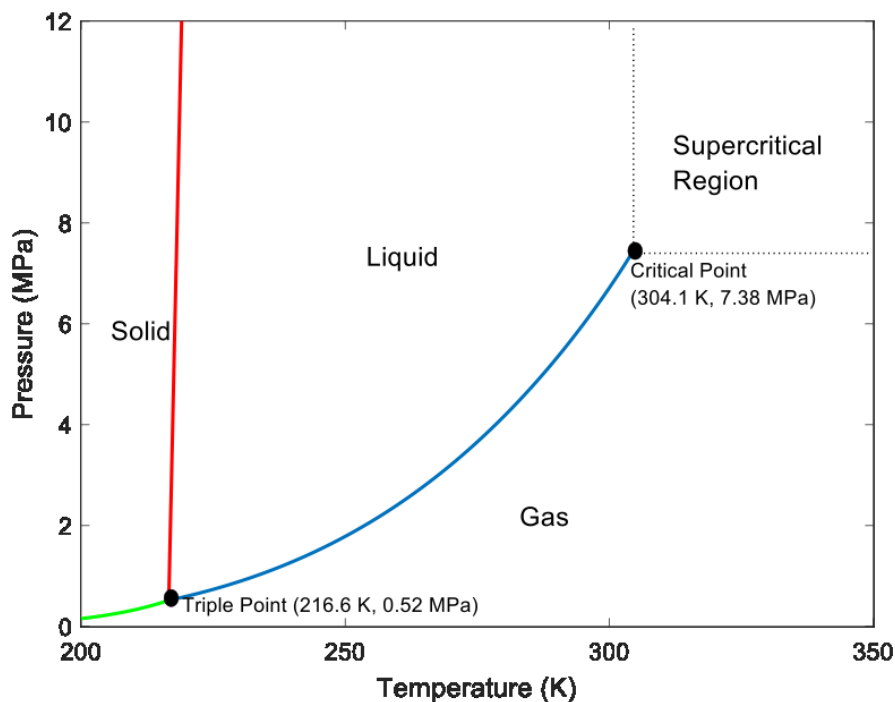


Figure 4. Phase diagram of carbon dioxide depicting the solid, liquid, gas, and supercritical phase regions (Roodpeyma 2017).

Based on the previous research efforts performed on studying the characteristics and behavioural properties of SCFs, it was observed that minor alterations made to the SCF's pressure and/or temperature can result in substantial changes to its extractability and dissolvability with targeted compounds (Herrero et al. 2006; McHugh and Krukoniš 1994). For instance, an increase in pressure when the SCF is near its critical point can elevate its density, and ultimately enhancing the fluid's solvating capabilities (Herrero et al. 2006; McHugh and Krukoniš 1994; Laitinen et al. 1994). As a result, SCFs can be applied to extract and remove certain desirable compounds in different matrices by simply manipulating and adjusting its temperature and/or pressure parameters. Similarly, when the desired compounds have been effectively isolated and extracted by the SCF, depressurization of the SCF can lower its density and solubility properties so that the dissolved compounds can be simply precipitated out of it (Brunner 2005).

Table 2. Properties of gas, liquid, and SCF (taken from Manivannan and Sawan 1998).

States	Density (g/mL)	Diffusivity (cm ² /s)	Dynamic Viscosity (g/cm·s)
Gas	1×10^{-3}	1×10^{-1}	1×10^{-4}
Liquid	1.0	5×10^{-6}	1×10^{-2}
Supercritical Fluid	3×10^{-1}	1×10^{-3}	1×10^{-4}

2.3.2 Supercritical Carbon Dioxide

Overall, an extensive selection of substances upon reaching their respective critical points can be effectively conveyed into their supercritical states of behaviour (Brunner 1994). As shown in Table 3, the critical temperatures and pressures corresponding to each of these compounds can widely differentiate from tens to hundreds of Kelvins and megapascals (Brunner 1994; McHugh and Krukoni 1994). Although many compounds can be brought to their supercritical states, the selection of a suitable SCF is crucial for its role as an extracting solvent (Płotka-Wasyłka et al. 2017). Factors such as the SCF's toxicity characteristic, its physiochemical behaviour and reactivity with the targeted solute, the technical applicability of achieving its supercritical condition, and the capital and operating costs of utilization are critical factors that should be comprehensively considered and examined (Płotka-Wasyłka et al. 2017).

Table 3. Critical temperatures and pressures of various compounds (taken from Brunner 1994).

Compounds	Critical Temperature (K)	Critical Pressure (MPa)
Methane	190.4	4.60
Ethylene	282.4	5.04
Carbon Dioxide	304.15	7.38
Ethane	305.4	4.88
Propylene	364.95	4.60
Propane	369.8	4.25
Ammonia	405.55	11.35
Isopropanol	508.3	4.76
Methanol	512.6	8.09
Ethanol	513.9	6.14
Benzene	562.2	4.89
Toluene	591.8	4.10
Water	647.3	22.12

At its gaseous state, carbon dioxide is a highly undesirable and impractical solvent to be used in typical applications of extracting and purifying compounds dissolved in various medias (Manivannan and Sawan 1998). However, when pressurized and heated to its critical point at 304.15 K (31.1°C) and 7.38 MPa (74.8 atm), the now supercritical CO₂ (SC-CO₂) exhibits improved viscosity and solubility characteristics that can favour for enhanced extracting capabilities (Brunner 1994; Manivannan and Sawan 1998). Combined with its modestly achievable critical temperature and pressure parameters, its non-flammable, non-toxic, chemically inert, reusable, and relatively inexpensive characteristics have allowed SC-CO₂ to be preferably utilized in various industrial SFE applications (Khaw et al. 2017; Gupta and Shim 2007; Herrero et al. 2006; Wai et al. 2003). Unlike the conventional organic and liquid solvents that are utilized in traditional extraction methods, its chemical inertness makes SC-CO₂ significantly safer to handle and to be applied in applications such as food processing (Brunner 2005).

Although deemed as a preferential choice to be applied in SFE applications due to its advantageous characteristics, its non-polar behaviour can ultimately limit the extractability of SC-CO₂ to only compounds that are small, low molecular-weighted, non-polar, and CO₂-philic such as alkanes, terpenes, aldehydes, esters, alcohols, and fats (Khaw et al. 2017; Brunner 2005). However, the additions of organic modifiers (also known as co-solvents) can effectively enhance the polarity of SC-CO₂, allowing it to better solvate and extract the polar compounds that it may encounter (Płotka-Wasyłka et al. 2017; Phelps et al. 1996).

2.3.3 Common Applications for Supercritical Fluids

Substantial efforts to research and develop applications to utilize SFE in various industrial sectors have been extensively explored over the past decades (Knox 2005; McHugh and Krukoni 1994). The earliest full-size commercialization of SFE was first introduced in Germany during the late 1970's by the food industry for the decaffeination of coffee beans (Palmer and Ting 1995; Zosel 1963). Decaffeination of coffee beans prior to the utilization of SFE was commonly done by treating the beans with organic solvents such as methylene chloride and ethyl acetate (De Marco et al. 2017). However, the exposure and consumption to trace amounts of these solvents found in the treated coffee beans can lead to detrimental health impacts resulting in conditions of neuro and liver toxicity, respiratory tract damages, liver and

lung cancer, and kidney failure (Australian Government 2018; USEPA 2017; De Marco et al. 2017). The alternative utilization of SC-CO₂ in the decaffeination process effectively eliminates the usage of toxic organic agents in exchange for a solvent that is more chemically inert and less harmful (Arai et al. 2002). Subsequent developments within the food industry further advanced the SFE technology to extract other food and edible-related components such as cholesterol from butter oil, carotenes from carrots, and fatty acid contents from ground beef (Sun and Temelli 2006; Mohamed et al. 1998; Chandra and Nair 1997; King et al. 1996).

Adaptation by the pharmaceutical sector further saw the derivation of the SFE technology applied into the development of the supercritical solvent impregnation technique, the gas anti-solvent recrystallization process, and the rapid expansion supercritical solution procedure for enhancing drug delivery and drug powder production (García-Casas et al. 2018; De Zordi et al. 2014; Kumar et al. 2014; Tom et al. 1993). The adoption of the SFE technology for environmental remediating applications have been successfully demonstrated to effectively treat heavy metals, pesticides, polycyclic aromatic hydrocarbons (PAH), polychlorinated biphenyls (PCB), and other hydrocarbon constituents polluted in various soil and liquid mediums (Saldaña et al. 2005; Lin et al. 1995; Laitinen et al. 1994). Research and developmental efforts have also focused on further utilizing SCFs for the purpose of extracting bitumen from oil sands, hydrocarbons from crude oils, and bitumen from process waste streams (Cossey et al. 2019; Yan et al. 2015; Rudyk et al. 2014; Rose et al. 2000; Guiliano et al. 2000; Deo et al. 1992). However, a commercial-scale SFE process unit capable of extracting hydrocarbons and bitumen from these materials have yet to be successfully developed and reported in literature.

2.3.4 Initial Solubility in Supercritical Fluids

The initial solubility of bitumen in a SCF is the concentration of bitumen that can be dissolved into a SCF at equilibrium (Cansell et al. 1998). Measuring the solubility of bitumen in a SCF is a foundational step in determining the maximum achievable extraction efficiency of a SFE process. The following section discusses the solubility behaviour of bitumen and bitumen cuts in SC-CO₂.

2.3.4.1 Initial Solubility of Bitumen in SC-CO₂

Past experimental work from literature has predominantly been conducted to measure the solubility of CO₂ in bitumen, while the solubility of bitumen in CO₂ has been largely deemed negligible, partly due to its difficulty to be accurately measured (Han et al. 1998; Eastick et al. 1992; Yu et al. 1989). However, Huang and Radosz (1990) and Yu et al. (1989) measured the solubilities of a Cold Lake bitumen sample and three of its bitumen cuts in SC-CO₂ at a pressure of 16 MPa and a temperature of 323 and 373 K. As shown in Table 4, Cuts 1, 2, and 3 had molecular weights of 201, 304, and 572 g/mol (determined based on boiling point), respectively, while the Cold Lake bitumen sample had a molecular weight of 568 g/mol. The resulting solubilities of the bitumen/bitumen cuts in CO₂ are detailed in Table 4. From their study, Huang and Radosz (1990) and Yu et al. (1989) determined that as the molecular weights of the bitumen samples increased, their resulting solubilities in CO₂ decreased.

Table 4. Solubilities (weight fraction) of three Cold Lake bitumen cuts and bitumen with SC-CO₂ at 16 MPa and temperatures of 323 and 373 K (Huang and Radosz 1990; Yu et al. 1989).

Bitumen Samples	Molecular Weight (g/mol)		Temperature (K)	
			323	373
Cut 1	201	Bitumen in CO ₂ (Weight Fraction)	0.123	0.0205
Cut 2	304		0.021	0.0032
Cut 3	572		0.001	0.0002
Cold Lake Bitumen (Whole)	568		0.019	0.0044

Hwang and Ortiz (1998) measured the hydrocarbon solubility in CO₂ during a pilot flooding project where SC-CO₂ was injected at conditions of 31°C and 7.14 MPa into a crude oil reservoir at the McElroy Field area in Texas. Based on their measurements, Hwang and Ortiz (1998) determined that the solubility in the CO₂-rich phase decreased as the carbon number of the analyzed oil sample increased, indicating that heavier hydrocarbons (i.e. > C₂₅) were less soluble in CO₂ when compared to lighter hydrocarbons (i.e. < C₂₅). This further correlates to the findings of Huang and Radosz (1990) and Yu et al. (1989) examined earlier.

Based on these studies performed by Huang and Radosz (1990), Yu et al. (1989), and Hwang and Ortiz (1998), the solubility of hydrocarbons in SC-CO₂ are lower with hydrocarbons

that are more complex and molecularly heavier. This observation can be attributed to the non-polar nature of SC-CO₂ as mentioned in the earlier sections of this chapter. Although the addition of modifiers has been demonstrated to largely increase the solubility of a solute in a SCF, limited research has been performed to determine if this effect can be similarly replicated for enhancing the solubility of hydrocarbons in SC-CO₂ (Cansell et al. 1998).

2.3.4.2 Effects of Pressure, Temperature, and Density on Initial Solubilities of Bitumen in SC-CO₂

By increasing the overall pressure of the SC-CO₂ while maintaining its temperature constant, the density of the SC-CO₂ increases, hence enhancing its ability to solubilize compounds, including hydrocarbons found in bitumen (Geranmayeh et al. 2012; Al-Marzouqi et al. 2009; Rose et al. 2000; Guiliano et al. 2000; Cansell and Rey 1998; Phelps et al. 1996; Deo et al. 1992). Resultingly, a higher solubilization strength typically translates into a higher extraction efficiency (Guiliano et al. 2000). Aside from the higher solubilization that typically occurs at higher densities, research has shown that the solubilization of heavier and more complex hydrocarbons can also be achieved using SC-CO₂ at higher densities (Al-Marzouqi et al. 2009; Guiliano et al. 2000; Rose et al. 2000).

Temperature can also affect the solubility of hydrocarbons (bitumen) in SCFs. At a consistently maintained pressure, increases to temperature will result in a decrease in the SCF's density (Rose et al. 2000; Deo et al. 1992) and a reduced density typically results in a lower solvating power and lower solubilities and correspondingly, a lower extraction efficiency (Al-Marzouqi et al. 2009; Rose et al. 2000; Hwang and Ortiz 2000). However, if both the pressure and temperature are increased, the elevated vapour pressure and volatility of the target compound(s) may counteract the lower solvent power of the SC-CO₂ at the increased temperature (La and Guigard 2015; Geranmayeh et al. 2012; Low and Duffy 1995). Al-Marzouqi et al. (2007) further investigated the correlating effects between temperature and pressure by observing the changes to a SCF's extraction yield when oil was extracted from an oil-saturated soil sample using SC-CO₂. At 10 MPa and 40°C (SC-CO₂ density of 0.629 g/mL), a 46.5 wt% extraction yield of hydrocarbons from the sample was achieved. As the pressure and temperature increased to 30 MPa and 100°C, respectively (SC-CO₂ density of 0.662 g/mL), an increased extraction yield of 72.4 wt% was achieved.

Deo et al. (1992) observed that as temperatures were increased to levels that closely approached a SCF's critical temperature, extraction efficiencies of hydrocarbons were increased. At the highest temperature and pressure conditions examined for SC-CO₂ at 60°C and 24 MPa, La and Guigard (2015) observed high extraction efficiencies for bitumen from an oil sands sample. Based on the experimental results observed, La and Guigard (2015) believed that the higher temperature conditions allowed for an increase in the hydrocarbons' vapour pressure, resulting in an increase extraction by SC-CO₂. Studies of hydrocarbon extraction from shale samples performed at high temperatures by Allawzi et al. (2011) suggested that an increase in temperature also increases the volatility of the hydrocarbons and this ultimately enhances the diffusional rate of the targeted hydrocarbons while diminishing the intermolecular forces of the interacted components. These observations suggest that the density of the SCF is not the only parameter that can affect the ability of a SCF to extract a target compound but that temperature also plays an important role.

Furthermore, pressure and temperature parameters can also be adjusted to influence the hydrocarbons that can be effectively extracted from a mixture of hydrocarbons (such as bitumen) by a SCF. Al-Marzouqi et al. (2007) investigated the extraction of an oil-saturated soil sample in SC-CO₂ and found that higher molecular weight (heavier) hydrocarbons were extracted when pressure was increased. When the temperature and pressure was maintained at 120°C and 20 MPa, hydrocarbon chains of up to C₂₅ were extracted by SC-CO₂. However, when the pressure was increased to 30 MPa while the temperature was still maintained at 120°C, hydrocarbons of up to C₃₁ were extracted (Al-Marzouqi et al. 2007). Similarly, work done by Rose et al. (2000) also observed that when pressure of the SCF was increased, the resulting extracts collected were moderately heavier in molecular weight.

2.3.4.3 Modifier Addition

Modifiers can be added to SCFs to improve the solubility of the targeted compounds in the SCF, especially during the extraction of highly polar compounds using non-polar SCFs such as SC-CO₂ (Płotka-Wasyłka et al. 2017; La and Guigard 2015; Stubbs and Siepmann 2004; Phelps et al. 1996). Consideration of the type of compounds to be extracted and the affinity of the compound to the modifier are factors that are considered when selecting an appropriate modifier to be utilized (Płotka-Wasyłka et al. 2017). Selections of methanol, ethanol, and more

commonly, toluene have been widely used as modifiers for extracting hydrocarbons with SCFs (Płotka-Wasyłka et al. 2017; Rudyk et al. 2017; La and Guigard 2015; Rudyk et al. 2014).

Table 5 summarizes some studies that have investigated the SFE of hydrocarbons from various crude oil and oil sand feedstocks using modified SC-CO₂. As shown, the addition of modifiers can effectively increase the extraction efficiency compared to extractions with SC-CO₂ where no modifier is used (Rudyk et al. 2014; Al-Marzouqi et al. 2009; La and Guigard 2015). Furthermore, the use of toluene as a modifier in the studies by Guiliano et al. (2000) and Al-Marzouqi et al. (2009) appears to result in the highest extraction efficiencies compared to the other modifiers utilized in these studies. However, results from the study by Magomedov et al. (2017) exhibited a lower extraction efficiency for toluene when compared to o-xylene. The use of toluene has been widely demonstrated as an effective modifier for the extraction of asphaltenes and heteroatoms using SC-CO₂ (Hwang and Ortiz 2000).

Determination of the amount and concentration of modifier added and its corresponding effect to the extraction of hydrocarbons was examined by Magomedov et al. (2017). In the study performed, toluene was added at three various concentrations of 15, 20, and 30 wt% to the SC-CO₂ for the extraction of hydrocarbons from a vacuum residue feedstock. The resulting extraction efficiencies of 9.9, 24.3, and 52.4 wt% were respectively achieved. Evidently, an increase of 15 to 30 wt% toluene concentration led to a 42.5 wt% increase of extraction efficiency with the vacuum residue, demonstrating that as concentrations of an added modifier increased, the extraction of hydrocarbons was also enhanced. Al-Sabawi et al. (2011) further examined the use of modifiers such as acetone, ethyl acetate, methanol, and toluene added to supercritical n-pentane at 5 to 20 mol% concentrations for the extraction of a bitumen sample. It was determined that as the concentration of the acetone, ethyl acetate, and toluene modifiers increased in the SCF, a larger mass of hydrocarbons was extracted from the bitumen sample. However, the combination of supercritical n-pentane with methanol yielded the lowest hydrocarbon extraction despite increasing the methanol concentration that was added.

Table 5. Extraction efficiencies of various feed streams for SC-CO₂ when applied with different concentrations of modifiers.

Feed Stream	SCF	Modifier Type	Modifier Concentration	Extraction Efficiency (wt%)	Reference
BAL 150 Crude Oil Asphaltenes	CO ₂	Dichloromethane	8.6 wt%	11.1	Guiliano et al. 2000
		Toluene	10.7 wt%	11.5	
Crude Oil	CO ₂	-	-	53	Rudyk et al. 2014
		Acetone	5 g	62	
		Propanol	5 g	64	
		Methanol	5 g	66	
		Ethanol	5 g	71	
Soil-Containing Crude Oil	CO ₂	-	-	4.20	Al-Marzouqi et al. 2009
		Heptane	5 v/v%	49.85	
		Toluene	5 v/v%	91.52	
Athabasca Oil Sands Slurry	CO ₂	-	-	27.9	La and Guigard 2015
		Toluene	9.1 wt%	33.7	
Vacuum Residue	CO ₂	Methanol	20 wt%	6.3	Magomedov et al. 2017
		Ethanol	20 wt%	7.9	
		Acetone	20 wt%	12.0	
		n-heptane	20 wt%	21.9	
		o-xylene	20 wt%	34.9	
		Toluene	15 wt%	9.9	
			20 wt%	24.3	
30 wt%	52.4				

Furthermore, Al-Sabawi et al. (2011) examined the quality of extracts produced when extractions were performed with different modifiers added to supercritical n-pentane. Although the highest extraction efficiency was obtained with the addition of toluene as a modifier, the extraction also generated the heaviest extract quality compared to the other modifiers used. Overall, the addition of ethyl acetate, toluene, and methanol to supercritical n-pentane resulted in more metal and heteroatomic impurities (i.e. nickel, vanadium, sulfur, and nitrogen) in the collected extracts; the addition of toluene yielded the highest concentration of these compounds. This result was largely expected since asphaltene found in bitumen are highly soluble in toluene.

The effects of modifiers in SC-CO₂ were further examined by Hwang and Ortiz (2000) for extractions from dolomite rock spiked with crude oil. Like other similar studies performed, Hwang and Ortiz (2000) found that as modifiers were added to the SC-CO₂, the density and polarity of the SCF was increased and allowed for improved extraction efficiencies. Additionally, the chemically modified SC-CO₂ also increased the solvation of intermediate to heavy hydrocarbon ranges in SC-CO₂ compared to when only SC-CO₂ was used. When only SC-CO₂ was used at conditions of 31°C and 80 atm, hydrocarbons of up to C₁₂ were readily extracted, while little to no hydrocarbons that were heavier than C₂₂ were extracted at all. However, when 10% methanol was added to the SC-CO₂, hydrocarbons of up to C₃₀ were extracted.

From the results of the studies discussed above, it is evident that an appropriate addition of a chemical modifier can significantly enhance the solubility of hydrocarbons in a SCF, while also affecting the quality of hydrocarbons that can be extracted as a result.

2.4 Summary

A majority of Alberta's crude oil production comes from unconventional sources like oil sands bitumen. Producing bitumen in Alberta can be performed by one of two methods: in-situ or ex-situ recovery. For bitumen deposits that are deeply situated, in-situ recovery techniques are applied. For oil sands formations located at shallower depths, ex-situ methods of surface mining and hot water extraction recovery are utilized instead. Despite the advantages for recovering bitumen using the ex-situ approach, this method also utilizes substantial volumes of water during its operation that resultantly produces large quantities of process waste streams contained with substantial amounts of water, sand, clay, silty-solids, bitumen residues, and other detrimental chemicals. With no current effective ways to recover these process waste streams, large man-made tailings ponds have been created to temporarily store these large volumes of waste streams. However, the containment safety, environmental risks, and long-term sustainability of utilizing tailings ponds are some of the major concerns faced by the oil sands industry.

SFE using CO₂ is commonly described as an environmentally sustainable process and is utilized in many extractive applications due to CO₂'s advantages of being non-toxic, chemically-inert, non-flammable, recoverable, and recyclable. Furthermore, CO₂'s modest critical point and inexpensiveness to acquire have effectively allowed it to become a preferential choice as a SCF

to be largely utilized. In addition to its more widely known utilizations and developments in food and pharmaceutical processing, SFE has also been widely researched over the years for its application to extract bitumen from oil sands, soils, and process waste streams. If successfully developed on a much larger scale, SFE can ultimately replace the need for the current ex-situ recovery practices used by the oil sands industry and resolving many of its current issues relating to extensive water use, process waste stream production, and tailings ponds.

To further research and develop the SFE of bitumen with SC-CO₂, a more extensive understanding to the solubility of bitumen in SC-CO₂ is fundamental. Because bitumen has such a complex composition that is made up of various sizes and molecular weights of hydrocarbons and heteroatoms, understanding the corresponding relationships between how pressure and temperature variations can influence the densities of SC-CO₂, and ultimately affecting the solubilities of hydrocarbons in SC-CO₂ is crucial. In the literature examined, a higher solubility and extraction efficiency can be consistently achieved when the pressure of the SFE process was increased to provide a higher density to the SCF. Temperature modifications saw a more complexed effect. When temperatures were increased with pressure, increases to the rate of mass transfer, volatility, and diffusion between the SCF and solute interaction enhanced the solubility of the hydrocarbon in the SCF. However, when temperatures were increased and pressures were maintained at a constant level, decreases to the SCF's density and solubility was resulted. By adding a modifier to the SC-CO₂, like toluene, a significantly larger quantity of hydrocarbons was extracted compared to when no toluene was added to the SC-CO₂. Moreover, the added modifier also allowed for the extraction of a broader hydrocarbon range that included larger concentrations of intermediate to heavier hydrocarbons and heteroatoms.

CHAPTER 3: MATERIALS AND METHODS

This chapter provides a description of the materials (including the whole bitumen, bitumen cuts, and chemicals) used for the initial solubility measurements and a list of the main components of the SFE system utilized for the initial solubility experiments. Furthermore, the procedures used for both the initial solubility experiments and the HTSD analysis are detailed.

3.1 Summary of Experiments

Table 6 provides a summary of the experimental conditions examined in this thesis. Three main objectives were established for this research study. The first objective was to measure the initial solubilities for whole bitumen and the bitumen cuts of LGO, HGO, and resid in SC-CO₂ only, at a pressure and temperature of 24 MPa and 333 K, respectively (SC-CO₂ density of 0.78 g/mL) (NIST 2018). The second objective was to measure initial solubilities for whole bitumen and the bitumen cuts in SC-CO₂ with 5 and 15 mol% toluene addition when pressures and temperatures were maintained at 24 MPa and 333 K (SC-CO₂ density of 0.78 g/mL) (NIST 2018). Table 6 provides a summary of the experimental conditions examined in this thesis.

Table 6. Summary of the experiments conducted at 24 MPa and 333 K using SC-CO₂.

Sample	SCF	Toluene Concentration (mol%)
Whole Bitumen	SC-CO ₂ only	0
	SC-CO ₂ with toluene	5
		15
LGO	SC-CO ₂ only	0
	SC-CO ₂ with toluene	5
HGO	SC-CO ₂ only	0
	SC-CO ₂ with toluene	5
		15
Resid	SC-CO ₂ only	0
	SC-CO ₂ with toluene	5
		15

3.2 Materials

In this section, details of the whole bitumen and bitumen cut samples, chemicals, and equipment used in this thesis are listed and examined.

3.2.1 Samples

Three bitumen cuts of LGO, HGO, and resid were used in this thesis. These samples are described in the following sections.

3.2.1.1 Whole Bitumen

The whole bitumen sample was provided by Syncrude Canada Limited (hereafter referred to as Syncrude). By using the Dean & Stark extraction method, the bitumen naturally entrapped in the oil sands were recovered and collected by Syncrude and was then subsampled into 1 L glass jars and sent to the University of Alberta on January 7, 2015. The delivered bitumen samples were stored in the refrigerator at approximately 4°C in the Supercritical Fluid Extraction Lab, located at the Natural Resources Engineering Facility (NREF) at the University of Alberta. Naturally, the whole bitumen sample was dark brown to black in colour and has a relatively viscous consistency at room temperature. Appendix A further details the properties and characteristics of the whole bitumen material that is used.

3.2.1.2 Light Gas Oil, Heavy Gas Oil, and Vacuum Residue

The LGO, HGO, and vacuum residue (herein referred to as resid) samples were produced from a series of atmospheric and vacuum distillation columns installed at Syncrude's facility. The atmospheric distillation column is mounted with multiple levels of parallel trays used for disintegrating the bitumen feedstock at elevated temperatures (Oil Sands Magazine 2020). By doing so, this allows the lighter and heavier hydrocarbon components from the bitumen feed to be isolated based on the boiling points achieved in the column (USEIA 2012a). As the lighter hydrocarbon components (e.g. diluent naphtha and front-end cuts of the LGO) were effectively distilled and collected on the upper tray levels in the distillation tank, the remaining heavier hydrocarbon ends were resultantly settled to the lower and bottom levels of the column (Oil Sands Magazine 2020; USEIA 2012a). To further maximize its usability and optimize yield, the

produced heavier hydrocarbon components were directed to the vacuum distillation column to be further distilled and refined (USEIA 2012a). During vacuum distillation, the heavier hydrocarbon feed was processed at lowered pressures to allow any residual lighter hydrocarbon components to be vaporized away to produce the back-end cuts of the LGO, HGO, and resid (USEIA 2012b).

The front-end and back-end cuts of LGO were collected from Syncrude's atmospheric and vacuum distillation columns on an unknown date and were combined into a single LGO sample, while the HGO sample was similarly collected on an unknown date from the vacuum distillation unit. The resid material was sampled on January 2006 from Syncrude's vacuum distillation unit. All three samples of LGO, HGO, and resid were then delivered in barrels to the Syncrude Research Centre, subsampled into smaller jars, and delivered to the NREF building at the University of Alberta on October 2, 2017. Upon arrival, the delivered samples were stored in the refrigerator at approximately 4°C in the Supercritical Fluid Extraction Lab. At ambient conditions, the combined LGO sample is a translucent yellow liquid, and is slightly viscous (similar to cooking oil) in its consistency; the HGO sample is dark brown to black in colour and semi-viscous (similar to honey) in its general consistency; and the resid sample is black in colour and maintained in an extremely brittle, glass-like, and solid state at ambient conditions. However, when the resid sample is heated to approximately 120°C, the consistency of the material becomes soft and malleable.

3.2.2 Chemicals

Table 7 outlines a list of chemicals that were used during the initial solubility measurements.

Table 7. Summary of the chemicals used in experiments.

Chemicals	Usage	Supplying Company
Carbon Dioxide (liquid, grade 3 bone dry)	Supercritical solvent	Praxair (Edmonton, AB)
Toluene (ACS grade)	Modifier and cleaning solvent	Fisher Scientific (Fair Lawn, NJ)
Acetone (ACS/HPLC grade)	Acetone/dry ice bath	Fisher Scientific (Fair Lawn, NJ)

3.3 Supercritical Carbon Dioxide Extraction Apparatus

Initial solubility experiments were conducted on the laboratory-scale batch SFE apparatus as shown by the schematic diagram in Figure 5. A photograph of the SFE system used is displayed in Figure 10. The suppliers and technical specifications of the system's major components are listed in Table 8.

As shown in Figure 5, the liquid CO₂ used in the initial solubility experiments was supplied from the CO₂ cylinder (1). Sourced from the cylinder, the CO₂ passes through a filter (2) to remove any unwanted particulate material before entering the two ISCO syringe pumps (3). The pair of ISCO syringe pumps are managed by a pump controller (5) and operated in tandem to supply a continuous flow of pressurized CO₂ to the SFE apparatus. The primary Pump A is the first to pressurize the inflowing CO₂. As the supply of pressurized CO₂ is depleted from Pump A and the pump requires refilling, the secondary Pump B is used. To ensure that the supplied CO₂ remains in a liquid state, the ISCO syringe pumps are cooled to 2°C by a mixture of anti-freeze and water that is circulated through the syringe pump jackets. From the ISCO syringe pumps, the pressurized CO₂ passes through a two-way inlet ball valve (6) and a check valve (7) to prevent any backflow from the extraction vessel back to the ISCO syringe pumps. From the check valve, the pressurized CO₂ flows through a preheating coil (8) that is submerged within a circulating hot water bath (28) set to the experimental temperature. Following the

preheating coil, a pressure relief valve (9) set to a releasing pressure of 27.6 MPa is installed on the inflowing CO₂ delivery line to prevent the over-pressurization of the SFE system. A safety head contained with a rupture disc (13) is installed onto the vessel lid as a secondary pressure protection/relief system for the vessel. The pressurized CO₂ is then directed into the stainless-steel extraction vessel (14) that is surrounded by a hot water heating jacket. Hot water from the circulating hot water bath (shown by the blue lines in Figure 5) is used to maintain the vessel's temperature at the desired experimental conditions. A MagneDrive® motor (11) that is attached to a helical impeller is used for mixing within the extraction vessel.

The pressure and temperature readings of the SFE system are measured by a pressure transducer (10) attached to the CO₂ inlet line preceding to the extraction vessel, and a thermistor probe (12) in the stainless-steel lid of the vessel. Along with the pressure and temperature data, data regarding to the pressures of the ISCO syringe pumps and the CO₂ flow rate from the pumps are also relayed to the data acquisition system (24) and recorded to the LabVIEW™ software.

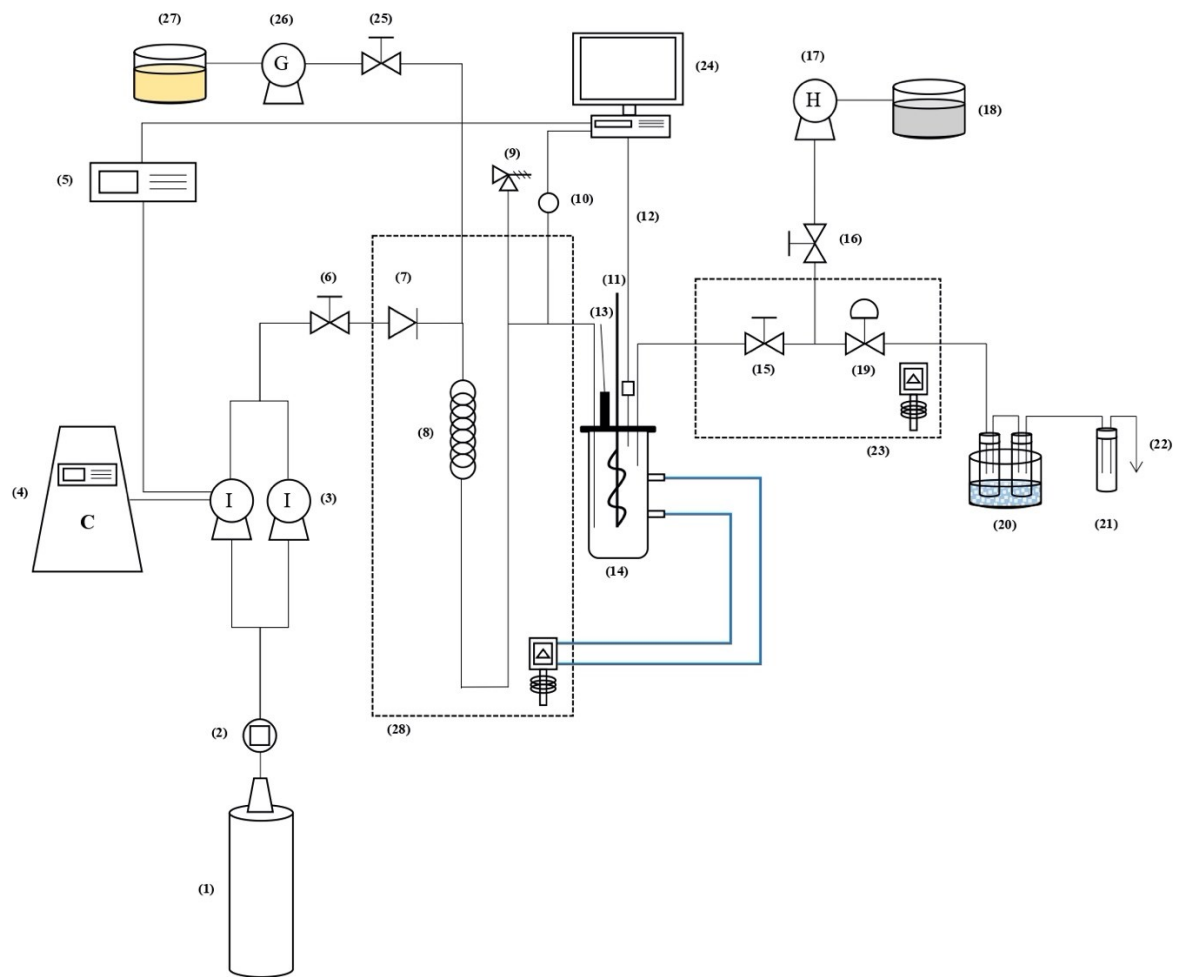
The SC-CO₂ containing dissolved hydrocarbons exits the extraction vessel and passes through a two-way outlet ball valve (15) and a metering valve (19). For initial solubility measurements, the metering valve is throttled so that a CO₂ flowrate of approximately 4 mL min⁻¹ is maintained at the ISCO pumps. The outlet ball valve and the metering valve are both submerged within a hot water bath (23) that is pre-set to 60°C. From the heated metering valve, rapid depressurization and cooling causes the CO₂ to be quickly vaporized, resulting in the collected hydrocarbons to be deposited within a series of three collection vials and are placed in an acetone/dry ice bath to reduce the volatilization of the contents. The first two vials (20) are the primary collection vials, while the third vial (21) is utilized for the carry-over collection of material within the released CO₂ that was not collected in the primary vials. After passing through the collection vials, the CO₂ is vented into the fume-hood (22).

Toluene is used to clean out system lines where hydrocarbons may have deposited onto during the dynamic collection process. The toluene used for cleaning is fed from a 1 L bottle (18) that is dispensed by a Hamilton® syringe pump (17) through a cleaning line installed between the outlet and metering valves. The cleaning line bypasses the system's extraction vessel to rinse the outlet line of any remaining hydrocarbons after each collection process. The outflowing toluene is regulated by a two-way ball valve (16) before being released into the outlet collection lines.

For experiments using toluene as a modifier, a Gilson pump (26) is utilized to deliver the chemical (27) into the pressurized CO₂ before it enters into the preheating coil. In other instances where toluene is not required, a two-way ball valve (25) is used to isolate the modifier line from the rest of the SFE system.

Stainless steel tubing from Swagelok[®] with outer diameter (OD) sizes of 1/16" and 1/8" are employed throughout the experimental system.

Additional details on the specific components used for the SFE system can be found in Table 8.



- | | | | |
|--|----------------------------------|--|---|
| 1. CO ₂ Cylinder | 8. Preheating Coiled Tubing | 15. Two-Way (Outlet) Ball Valve | 22. CO ₂ Release to Fumehood |
| 2. Filter | 9. Pressure Relief Valve | 16. Two-Way (Cleaning) Ball Valve | 23. Circulating Hot Water Bath |
| 3. ISCO Syringe Pumps | 10. Pressure Transducer | 17. Hamilton® Syringe Pump | 24. Data Acquisition System |
| 4. Refrigerated Cooling Circulating Bath | 11. MagneDrive® Mixer | 18. Toluene Reservoir | 25. Two-Way (Co-solvent) Ball Valve |
| 5. ISCO Pump Controller | 12. Thermistor Probe | 19. Metering Valve | 26. Gilson Pump |
| 6. Two-Way (Inlet) Ball Valve | 13. Safety Head and Rupture Disc | 20. Primary Collection Vials in Acetone/Dry Ice Bath | 27. Co-solvent Reservoir |
| 7. Check Valve | 14. Extraction Vessel | 21. Carry-Over (c/o) vial in Ambient Conditions | 28. Circulating Hot Water Bath |

Figure 5. Schematic of laboratory-scale SFE system used for initial solubility measurements.

Table 8. List of components, their suppliers, and pressure ratings (if applicable) used for the SFE system.

System Components	Manufacturers/Suppliers	Pressure Rating (MPa)
CO ₂ Cylinder	Praxair (Edmonton, AB)	-
Filter	Swagelok (Edmonton, AB)	-
ISCO Syringe Pumps with Controller Module (Model 500D)	Teledyne ISCO (Lincoln, NE)	25.9
Isotemp 3013 Refrigerated Cooling Circulating Bath	Fisher Scientific (Fair Lawn, NJ)	-
Isotemp 2100 Immersion Circulator (Circulating Hot Water Bath)	Fisher Scientific (Fair Lawn, NJ)	-
Isotemp Hot Water Bath	Fisher Scientific (Fair Lawn, NJ)	-
Stainless Steel Tubing 1/16" OD and 0.020" Wall Thickness (SS-T1-S-020-20)	Swagelok (Edmonton, AB)	82.7
Stainless Steel tubing 1/8" OD and 0.028" Wall Thickness (SS-T2-S-028-20)	Swagelok (Edmonton, AB)	58.6
Two-Way Ball Valve (SS-4SKPS4)	Swagelok (Edmonton, AB)	41.4
Check Valve (SS-CHS2-1/3)	Swagelok (Edmonton, AB)	41.4
305 Gilson Pump (25-SC Pump-head)	Mandel Scientific (Guelph, ON)	28
Stainless Steel High Pressure Proportional Relief Valve with R3A-F Spring (SS-4R3A)	Swagelok (Edmonton, AB)	41.4 (Relief Valve) 27.6 (Spring)
Pressure Transducer (MMG5.0KV1P4C0T3A6)	OMEGA Engineering (Stamford, CT)	34.5
Stainless Steel Extraction Pressure Vessel, 300 mL	Autoclave Engineers (Erie, PA)	37.9
MagneDrive® Mixer Assembly (II, Series 0.75)	Autoclave Engineers (Erie, PA)	37.9
Helical Impeller	Custom-made	-
Thermistor Probe (YSI 406)	Labcor Technical Sales Inc. (Anjou, QC)	-
Stainless Steel Medium Flow High Pressure Metering Valve (SS-31RS4)	Swagelok (Edmonton, AB)	34.5
Hamilton Microlab® Syringe Pump (500 Series)	Hamilton (Reno, NV)	-

3.3.1 Extraction Vessel, MagneDrive® Mixer, and Helical Impeller

The extraction vessel used for the initial solubility measurements is constructed from 316 stainless-steel and has an empty bed volume of 300 mL. Figure 6 depicts a cross-sectional view of the pressure vessel with its respective dimensions. Not shown in Figure 6 is the aforementioned hot water heating jacket that is weld-fitted onto the vessel body. Figure 7 provides an overhead schematic of the extraction vessel lid that is connected to the MagneDrive assembly. A stainless-steel sleeve (see Figure 8) is inserted into the extraction vessel to secure the CO₂ inlet delivery line from interfering with the rotating helical impeller (see Figure 9). The sleeve and impeller reduce the volume of the vessel to 205 mL.

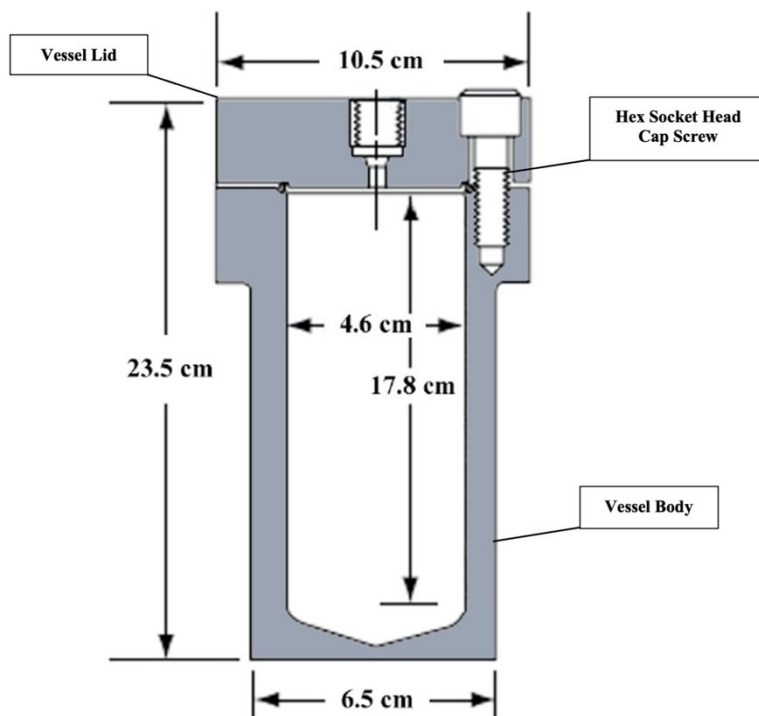


Figure 6. Cross-sectional display of the 300 mL extraction vessel (modified from Autoclave Engineers 2002).

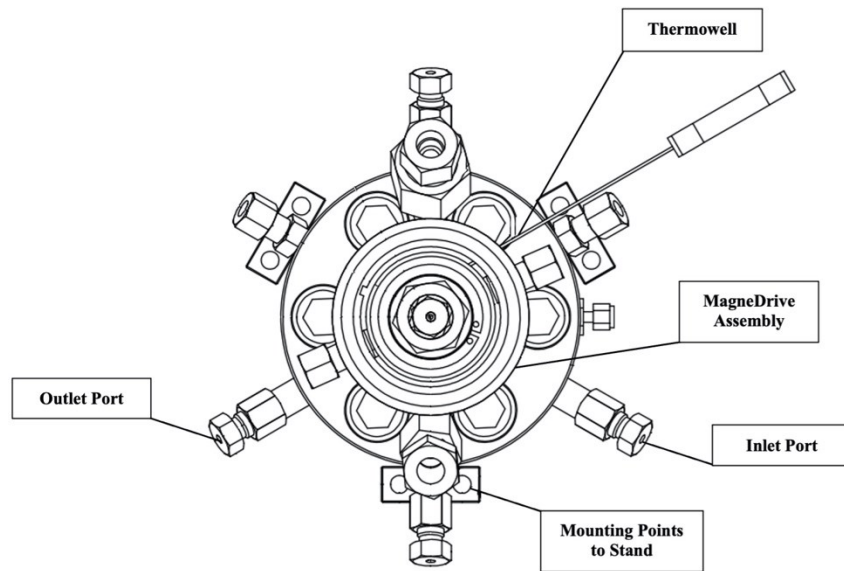


Figure 7. Overhead view of the stainless-steel vessel and a part of the MagneDrive assembly (modified from Autoclave Engineers 2002).



Figure 8. The stainless-steel extraction vessel sleeve (left) and the detached stainless-steel helical impeller (right).

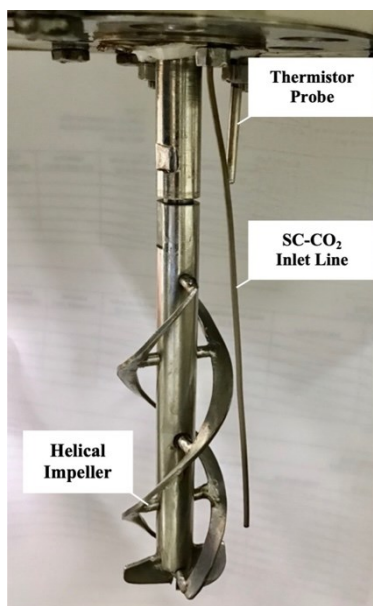


Figure 9. Stainless steel helical impeller attached to the driveshaft of the MagneDrive®, SC-CO₂ inlet tubing, and thermistor temperature probe.

As shown in Figure 7, the body of the vessel and the vessel lid are joined together by six hexagonally aligned bolts that are tightened to a maximum torquing force of 50 ft-lb. To further ensure a pressure seal is maintained between the lid and the vessel body, a Teflon o-ring is inserted onto the lip of the vessel opening. The vessel lid includes multiple opening ports used for the placement and insertion of the thermistor probe, the CO₂ inlet and outlet lines, and a rupture disc (see Figure 7). Other ports that are not required are sealed.

The helical impeller is attached to a driveshaft that protrudes out beneath the extraction vessel lid. An external rotating magnet is then connected to the driveshaft above the extraction vessel lid and is driven by a rubber belt that is linked to the MagneDrive® motor. A digital controller regulates the rotations per minute (RPM) of the motor. As the motor rotates at the designated speed, it mechanically drives the rubber belt and the connected driveshaft, causing the attached helical impeller to revolve. A photograph of the SFE system is shown in Figure 10.

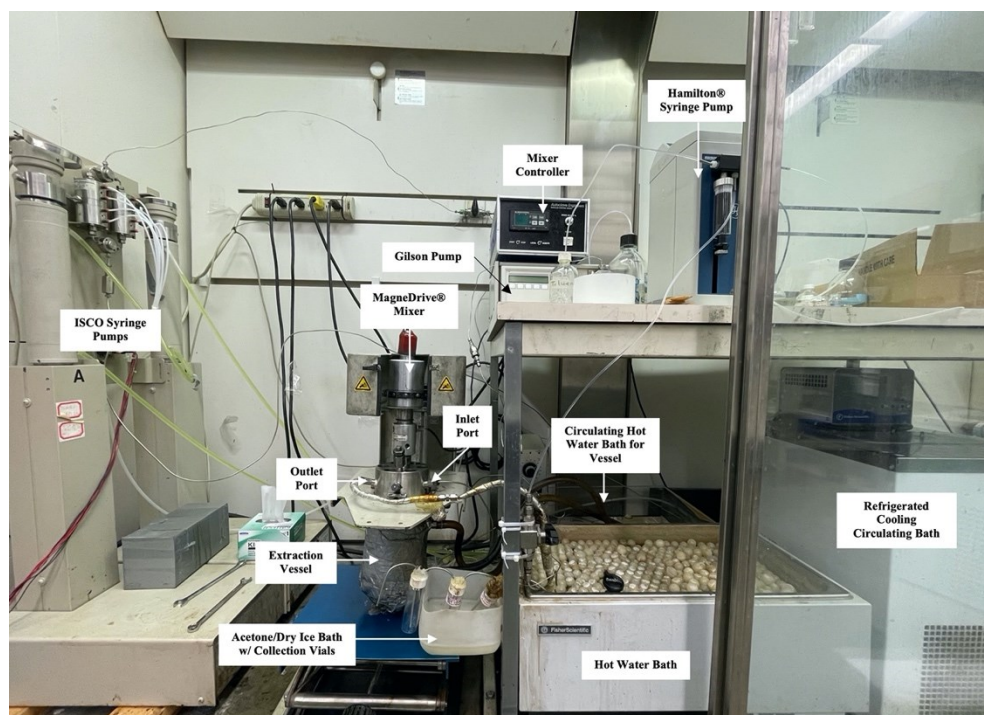


Figure 10. The SFE system.

3.3.2 Toluene (Modifier) Addition

For experiments involving toluene addition as a modifier, toluene is added to the SFE system using a Gilson 305 piston pump equipped with a 25-SC pump head that is connected to a 1 L jar. Toluene withdrawn from the jar passes through a filter, into the Teflon tubing, and into the pump head inlet unit. The outflowing toluene is then dispensed from the pump head, past a section of a 1/16 in. stainless steel tubing, and into the SFE system through a tee connection placed upstream of the extraction vessel. A series of inlet and outlet check valves rated to a pressure of up to 28 MPa, are utilized by the 25-SC pump head unit to prevent the backflowing of pressurized CO₂ from the SFE system.

Figure 11 below shows the 1 L reservoir bottle that is connected by a section of Teflon tubing (with a filter submerged into the reservoir) to the 25-SC pump head unit affixed to the 305 Gilson piston pump. The outflowing modifier chemical is then fed by a 1/16 in. stainless steel tubing from the pump head outlet and into the SFE system.

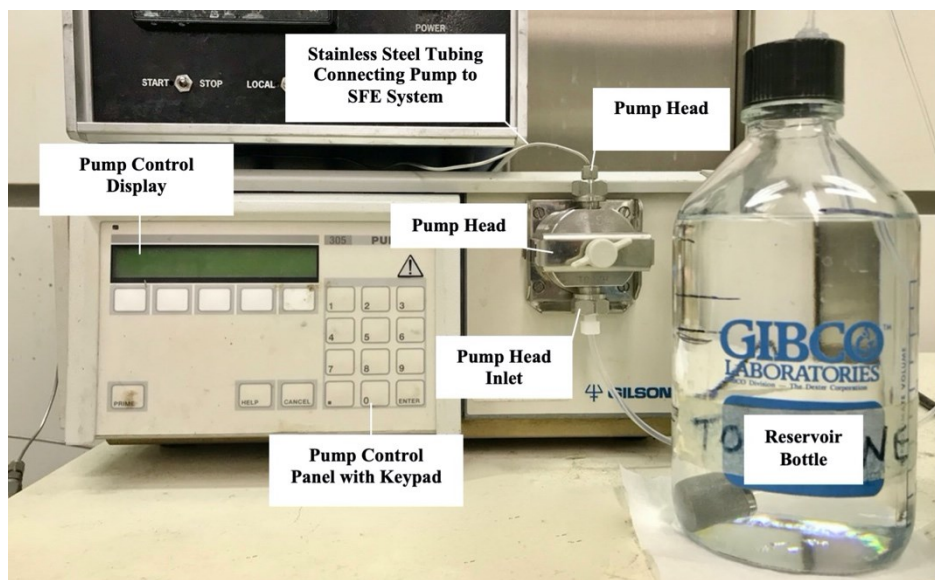


Figure 11. Front view of the chemical modifier setup for the SFE system.

3.3.3 LabVIEW™ Data Collection

The LabVIEW™ software is installed onto the data acquisition system to record the experimental temperatures and pressures measured by the thermistor probe and pressure transducer, respectively. The ISCO syringe pumps' pressures and flowrates are measured by the pump controller and recorded by LabVIEW™. Figure 12 shows a screenshot of the LabVIEW™ display.

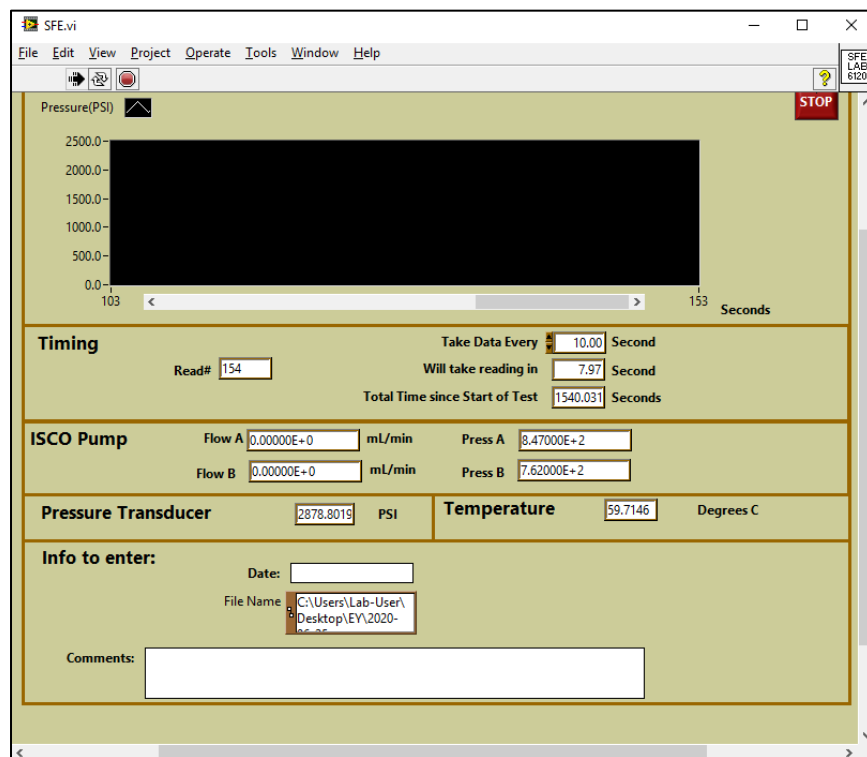


Figure 12. A screenshot of the LabVIEW™ software, displaying pressure, temperature, and flow rates during an experiment.

3.4 Procedure for Initial Solubility Measurement Experiments

All initial solubility experiments were conducted at a pressure of 24 MPa and a temperature of 333 K. The experimental pressure and temperature were selected based on the previous work conducted by Fang (2010), La (2011), Cossey (2018), and other unpublished experimental data collected by the SFE research group. At these conditions of pressure and temperature, SC-CO₂ has a density of 0.78 g/mL (NIST 2018).

Initial solubility experiments were conducted for whole bitumen, LGO, HGO, and resid, with SC-CO₂ and SC-CO₂ with toluene as a modifier (see Table 6). The following sections provide a brief description of the procedures used for the experiments. More detailed procedures can be found in Appendix C. An example of the spreadsheet used for documenting the results of the initial solubility experiments is provided in Appendix D.

3.4.1 Procedures for Initial Solubility Experiments with SC-CO₂ Only

The following summarizes the procedure used when conducting initial solubility experiments with SC-CO₂ only, which includes three distinct periods:

- i. Pressurization and static periods;
- ii. Dynamic period; and
- iii. Depressurization

Pressurization and Static Period

- Turn on the refrigerated circulating bath and set to 2°C to cool the ISCO syringe pumps.
- Turn on the water bath for circulating hot water to the vessel heating jacket and set to 65°C (because of heat losses in the system, a temperature of 65°C is needed in the water bath to achieve an extraction vessel temperature of 60°C).
- Turn on the water bath for heating the metering and outlet valves and set to 60°C.
- Weigh a known mass of sample (whole bitumen, LGO, HGO, or resid) using an analytical balance scale (Mettler Toledo AX205 DeltaRange®) into a 500 mL jar. Sample sizes of 50 g are used for most experiments. In some cases, smaller sample (either 10 or 25 g) were used. For example, experiments with resid had sample sizes of 10 and 25 g.
- Transfer the weighed sample from the 500 mL jar to the extraction vessel. Transfer a small amount of sample into a *time zero* vial.
- Place the Teflon o-ring onto the extraction vessel and connect the vessel to the vessel lid using the bolts and by tightening the bolts according to the specifications suggested by Autoclave.
- Ensure the inlet, metering, outlet, modifier addition, and cleaning valves are all closed.
- Connect the circulating water bath to the vessel and heat the vessel to approximately 55°C.
- Turn on the ISCO syringe pumps and set to “Constant Pressure” mode at 24 MPa.
- Open the inlet valve to the extraction vessel and allow CO₂ from the ISCO pumps to pressurize the extraction vessel.

- Turn on the MagneDrive® mixer at 50 RPM and begin the 60-minute static period. For initial solubility measurements with resid, no mixing was performed during the static and dynamic collection periods.
- During the static period, a series of three 40 mL glass vials labelled as *a*, *b*, and *c/o* were fastened to the system's outlet line to collect any hydrocarbons that condense out of the CO₂. Vials labelled as *a*, *b*, and *c/o* were the primary, secondary and carry-over collection vials, respectively. Vials *a* and *b* were placed in an acetone-dry ice bath, while vial *c/o* was maintained at ambient conditions during the dynamic sampling period. Vial *a* was partly filled with glass beads (4 mm diameter) to provide a larger surface area for the collection of the hydrocarbon extracts, while vial *b* contained 20 mL of toluene to capture any remaining hydrocarbons.

Dynamic Collection Period

- Open the extraction vessel's outlet valve and begin the 25-minute dynamic collection period.
- Gradually open the metering valve and adjust to obtain a steady flow of CO₂ ranging between 2 to 4 mL min⁻¹, as indicated on the ISCO pump controller.
- At 5-minute intervals, change the *a* and *b* collection vials (the *c/o* vial is not changed during the dynamic collection period).
- At the end of the 25-minute dynamic collection period, close the metering and outlet valves and remove the *a*, *b*, and *c/o* vials.

Depressurization

- Attach a collection vial (*rinse* vial) in the position of vial *a*.
- With the outlet line depressurized, open the valve to the Hamilton® syringe pump and deliver a pre-determined volume of toluene through the outlet collection line to thoroughly rinse this line and collect the rinsing toluene in the *rinse* vial.
- Close both the valve to the Hamilton® syringe pump and the metering valve.
- Close the inlet valve and both the CO₂ and air cylinders.
- Turn off the ISCO pumps and controller, the MagneDrive® mixer, and all circulating and heating baths.

- Remove the *rinse* vial from the SFE system and attach two depressurization vials labelled *8-dep* and *9-dep* to the position of vials *a* and *b*, respectively. The depressurization vials will collect any residual hydrocarbon contents discharged from the SFE system during the depressurization process.
- Carefully open the outlet and metering valves to gradually depressurize the extraction vessel. Depressurization of the vessel must be conducted slowly to avoid any of the residual sample to be carried over from the extraction vessel to the outlet collection line.
- Once the extraction vessel is fully depressurized, remove the vessel from the vessel lid and collect any residual sample into a 250 mL jar labelled as *vessel residue* (including any toluene used to rinse the vessel).

3.4.2 Procedure for Initial Solubility Experiments with SC-CO₂ and Toluene

The experimental procedure for initial solubility experiments with SC-CO₂ and toluene were conducted in the same manner as outlined in Section 3.4.1, with modifications as follows:

- During pressurization and prior to the beginning of the static period, a pre-determined volume of toluene was added to the SC-CO₂ through a tee connection upstream of the extraction vessel. Once the toluene was added, the MagneDrive® mixer was turned on.
- At the beginning of the dynamic collection period, the valve to the Gilson pump was opened at this time to allow a continuous flow of toluene into the vessel during the collection process.

Depending on the desired toluene concentration levels (5 or 15 mol%), the amount of toluene added during the static period and the flow rate of the toluene during the dynamic collection period is different. Both the volume of toluene added during the static period and the flow rate of toluene during the dynamic collection period for experiments with SC-CO₂ and toluene at 5 and 15 mol% concentration levels are provided in Table 9. Note that any change to the mass of sample added to the extraction vessel (10, 25, or 50 g) will also result in changes to the volume of toluene added during the pressurization period.

Table 9. Volumes and flow rates of toluene added at various concentrations for whole bitumen, light gas oil, heavy gas oil, and resid samples.

Modifier Type	Sample Material	Sample Size (g)	Concentration (mol%)	Modifier Volume Added During Pressurization (mL)	Modifier Flowrate During Extraction (mL min ⁻¹)
Toluene	Whole Bitumen	50	5	15.383	0.5230
			15	38.750	1.7525
	LGO	50	5	15.383	0.5230
		25	5	17.818	0.5230
	HGO	50	5	15.383	0.5230
			15	38.750	1.7525
		25	15	44.876	1.7525
		10	15	48.554	1.7525
	Resid	10	5	28.662	0.5230
			15	72.195	1.7525

3.4.3 Samples

For each experiment, a total of 12 samples (Vials: *1a, 1b; 2a, 2b; 3a, 3b; 4a, 4b; 5a, 5b; c/o; and rinse*) are produced. The collected hydrocarbon extracts in the sample vials were dried for 48 hours through an air-blowing apparatus under the fume-hood to remove any remaining dissolved CO₂ or toluene. The samples were then weighed to determine the amount of hydrocarbons collected in each vial during the dynamic collection process.

3.5 High Temperature Simulated Distillation

Air-dried samples collected in vials *a, b, c/o, time zero, and vessel residue* were delivered to Syncrude's research facility for HTSD analyses to be performed. The HTSD results generated for these samples will provide the mass percentages of the hydrocarbons that distill at a given temperature. This information is used to determine the quality of the hydrocarbons that were dissolved and collected during the initial solubility experiments. In general, hydrocarbons distilled at lower temperatures have lower molecular weights, while hydrocarbons distilled out at higher temperatures have heavier molecular weights. HTSD conducted by Syncrude was performed using an analytical method equivalent to ASTM D7169: "Standard Test Method for

Boiling Point Distribution of Samples with Residues Such as Crude Oils and Atmospheric and Vacuum Residues by High Temperature Gas Chromatography” (ASTM 2011). A summary of the ASTM D7169 process is provided below, while a more comprehensive description of the process can be found in Appendix E.

A gas chromatograph (GC) with a flame ionization detector (FID) was used for HTSD. The MXT-1HT SimDist column manufactured by Restek® was used in the GC. The column had an inner diameter of 0.53 mm and was covered with a 0.10 to 0.20 μm 100% polydimethylsiloxane (PDMS) coating. Helium (with 99.999% purity) was utilized as the carrier gas. The electrical signal from the FID was digitized and collected by the data system consisting of a computer installed with the required data acquisition software. The data system was operated at acquisition rates of 10 Hz, which slices the data into 0.1 s time intervals.

Carbon disulfide (CS_2) applied at +99% purity was utilized as a diluting solvent for the samples and for calibration. Both Polywax (either P655 or P1000) and a variety of paraffins were added to produce a retention time calibration mixture. The produced mixture was then used to generate a retention time – boiling point plot. By having both Polywax and paraffins added to the retention time calibration mixture, the system can be effectively standardized to detect for a carbon range between C_5 to C_{100} and analyze hydrocarbon samples with boiling points of 36.1 to 735°C. To establish the response factor, a completely eluted Reference Oil 5010 is used.

A 2 mL aliquot of each sample mixture was placed in auto sampler vials and were injected into the GC for analysis. By using the response factor, the net area of the sample chromatograph, the mass of the sample, and the mass of the solvent, the recovery percentage of the eluted sample at each time interval was calculated. The retention times required to exactly produce 0.5, 1, 2, 3, 4... percent recoveries were determined for each sample. From the retention time – boiling point calibration curve, the determined retention times were converted to the corresponding boiling points from the plot. The cumulative percent recoveries of each analyzed sample were then plotted as a function of temperature to produce the required HTSD curve.

3.6 Calculating Initial Solubility

Initial solubility is a concentration of the hydrocarbon components that are dissolved into the supercritical fluid (SC-CO_2 only or SC-CO_2 modified with toluene) at equilibrium. Theoretically, initial solubility is measured as an infinite bitumen to carbon dioxide ratio such

that the dissolving of the bitumen's hydrocarbon components into the SC-CO₂ will not change the natural composition of the starting sample.

The initial solubilities were calculated by using the cumulative masses of the hydrocarbons collected in the sampling vials during the dynamic collection period and dividing it by the total mass of CO₂ that passed through the extraction vessel during the dynamic collection period:

$$\text{Initial solubility (g of extracted hydrocarbons/g of CO}_2\text{)} = \frac{\text{Mass of hydrocarbons collected in vials}}{\text{Mass of CO}_2} \quad (1)$$

To calculate the total mass of CO₂ that was passed through the extraction vessel during the dynamic collection process, it should first be understood how the total volume of CO₂ used during the collection process is determined. The LabVIEW™ program records the CO₂ flow rate (mL min⁻¹) measured at the ISCO syringe pumps at every 10 seconds. The CO₂ flow rate at each 10-second increment is then converted from a per minute basis to a per second basis and is then multiplied by 10 seconds to determine the volume of CO₂ used over that 10-second period. The CO₂ volumes are then summed over the duration of the dynamic collection period and the total CO₂ volume is determined. By using the density of CO₂ at the experimental condition (i.e. 0.78 g/mL), the total mass of CO₂ used over the dynamic collection period can be calculated.

CHAPTER 4: RESULTS AND DISCUSSION

This chapter details the results of the 37 initial solubility measurements performed for whole bitumen, LGO, HGO, and resid in SC-CO₂ when 0, 5, and 15 mol% of toluene is added. The initial solubilities measured for the whole bitumen and the bitumen cut samples are first presented and discussed in Section 4.1. The HTSD results for the hydrocarbon extracts collected from the initial solubility experiments are further analyzed and discussed in Section 4.2.

4.1 Initial Solubility Measurements for Whole Bitumen and Bitumen Cuts

The initial solubility measurements for whole bitumen were first examined so that these values could be compared to those of the bitumen cuts. Experiments were conducted with only SC-CO₂ and SC-CO₂ with toluene added as a modifier. Three toluene concentrations of 0 (SC-CO₂ only), 5, and 15 mol% were added to the SC-CO₂, while a CO₂ flow rate ranging between 2 to 4 mL min⁻¹ (measured at the pump at 24 MPa and 275 K) was maintained throughout the duration of the sampling period. The solubility measurements for whole bitumen were performed at 24 MPa (3480 psi) and 333 K (60°C). Table 10 and Table 11 displays the initial solubility results for these experiments. Tables D1 and D2 in Appendix D displays a sample spreadsheet documenting the hydrocarbon collection data from the experiments performed on June 17, 2020. A sample calculation of the initial solubility measured from the run is also detailed in Appendix D.

4.1.1 Initial Solubility Measurements for Whole Bitumen with SC-CO₂ only

Solubility measurements for whole bitumen using only SC-CO₂ (0 mol% toluene) were performed in triplicate. A bitumen sample size of approximately 50 g is utilized in all three initial solubility measurements. The first row in Table 10 summarizes the three initial solubilities measured for the whole bitumen sample using only SC-CO₂.

Table 10. Initial solubilities of whole bitumen with SC-CO₂ modified with toluene (0, 5, and 15 mol%) at 24 MPa and 333 K.

	Run #	Date Performed	<i>Cumulative mass of hydrocarbons collected (g)</i>	<i>Cumulative mass of CO₂ used (g)</i>	<i>Average CO₂ flow rate (mL min⁻¹)</i>	Initial Solubility* (g/g)	Average Initial Solubility (g/g)
SC-CO ₂ only	1	12/09/2019	1.678	122.47	4.59	1.37 x 10 ⁻²	1.3 x 10 ⁻²
	2	01/06/2020	1.608	126.25	4.76	1.27 x 10 ⁻²	
	3	06/22/2020	1.261	107.64	4.06	1.17 x 10 ⁻²	
SC-CO ₂ with 5 mol% Toluene	4	06/23/2020	2.641	84.04	3.17	3.14 x 10 ⁻²	3.5 x 10 ⁻²
	5 **	06/24/2020	8.088	94.61	3.57	8.55 x 10 ⁻²	
	6	06/25/2020	2.832	81.75	3.08	3.46 x 10 ⁻²	
	7	06/26/2020	3.427	87.06	3.28	3.94 x 10 ⁻²	
SC-CO ₂ with 15 mol% Toluene	8	07/10/2020	16.070	93.58	3.53	1.72 x 10 ⁻¹	1.1 x 10 ⁻¹
	9	07/13/2020	6.060	85.77	3.23	7.06 x 10 ⁻²	
	10	07/14/2020	8.104	79.74	3.00	1.02 x 10 ⁻¹	
	11	07/15/2020	9.205	85.55	3.22	1.08 x 10 ⁻¹	

* *Initial solubility calculated using Equation 1*

** *Initial solubility data from run was omitted due to experimental errors*

The average initial solubility for whole bitumen in SC-CO₂ only is 1.3×10^{-2} g/g, with very little variability between replicates. This initial solubility value obtained for whole bitumen in SC-CO₂ only is in close agreement with previously published data from Huang and Radosz (1990) and Yu et al. (1989) where the solubility for Cold Lake bitumen in CO₂ was reported as 1.9×10^{-2} (weight fraction) at conditions of 323 K and 16 MPa. An initial solubility of 1.3×10^{-2} g/g is also in agreement with the initial solubility of 1.14×10^{-2} g/g reported by Underwood et al. (2018) for whole bitumen; the initial solubility measured by Underwood et al. (2018) was conducted on the same SFE system used for this research study and at the same conditions of 333 K and 24 MPa.

The important experimental parameters affecting this initial solubility measurement are the temperature and pressure (through their combined effect on the density of the SC-CO₂) and the CO₂ flow rate. For the initial solubility experiments with SC-CO₂ only, the temperature was maintained at $333 \text{ K} \pm 3 \text{ K}$ and the pressure was maintained at $24 \text{ MPa} \pm 0.12 \text{ MPa}$. These magnitudes of variation in temperature and pressure may translate to a variability in the SC-CO₂ density of 0.76 to 0.79 g mL^{-1} , which is not expected to have a large effect on the measured initial solubility.

The CO₂ flow rate is maintained between 2 to 4 mL min⁻¹ (as measured at the ISCO pumps). The flow rate is important for two main reasons. First, the CO₂ flow rate must be maintained sufficiently low to allow sufficient time for equilibrium to be reached between the sample and the flowing CO₂. Second, the CO₂ flow rate must be sufficiently high to ensure that any hydrocarbons that deposit in the metering valve or in the lines after depressurization move through the lines and are collected in the collection vials. Past experimental work conducted on the same apparatus in the SFE lab at the University of Alberta (unpublished) has shown that a CO₂ flow rate between 2 to 4 mL min⁻¹ is sufficiently low to ensure that equilibrium could be achieved between the CO₂ and the bitumen or bitumen-containing sample, while still high enough to ensure that any hydrocarbons depositing in the metering valve or the lines after depressurization of the CO₂ would move to the collection vials. Therefore, this flow rate range was selected for this research study. It should be noted that even if some hydrocarbons are not effectively removed from the metering valve and lines downstream of the metering valve by the flowing CO₂, the hydrocarbons should be effectively collected during the rinse.

Although every effort is made to maintain the CO₂ flow rate constant during an experiment, the CO₂ flow rate may change if hydrocarbons are deposited or dislodged from the metering valve or the lines downstream of the metering valve. If the CO₂ flow rate changes, the metering valve must be manually adjusted to correct the CO₂ flow rate. Considerable effort and attention is needed to ensure that the metering valve is adjusted in such a way that the CO₂ flow rate was maintained as consistent as possible however, in some cases, the CO₂ flow rate would fluctuate but the average CO₂ flow rate was still successfully maintained between 2 and 4 mL min⁻¹ (as shown in Table 10).

4.1.2 Initial Solubility Measurements for Whole Bitumen with Toluene Added to SC-CO₂

The effects of adding a modifier on the solubility of bitumen in SC-CO₂ was investigated with the addition of toluene at concentrations of 5 and 15 mol%. Four initial solubility measurements were each performed at the 5 and 15 mol% concentration conditions, while a bitumen sample size of 50 g was utilized in all four measurements. Table 10 summarizes the solubility results measured for whole bitumen using SC-CO₂ with toluene added at 5 and 15 mol%.

With toluene added as a modifier to the SC-CO₂, an assumption is made that the SC-CO₂ – toluene mixture will behave as a single homogenous phase. This assumption is based on the approximated critical points of binary mixtures (CO₂ and toluene) that were examined by Wu et al. (2005) and Ziegler et al. (1995).

The decision to select toluene as the modifier for this research study was largely based on its demonstrated effectiveness on enhancing the dissolution and extraction of heavy hydrocarbons when added to SC-CO₂ (La and Guigard 2015; Al-Marzouqi et al. 2009; Guiliano et al. 2000). Furthermore, heavier components found in bitumen such as asphaltenes, heteroatoms, and metal impurities were found to be more soluble in SCFs where toluene was added as a modifier, as compared to other modifiers such as ethyl acetate and methanol (Al-Sabawi et al. 2011).

Toluene was added at a 5 mol% concentration to the SC-CO₂ during the pressurization and the dynamic collection periods in Runs 4 to 7. During pressurization, 15.383 mL of toluene was added to the extraction vessel. During the dynamic collection period, a toluene feed rate of

0.523 mL min⁻¹ was maintained during the 25-minute sampling period so that approximately 13 mL of toluene was added. However, since the Gilson pump used for delivering the toluene modifier into the vessel is operated on a flow rate basis, slight time variations between the pressurization and dynamic collection periods may result in minor differences to the amount of toluene added to the extraction vessel. It is not anticipated that this variation will have a large effect on the measured initial solubilities.

The initial solubilities measured for whole bitumen in SC-CO₂ with 5 mol% toluene addition were 3.14 x 10⁻² (Run 4), 8.55 x 10⁻² (Run 5), 3.46 x 10⁻² (Run 6), and 3.94 x 10⁻² (Run 7) g/g. Despite having conducted four initial solubility measurements, results from only Runs 4, 6, and 7 were used. During the static period for Run 5, the pressure within the extraction vessel was not consistently maintained at 24 MPa for the 60-minute static period due to a malfunction of the ISCO pumps; a pressure of 20 MPa was achieved in the extraction vessel instead of the target 24 MPa. Because of this decrease in pressure during the static period, the initial solubility measured for Run 5 was excluded from the average initial solubility calculation.

The average initial solubility from Runs 4, 6, and 7 was calculated to be 3.5 x 10⁻² g/g. The highest solubility measurement was achieved during Run 7, while the lowest solubility was measured in Run 4. Although this variability is quite small, it might be explained by the fluctuation on the CO₂ flow rate.

Although the average CO₂ flow rates maintained during the triplicated runs for the 5 mol% toluene condition as documented in Table 10 were all kept within the desired 2 to 4 mL min⁻¹ range, a closer examination of the flow data recorded during the dynamic collection periods from Runs 4, 6, and 7 saw larger fluctuations to the CO₂ flow rates during Runs 4 and 6; Run 7 showed a more consistent flow rate range during the dynamic collection process. The consistencies of the CO₂ flow rates maintained for the duration of the dynamic collection process is an important factor that can largely influence the quantity of extracts collected in the sampling vials. As mentioned earlier, if too low of a flow is sustained, hydrocarbons may not be collected in the sampling vials. Alternatively, if the flow is too high, insufficient equilibration between the bitumen and CO₂ components may occur. Fluctuations in the CO₂ flow rate, either too high or too low, can impact the solubility measurements. The average CO₂ flow rates recorded during the sampling intervals ranged between 2.56 to 4.78 mL min⁻¹ for Run 4, 2.59 to 4.28 mL min⁻¹ for Run 6, and 2.96 to 4.25 mL min⁻¹ for Run 7. Evidently, a larger flow rate fluctuation was

observed in Run 4 which correspondingly yielded the lowest initial solubility measurement out of the three measurements performed. Alternatively, Run 7 had the smallest CO₂ flow rate fluctuation which subsequently provided the highest initial solubility measured out of the three runs. However, despite the slight variability, the agreement between the three experiments is quite good.

The average initial solubility measured for whole bitumen in SC-CO₂ with 5 mol% toluene was approximately 3 times larger than the average initial solubility that was measured for whole bitumen using SC-CO₂ only. This higher solubility implies that a greater mass of hydrocarbons was collected over the same time period (and thus in roughly the same amount of CO₂). This trend was also observed by Al-Sabawi et al. (2011) i.e., as the concentration of toluene added to the SCF increased, a larger mass of hydrocarbons was collected. This observation is also consistent with the findings of Rudyk et al. (2014) and Al-Marzouqi et al. (2009) where the SCF extraction efficiencies were increased when modifiers were added.

Toluene was added as a modifier at a 15 mol% concentration to the SC-CO₂ during the pressurization and the dynamic collection periods in Runs 8 to 11. Given a bitumen size of 50 g, 38.75 mL of toluene was added to the SFE system during the pressurization period so that a 15 mol% toluene concentration can be achieved. During the dynamic sampling period, a flow rate of 1.7525 mL min⁻¹ was later maintained by the Gilson pump for toluene delivery during the 25-minute sampling process so that approximately 44 mL of toluene was added during the dynamic collection period.

The initial solubilities measured for whole bitumen in SC-CO₂ with 15 mol% toluene addition were 1.72 x 10⁻¹ (Run 8), 7.06 x 10⁻² (Run 9), 1.02 x 10⁻¹ (Run 10), and 1.08 x 10⁻¹ (Run 11) g/g, with an average initial solubility of the four runs being 1.1 x 10⁻¹ g/g. Of the four measurements taken, Run 8 achieved a higher initial solubility compared to the other three runs performed with 15 mol% toluene. Noticeably, Run 8 also collected a much larger hydrocarbon mass as well, despite only using a slightly larger amount of CO₂ during the dynamic collection process. Based on the experimental data recorded for Run 8, an exceedingly high CO₂ flow rate of up to 62 mL min⁻¹ was briefly achieved during the early periods of the dynamic collection process. As the run further progressed, the CO₂ flow rates were more carefully maintained between the ideal 2 to 4 mL min⁻¹ range. The high flow rates observed during the early periods of the run may have driven the bitumen starting material out from the vessel and into the outlet

collection lines without being fully dissolved in the SC-CO₂ – toluene mixture. As the CO₂ flow rates diminished and were maintained at the desired 2 to 4 mL min⁻¹ range, entrained sample trapped in the outlet portion of the SFE system would slowly begin to move out of the lines and be deposited in the sampling vials. This phenomenon can further explain the dark brown/black colour similar to that of the starting material. However, HTSD analysis needs to be done on the extracts collected from Run 8 to verify if the extracts collected are compositionally similar to the whole bitumen starting material (see Section 4.2.2).

The average initial solubility measured for whole bitumen in SC-CO₂ with 15 mol% toluene was approximately 9 times larger than the average initial solubility that was measured for whole bitumen using SC-CO₂ only. Compared to the average initial solubility for whole bitumen in SC-CO₂ with 5 mol% toluene added, the average initial solubility measured for whole bitumen in SC-CO₂ with 15 mol% toluene was approximately 3 times larger.

4.1.3 Initial Solubility Measurements for Bitumen Cuts with SC-CO₂ only

Initial solubility measurements for LGO, HGO, and resid using only SC-CO₂ (0 mol% toluene) were performed in triplicate for each bitumen cut material. A sample size of approximately 50 g is utilized for LGO and HGO, while a smaller sample size of approximately 10 g is utilized for resid. Due to the glass-like solid and brittle nature of the resid sample at temperatures below 120°C, mixing by the helical impeller was unable to be performed during the experiment. As a result, to ensure that equilibrium between the SC-CO₂ and the resid components can still be effectively achieved, glass beads (4 mm diameter) were added to the resid material to increase its contacting surface area with the SC-CO₂. Furthermore, a much longer static period of 6 hours was also applied as well. With 50 g of the resid material mixed with the added glass beads, the volume of the sample mixture would obstruct the CO₂ inlet line coming into the extraction vessel. Because of this, a reduced resid mass of 10 g was used instead so that a better clearance space can be provided to the CO₂ inlet line in the extraction vessel.

The initial solubility measured for LGO using only SC-CO₂ were 1.03 x 10⁻¹ (Run 12), 7.08 x 10⁻² (Run 13), and 8.63 x 10⁻² (Run 14) g/g, with an average initial solubility of 8.7 x 10⁻² g/g. The highest solubility of the three runs was measured during Run 12, while lower solubilities were obtained in Runs 13 and 14. The average CO₂ flow rates maintained from Runs 12 to 14 ranged largely between 3.51 to 4.37 mL min⁻¹, where approximately 93 to 116 g of CO₂

flowed through the system. Run 12 maintained the lowest average CO₂ flow rate at 3.51 mL min⁻¹ but yet, it resulted in the highest initial solubility measured. Alternatively, Runs 13 and 14 maintained some of the highest CO₂ flow rates and yielded the lowest initial solubilities. Although average CO₂ flow rates of between 3 to 4 mL min⁻¹ were largely maintained during sampling for Runs 13 and 14, a significantly higher flow rate of greater than 6.5 mL min⁻¹ was sustained during the 0 to 5-minute sampling interval during Runs 13 and 14. The higher flow may have resulted in insufficient equilibration between the SC-CO₂ and LGO, resulting in lower initial solubilities being measured, as shown in Table 11.

The average initial solubility measured for LGO during Runs 12 to 14 was almost 7 times larger than the average initial solubility measured for whole bitumen. The higher average initial solubilities achieved from Runs 12 to 14 can be largely attributed to the naturally lighter hydrocarbon composition found in the LGO starting material (see Figure 13 and Table 12). Huang and Radosz (1990) also measured higher initial solubilities when a light bitumen cut that is compositionally similar to LGO was dissolved in SC-CO₂.

Initial solubilities for HGO measured in Runs 19 to 21 with only SC-CO₂ were reported at 1.16×10^{-2} (Run 19), 1.13×10^{-2} (Run 20), and 9.72×10^{-3} (Run 21) g/g, with an average of the three runs being 1.1×10^{-2} g/g as shown in Table 11. Of the three measurements performed, Runs 19 and 20 yielded the two highest solubilities, while Run 21 measured the lowest solubility. Average CO₂ flow rates ranging between 3.68 to 4.15 mL min⁻¹ were maintained during all three runs so that approximately 98 to 110 g of CO₂ was delivered through the extraction vessel during the dynamic collection processes. The slightly lower initial solubility measured during Run 21 may be attributed to the higher CO₂ flow rate of 6 mL min⁻¹ maintained during the 0 to 5-minute dynamic collection period.

The average initial solubility measured for LGO was approximately 8 times larger than the average initial solubility for HGO. However, the average initial solubility for whole bitumen was only 1.2 times larger than the average initial solubility for HGO. Since a large percentage (~37 wt%) of the whole bitumen sample is distilled out at the HGO boiling temperature range (343 to 524°C), this can indicate that HGO makes up a large percentage of whole bitumen's composition (see Table 12). Due to this, the similarities between the average initial solubilities measured between HGO and whole bitumen is largely expected.

Table 11. Initial solubilities of LGO, HGO, and resid with SC-CO₂ modified with toluene (0, 5, and 15 mol%) at 24 MPa and 333 K.

	Modifier Addition	Run #	Date Performed	<i>Cumulative mass of hydrocarbons collected (g)</i>	<i>Cumulative mass of CO₂ used (g)</i>	<i>Average CO₂ flow rate (mL min⁻¹)</i>	Initial Solubility* (g/g)	Average Initial Solubility (g/g)
LGO	SC-CO ₂ only	12	08/12/2020	9.580	93.09	3.51	1.03 x 10 ⁻¹	8.7 x 10 ⁻²
		13	08/13/2020	8.166	115.32	4.35	7.08 x 10 ⁻²	
		14	08/14/2020	9.999	115.93	4.37	8.63 x 10 ⁻²	
	SC-CO ₂ with 5 mol% Toluene	15	08/17/2020	17.718	100.32	3.78	NC	NC
		16	08/19/2020	10.061	113.67	4.28	NC	
		17	08/20/2020	9.016	111.04	4.18	NC	
		18	08/21/2020	9.646	117.16	4.42	NC	
	HGO	SC-CO ₂ only	19	06/05/2020	1.274	110.04	4.15	1.16 x 10 ⁻²
20			06/08/2020	1.101	97.74	3.68	1.13 x 10 ⁻²	
21			06/12/2020	1.064	109.51	4.13	9.72 x 10 ⁻³	
SC-CO ₂ with 5 mol% Toluene		22	06/15/2020	2.383	83.73	3.16	2.85 x 10 ⁻²	4.5 x 10 ⁻²
		23	06/17/2020	3.852	99.16	3.74	3.88 x 10 ⁻²	
		24	06/18/2020	4.469	81.16	3.06	5.51 x 10 ⁻²	
		25	07/20/2020	6.200	105.78	3.99	5.86 x 10 ⁻²	
SC-CO ₂ with 15 mol% Toluene		26	07/09/2020	22.851	94.80	3.57	NC	NC
		27	07/17/2020	12.903	104.44	3.94	NC	
		28	07/27/2020	4.736	94.66	3.57	NC	

* Initial solubility calculated by using Equation 1

NC Not Calculated – see Section 4.1.4 for details

Table 11. (cont.) Initial solubilities of LGO, HGO, and resid with SC-CO₂ modified with toluene (0, 5, and 15 mol%) at 24 MPa and 333 K.

	Modifier Addition	Run #	Date Performed	<i>Cumulative mass of hydrocarbons collected (g)</i>	<i>Cumulative mass of CO₂ used (g)</i>	<i>Average CO₂ flow rate (mL min⁻¹)</i>	Initial Solubility* (g/g)	Average Initial Solubility (g/g)
Resid	SC-CO ₂ only	29	07/22/2020	0.0638	90.84	3.43	7.02 x 10 ⁻⁴	5.9 x 10 ⁻⁴
		30	08/04/2020	0.0529	95.97	3.62	5.51 x 10 ⁻⁴	
		31	08/06/2020	0.0482	94.70	3.56	5.09 x 10 ⁻⁴	
	SC-CO ₂ with 5 mol% Toluene	32	08/31/2020	0.626	115.46	4.35	5.42 x 10 ⁻³	5.6 x 10 ⁻³
		33	09/04/2020	0.603	125.82	4.74	4.79 x 10 ⁻³	
		34	09/15/2020	0.787	117.80	4.44	6.68 x 10 ⁻³	
	SC-CO ₂ with 15 mol% Toluene	35	09/02/2020	2.734	109.15	4.11	2.50 x 10 ⁻²	2.4 x 10 ⁻²
		36	09/14/2020	2.223	95.85	3.61	2.32 x 10 ⁻²	
		37	09/18/2020	2.852	119.14	4.49	2.39 x 10 ⁻²	

* Initial solubility calculated by using Equation 1

NC Not Calculated – see Section 4.1.4 for details

Initial solubilities measured for resid using only SC-CO₂ were reported at 7.02×10^{-4} (Run 29), 5.51×10^{-4} (Run 30), and 5.09×10^{-4} (Run 31) g/g, with an average of the three runs being 5.9×10^{-4} g/g. The average initial solubility measured for resid was approximately 22 times smaller than the average initial solubility measured for whole bitumen, approximately 147 times smaller than LGO, and approximately 19 times smaller than HGO as shown in Table 10 and Table 11. Of the three bitumen cuts examined, resid has the heaviest hydrocarbon composition (see Figure 13) and is predominantly made up of large concentrations of asphaltenes and other heteroatomic and metal impurities (Chung et al. 1997). The large concentrations of asphaltenes and impurities found in resid have a very low solubility in SC-CO₂ (Hwang and Ortiz 2000). This effect is evident from Table 11 where the mass of hydrocarbons collected from Runs 29 to 31 was much smaller than the mass of hydrocarbon extracted from LGO, HGO, and whole bitumen, despite providing similar amounts of CO₂ at the same experimental temperature and pressure. From Runs 29 to 31, average CO₂ flow rates ranging between 3.43 to 3.62 mL min⁻¹ were maintained throughout the dynamic collection period so that approximately 90 to 96 g of CO₂ were passed through the extraction vessel. Past research work from Huang and Radosz (1990) and Eastick et al. (1992) similarly demonstrated that lower solubilities were measured for heavier bitumen cuts in SC-CO₂. Specifically, from the works of Huang and Radosz (1990) (see Table 4), a resid equivalent of a bitumen Cut 3 used in their experiments measured a solubility of 0.001 w/w in SC-CO₂ at 323 K and 16 MPa. When compared with the solubilities of the lighter bitumen fractions of Cuts 1 and 2 (LGO and HGO equivalents) that were also examined, the solubility for Cut 3 was the lowest among all of the bitumen cuts.

Of all of the bitumen cuts examined, LGO consistently achieved the highest initial solubility in SC-CO₂ when no toluene was added. It was noted that as the hydrocarbon composition of the bitumen cuts became heavier, as in the HGO and resid samples, the initial solubilities measured in SC-CO₂ decreased. Furthermore, it was noted that the solubility of resid was much lower than that of the other bitumen cuts and whole bitumen. This trend was also shown in the works of Huang and Radosz (1990) and Eastick et al. (1992).

4.1.4 Initial Solubility Measurements for Bitumen Cuts with Toluene Added to SC-CO₂

Toluene was added to SC-CO₂ at concentrations of 5 and 15 mol% so that its effect on the initial solubility of the bitumen cuts in SC-CO₂ could be further investigated. The 15 mol% toluene concentration condition was not performed on the LGO sample. The reason for this decision was largely based on the thought that increasing the concentration of toluene added to the SC-CO₂ would unlikely result in any additional benefits or enhancements to the solubilization of heavier hydrocarbon components from the LGO sample. Both of the 5 and 15 mol% toluene concentration conditions were examined for the HGO and resid samples.

During the dynamic collection period for Run 15 with LGO using SC-CO₂ with 5 mol% toluene, the extracts collected in the “a” vials were visually similar in colour and viscosity when compared to the *time zero* LGO sample. Without performing any further HTSD analysis on the collected extracts at the time, it was speculated that the LGO starting material was being carried over from the extraction vessel and being deposited into the sampling vials without solubilization. Factors such as volume expansion and/or density flip in the LGO, SC-CO₂, and toluene mixture were considered to be probable causes of why this was occurring. Volume expansion occurs when the SC-CO₂ – toluene binary mixture dissolves into the bitumen sample and causes the volume of the sample mixture to expand. If the volume of the sample mixture expands to a volume greater than that of the extraction vessel, the sample overflows and is “pushed out” of the extraction vessel. To examine if volume expansion was causing the issues seen with the LGO sample, the starting sample mass of the LGO was reduced from 50 g to 25 g, so that the sample volume is less and thus the expanded volume would be less. In theory, the initial solubility measured for LGO in SC-CO₂ should not be affected when the mass of the starting sample is changed since solubility is defined as a property of a substance.

To maintain a 5 mol% toluene concentration in the SC-CO₂ during the run, 15.383 mL of toluene was added by the Gilson pump during the pressurization period into the extraction vessel. A toluene feed rate of 0.523 mL min⁻¹ was maintained during the 25-minute sampling period so that approximately 13 mL of toluene was added during the dynamic collection process when a starting sample mass of 50 g is used. When the starting sample mass was reduced to 25 g in Runs 16 to 18, 17.818 mL of toluene was added by the Gilson pump during the pressurization

period instead. Similarly, a toluene feed rate of $0.523 \text{ mL min}^{-1}$ was maintained during the 25-minute sampling period.

Four initial solubilities were measured for LGO in SC-CO₂ with 5 mol% toluene and were reported to be 1.77×10^{-1} (Run 15 with 50 g of starting sample mass), 8.85×10^{-2} (Run 16 with 25 g of starting sample mass), 8.12×10^{-2} (Run 17 with 25 g of starting sample mass), and 8.23×10^{-2} (Run 18 with 25 g of starting sample mass) g/g. The initial solubilities measured from Runs 16 to 18 using 25 g of LGO starting sample mass were relatively similar, with only the solubility measured from Run 16 to be slightly higher than the other two measurements. It can be seen that as the LGO starting sample size was halved from 50 to 25 g in Runs 15 to 16, 17, and 18, the initial solubilities measured were also roughly reduced by half as well. The change in the solubility measured when the LGO starting sample size was also reduced can indicate that unreliable initial solubility measurements were obtained during Runs 15 to 18. Since solubility is a property of a substance, it theoretically should not be affected by the initial sample mass. Furthermore, it was noted that the colour and consistencies of the extracts collected from Runs 16 to 18 with the reduced sample size still closely resembled the LGO *time zero* sample. Based on these observations, it was probable to suggest that the suspected volume expansion theory is unlikely occurring. Due to the limitations of the SFE equipment (i.e. lack of a view cell on the extraction vessel), it was unfeasible to further explore if the carry-over issues observed were caused by a density flip among the components in the extraction vessel. Further pursuant to determine the cause of this issue would be work performed beyond the scope of this specific research study. Therefore, the initial solubility for LGO in SC-CO₂ added with 5 mol% toluene remains undetermined at this point.

The average initial solubility supposedly measured from Runs 16 to 18 was 8.3×10^{-2} g/g. This is a mere 3.5% difference between the average solubility measured from Runs 12 to 14 where no toluene was added to the SC-CO₂. The small difference in their initial solubilities can likely suggest that the addition of the toluene modifier at 5 mol% concentration did not provide any significant solubility enhancement to the SC-CO₂ when dissolving with the heavier hydrocarbons found in the LGO sample. Typically, modifiers are preferably supplemented in SCFs (e.g. SC-CO₂) to help improve its solubility with heavier hydrocarbons (Płotka-Wasyłka et al. 2017; Stubbs and Siepmann 2004; Phelps et al. 1996). The predominantly lighter composition of the LGO sample likely consist of low concentrations of heavy hydrocarbons such as

asphaltenes. Therefore, even if a toluene modifier was added to the SC-CO₂, the solubility of LGO in the SC-CO₂ could unlikely see a considerable increase.

The average CO₂ flow rates maintained during Runs 15 to 18 were between 3.78 to 4.42 mL min⁻¹. Approximately 100 to 117 g of CO₂ were passed through the extraction vessel during the dynamic collection periods.

Four initial solubilities were measured for HGO with 5 mol% toluene added to the SC-CO₂. For a 5 mol% toluene concentration to be consistently maintained during Runs 22 to 25, 15.383 mL of toluene was added by the Gilson pump into the vessel during the pressurization process. A toluene feed rate of 0.523 mL min⁻¹ was maintained during the 25-minute sampling period, where approximately 13 mL of toluene was added during the dynamic collection process. All of the initial solubilities measured were performed with using a starting HGO sample mass of 50 g. Initial solubilities of 2.85×10^{-2} (Run 22), 3.88×10^{-2} (Run 23), 5.51×10^{-2} (Run 24), and 5.86×10^{-2} (Run 25) g/g were measured from each of these runs; an average initial solubility of 4.5×10^{-2} g/g was calculated based on the solubilities obtained from Runs 22 to 25. The initial solubility measured from Run 22 was observed to be somewhat lower than the solubilities obtained from Runs 23 to 25. Upon further analysis of the experimental data and observations during each of these runs, it was noted that the CO₂ flow rates maintained during Run 22 had largely fluctuated between 1.99 to 5.39 mL min⁻¹ during the 25-minute dynamic collection period. As previously discussed, maintaining a consistent and adequate CO₂ flow rate during the initial solubility measurement is crucial. The large CO₂ flow rate fluctuations during Run 22 may have resulted in a lower initial solubility.

Based on Table 11, the average initial solubility measured for HGO when 5 mol% toluene was added was approximately 4 times larger than the average solubility measured when no toluene was added to the SC-CO₂. The addition of toluene as a modifier to the SC-CO₂ likely increased the solubilization of the heavier hydrocarbons found in HGO. When 5 mol% of toluene was added to the SC-CO₂, the heavier hydrocarbon components in HGO that were largely insoluble when only SC-CO₂ were extracted. The increased masses of hydrocarbons collected from Runs 22 to 25 with the addition of the 5 mol% of toluene added to the SC-CO₂ largely correlates with the findings of Magomedov et al. (2017), Al-Sabawi et al. (2011), and Guiliano et al. (2000), where larger masses of hydrocarbons were generally collected as concentrations of modifiers added to the SCF increased.

Three initial solubility measurements performed with 50, 25, and 10 g of starting sample material was performed for HGO with 15 mol% of toluene added to the SC-CO₂. To achieve a 15 mol% toluene concentration when a HGO starting sample mass of 50 g is used, 38.75 mL of toluene was added to the system during pressurization, while a toluene flow rate of 1.7525 mL min⁻¹ was maintained by the Gilson pump during the 25-minute sampling process so that approximately 44 mL of toluene in total was supplemented into the extraction vessel. With a 25 g HGO starting sample size, 44.876 mL of toluene was added to the system during pressurization while a toluene flow rate of 1.7525 mL min⁻¹ was maintained during the 25-minute sampling process. For a HGO starting sample size of 10 g, 48.554 mL of toluene was added to the system during pressurization while a toluene flow rate of 1.7525 mL min⁻¹ was maintained for the whole 25-minute sampling process.

The initial solubilities measured for the three runs were 0.241 (Run 26 with 50 g of starting sample mass), 0.124 (Run 27 with 25 g of starting sample mass), and 5.00×10^{-2} (Run 28 with 10 g of starting sample mass) g/g. Similar to what was observed during Runs 15 to 18, the extracts sampled in the “*a*” vials during the dynamic collection process from Run 26 displayed a dark brown and viscous consistency that largely resembled the *time zero* HGO material. Without performing any further HTSD analyses on the extracts at the time, it was largely speculated that the HGO starting material was being directly carried over from the extraction vessel and into the outlet portions of the SFE system. Similar to Runs 15 to 18, the starting sample mass for HGO was reduced from 50 g to 25 g for Run 27, and from 25 g to 10 g for Run 28 to examine if volume expansion was the contributing factor. Based on the calculated initial solubilities from Runs 26 to 28, as the HGO starting sample size was reduced from 50 g to 25 g, and then from 25 g to 10 g in Runs 26 to 27 and 27 to 28, the initial solubilities measured respectively were also roughly reduced by half as well. The change in solubility measured when the HGO starting sample size was also changed can indicate that unreliable initial solubility measurements were obtained during Runs 26 to 28. Since solubility is a property of a substance, it theoretically cannot be altered despite changes to the substance’s mass. Furthermore, the colour and consistency of the extracts collected in Runs 27 and 28 were also noted to be largely similar to the HGO *time zero* material. Based on these observations and results, it is probable that volume expansion was unlikely occurring during Runs 26 to 28. Additional efforts to further determine what may be happening were hindered by the limitations of the available SFE equipment.

Therefore, the initial solubility for HGO with 15 mol% toluene added to the SC-CO₂ remains undetermined at this point.

Average CO₂ flow rates ranging between 3.57 to 3.94 mL min⁻¹ were maintained during Runs 26 to 28. Approximately 94 to 104 g of CO₂ were passed through the extraction vessel during the three 25-minute dynamic periods.

Similar to Runs 29, 30, and 31, a much smaller starting sample size of approximately 10 g of resid material was used for the initial solubility measurements in Runs 32 to 34 with 5 mol% of toluene added to the SC-CO₂. Likewise, mixing was not performed during the static and dynamic collection periods during Runs 32 to 34 and a much longer static period of 6 hours was utilized. To maintain a 5 mol% toluene concentration in the SC-CO₂ during Runs 32 to 34, 28.662 mL of toluene was added to the SFE system during the pressurization period. A toluene flow rate of 0.523 mL min⁻¹ was maintained by the Gilson pump during the full 25-minute dynamic sampling process so that approximately 13 mL of toluene would be supplemented into the extraction vessel.

Three initial solubility measurements were performed for resid with 5 mol% of toluene added to the SC-CO₂ in Runs 32 to 34. The initial solubilities measured were 5.42 x 10⁻³ (Run 32), 4.79 x 10⁻³ (Run 33), and 6.68 x 10⁻³ (Run 34) g/g; an average solubility of 5.6 x 10⁻³ g/g was calculated based on the solubilities obtained from the three runs. By adding 5 mol% of toluene to the SC-CO₂, the average initial solubility from Runs 32 to 34 was approximately increased by a factor of ten when compared to the average solubility measured from Runs 29 to 31 where no toluene was added to the SC-CO₂. As a “bottom of the barrel” residual material that is generated at the end of the crude oil distillation process, resid is largely made up of large concentrations heavy hydrocarbons. Without the addition of a modifier (e.g toluene), the solubility of resid in SC-CO₂ was extremely low as demonstrated in Runs 29 to 31. Similar results were observed from the works of Hwang and Ortiz (2000) where only hydrocarbons of up to C₁₂ from a sample of crude oil were readily extracted when CO₂ without the addition of a modifier was used, in fact, no hydrocarbons greater than C₂₂ were extracted at all. By adding the 5 mol% of toluene to the SC-CO₂ during Runs 32 to 34, it allowed the SC-CO₂ to be more soluble with molecularly heavier hydrocarbons like asphaltenes (Al-Sabawi et al. 2011; Hwang and Ortiz 2000).

Average CO₂ flow rates were maintained from between 4.35 to 4.74 mL min⁻¹ during Runs 32 to 34, where roughly 115 to 125 g of CO₂ were delivered through the extraction vessel during the three dynamic collection periods. The highest initial solubility from the three runs performed was achieved in Run 34, while the lowest solubility was attained during Run 33. The slightly higher CO₂ flow rates maintained during Run 33 may have impacted the equilibration between the SC-CO₂ and resid components; this may have reduced the mass of hydrocarbons effectively dissolved into the SC-CO₂ and thus may have resulted in a lower initial solubility.

Three initial solubility measurements were performed for resid with 15 mol% of toluene added to the SC-CO₂ during Runs 35 to 37. For a 15 mol% toluene concentration to be maintained when approximately 10 g of resid starting sample is used, 72.195 mL of toluene needs to be added to the extraction vessel during the pressurization period. A toluene flow rate of 1.7525 mL min⁻¹ is then maintained throughout the 25-minute dynamic collection process during the run by the Gilson pump.

The solubilities measured from the three runs performed were 2.50×10^{-2} (Run 35), 2.32×10^{-2} (Run 36), and 2.39×10^{-2} (Run 37) g/g. An average solubility from the three runs was calculated to be 2.4×10^{-2} g/g. With the added 15 mol% of toluene, the average initial solubility measured from Runs 35 to 37 was increased by a factor of approximately 10 when compared to the average solubility that was measured from Runs 32 to 34 when only 5 mol% of toluene was used. When compared to the average initial solubility from Runs 29 to 31 where no toluene was used, the average initial solubility measured for Runs 35 to 37 saw a further increase by a factor of 100. The significant increases to the solubilities measured during Runs 35 to 37 can be largely attributed to the larger concentration of toluene that was supplemented to the SC-CO₂. By increasing the concentration of the toluene from 5 to 15 mol%, the SC-CO₂ was able to further enhance its solubility with more heavier hydrocarbons from the resid material. The results from Runs 35 to 37 similarly correlates with the findings of Magomedov et al. (2017), where a study was performed to investigate the effects of a toluene modifier on the solubility and extraction of hydrocarbons using SC-CO₂. During their study, a vacuum residue sample was extracted by SC-CO₂ modified with toluene at 15 and 30 wt%. Their results showed that as the toluene concentration was increased from 15 to 30 wt%, the extraction efficiency increased from 9.9 to 52.4 wt%.

Average CO₂ flow rates ranging between 3.61 to 4.49 mL min⁻¹ were maintained during Runs 35 to 37 so that roughly 95 to 119 g of CO₂ were delivered through the extraction vessel during the dynamic collection period. The CO₂ flow rates maintained during Runs 35 to 37 were largely within the desired flow rate range of 2 to 4 mL min⁻¹.

4.2 Compositional Analysis for Whole Bitumen and Bitumen Cuts

To provide a more comprehensive understanding of the compositional characteristics of the whole bitumen, LGO, HGO, and resid starting materials, HTSD analyses were performed to identify the boiling ranges of these starting samples. Figure 13 presents the HTSD curves for the whole bitumen and bitumen cut samples; the HTSD curves are graphed as a function of the boiling temperatures at which mass percentages of the sample's hydrocarbons are distilled out at. Fundamentally, higher boiling temperature ranges are required to distill heavier hydrocarbons, while lower boiling temperatures can distill lighter hydrocarbons. Based on Figure 13, the HTSD curve for LGO has the lowest boiling temperature distribution and therefore LGO contains the largest percentage of the light hydrocarbons as compared to whole bitumen, HGO, and resid. Of all four samples analyzed, resid has material that distills at the highest temperature and therefore contains the heaviest hydrocarbons.

As displayed in Figure 13, the HTSD results for whole bitumen, LGO, HGO, and resid all show an unresolved fraction of hydrocarbons that were not distilled at the maximum temperature of 735°C. While unresolved fractions seen in the whole bitumen and resid samples can be justified by the heavier hydrocarbons (with distillation temperatures greater than 735°C) that are present in the material, there is no reason to see any unresolved fractions in the LGO and HGO samples due to their lighter hydrocarbon compositions. After consulting with Syncrude, it was determined that the unresolved fractions seen in LGO and HGO was an artefact of the HTSD analytical method. As a result, a decision was made that it would be best to normalize all future HTSDs performed on the extract, *time zero*, and *vessel residue* samples for LGO and HGO to 100 wt%. Because the unresolved fractions seen in whole bitumen and resid is real, only the extract HTSDs will be normalized to 100 wt% for these specific samples; the HTSDs for the *time zero* and *vessel residue* samples from whole bitumen and resid will not be normalized. To normalize the HTSD data, it is simply done by dividing each individual mass data point by the

final mass fraction resolved by the HTSD and multiplying it by 100 to get the normalized mass percentage.

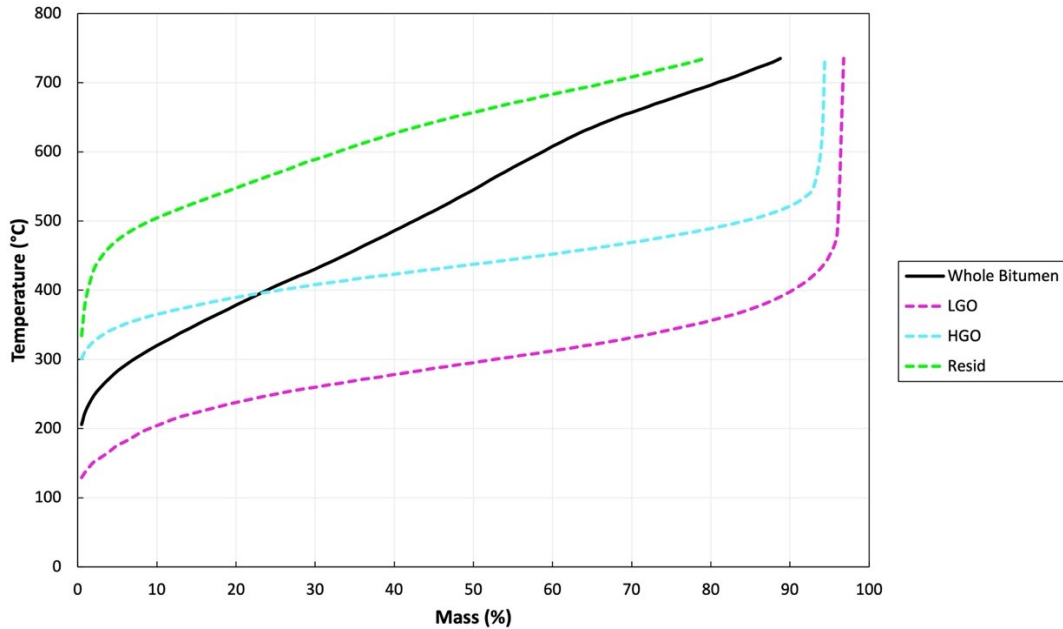


Figure 13. HTSD curves for whole bitumen, LGO, HGO, and resid starting materials.

Using the information provided in Figure 13, Table 12 details the recovery mass percentages of the hydrocarbons that are distilled out at temperature ranges of 177 to 343°C, 343 to 524°C, and +524°C from the whole bitumen and bitumen cuts. The provided distillation temperature ranges are provided by Syncrude. Based on Table 12, a majority of LGO's hydrocarbons were distilled between the temperatures of 177 to 343°C, HGO's hydrocarbons were mostly recovered between 343 to 524°C, and resid's hydrocarbons were largely distilled at greater than 524°C. Based on Table 12, whole bitumen consist of approximately 14 wt% of LGO, 33 wt% of HGO, and 53 wt% of resid.

Table 12. Recovery mass percentages for whole bitumen, LGO, HGO, and resid starting materials at various distillation temperature ranges.

Sample	RAS #	Recovery Mass Percentage (wt%)			
		177 – 343°C	343 – 524°C	524 – 735°C	> 735°C
Whole Bitumen	34807	14	33	42	11
LGO	E203140-N	75	21	1	3
HGO	E226483_37HVGO	4	86	5	5
Resid	21127	1	13	65	21

4.2.1 Compositional Analysis of Samples from Whole Bitumen with SC-CO₂ only

Photographs of the extracts that were collected from Runs 1, 2, and 3 (whole bitumen no toluene) are displayed in Figure 14. By visually comparing the contents collected from all three runs performed, the *1a* vials from both Runs 1 and 2 had noticeably darker coloured (dark brown/black) extracts compared to the contents collected in the other *2a*, *3a*, *4a*, and *5a* vials; the extracts collected in the *2a*, *3a*, *4a*, and *5a* vials from Runs 1 and 2 had a pale yellow/light gold colour. In comparison to the extracts in the *1a* vial from Run 3, extracts in the *1a* vial from Runs 1 and 2 were also noticeably darker in colour; the extracts collected in the *1a*, *2a*, *3a*, *4a*, and *5a* vials from Run 3 has a pale yellow/light gold colour (see Figure 14).

The darker coloured extracts collected in the *1a* vials in Runs 1 and 2 can likely be attributed to some of the bitumen starting material being carried over from the vessel and into the outlet lines, or from the dislodging of residual bitumen that were left in the SFE system’s outlet collection lines from previous experiments. As previously discussed in Section 4.1.2, issues of carry-over can occur when high CO₂ flow rates are maintained, causing a small amount of the bitumen starting material to be “pushed out” of the extraction vessel, into the system’s outlet collection lines, and subsequently collected into the sampling vials. Based on the experimental data recorded during Runs 1 and 2, the average CO₂ flow rates during the dynamic collection period for vial *1a* was approximately 10 mL min⁻¹ for Run 1 and 5.4 mL min⁻¹ for Run 2. Both of these flow rates exceed the desired 2 to 4 mL min⁻¹ range for initial solubilities and can further increase the chances of having the bitumen starting material being carried over into the outlet lines and into the sampling vials.

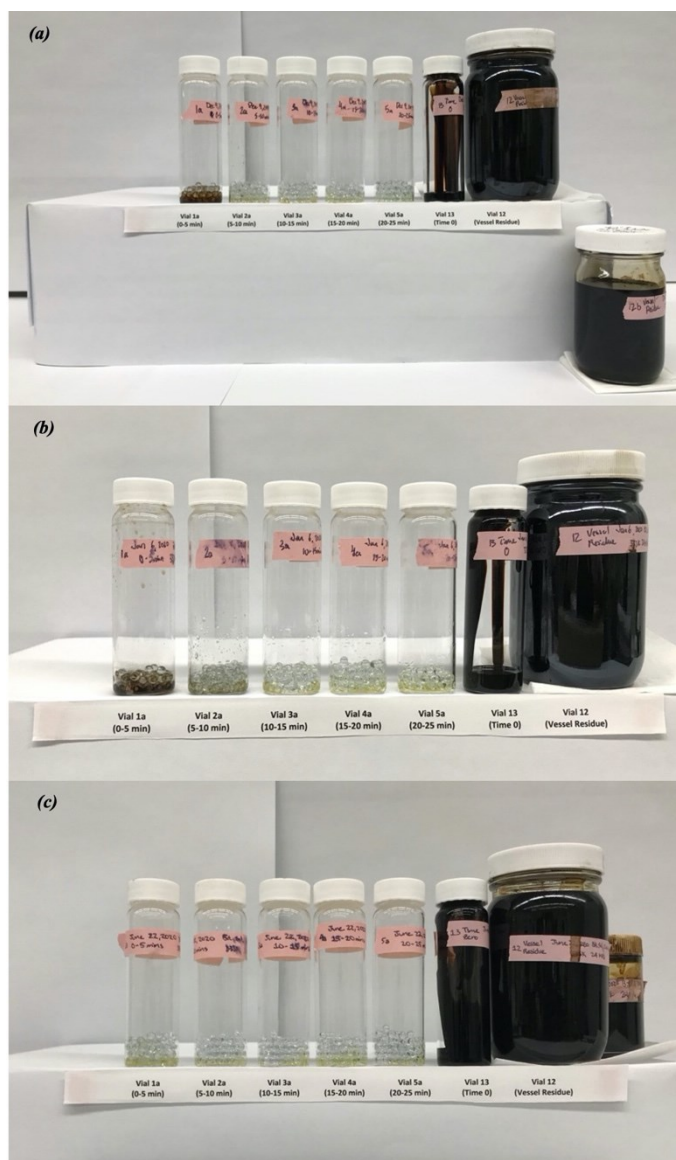


Figure 14. Visual comparison of extracts, starting materials, and vessel residue from initial solubility experiments for whole bitumen with SC-CO₂ only: (a) Run 1, (b) Run 2, and (c) Run 3.

Insufficient cleaning of the SFE system's outlet lines can also be a contributing factor to the darker coloured extracts collected in the *1a* vials from Runs 1 and 2. Although a high-pressure cleaning process is performed after each experiment with the SFE system, some residual bitumen may still remain in the outlet lines of the system. Over time, these bitumen residues may loosen up, dislodge, carried out of the SFE system, and be deposited into sampling vials during subsequent experiments like in Runs 1 and 2. Because the extracts are typically lighter in colour, any bitumen that is collected into the sampling vial can drastically taint the colour of the extract

material into a much darker brown or black colour; this is likely what occurred for the *1a* vials from Runs 1 and 2.

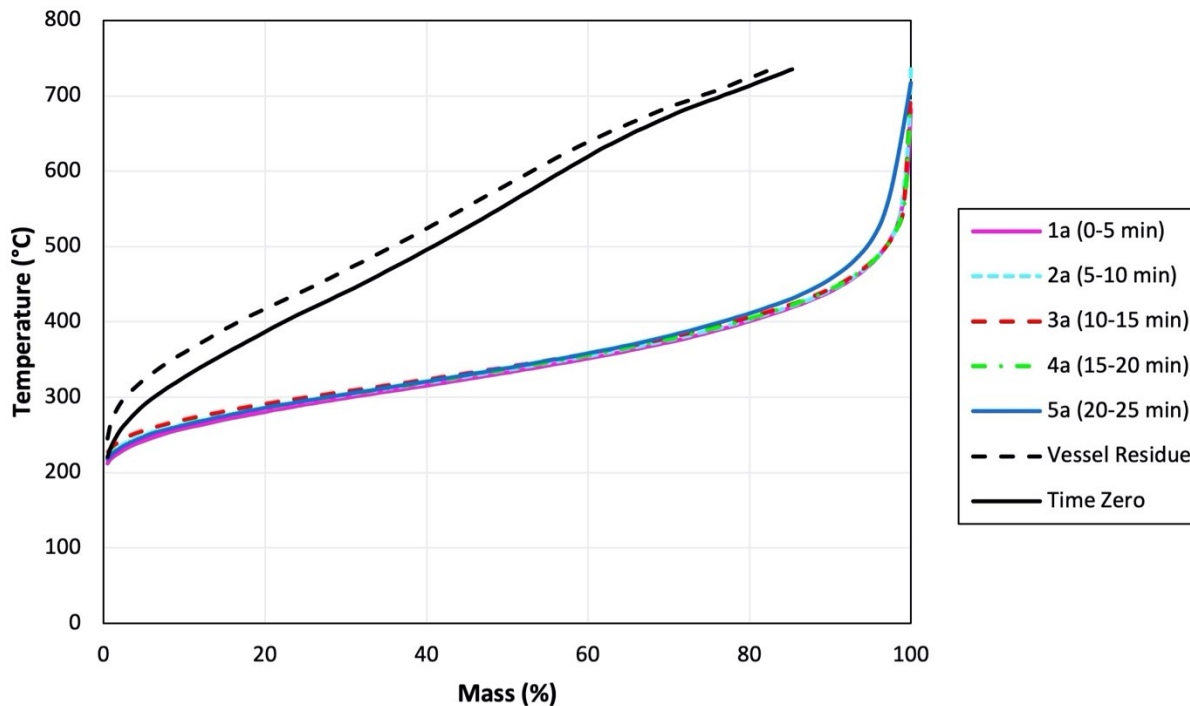


Figure 15. HTSD curves for samples from Run 3 (whole bitumen in SC-CO₂ only).

Select extract samples collected in vials *1a*, *2a*, *3a*, *4a*, *5a*, *time zero* samples, and *vessel residue* samples from Runs 1, 2, and 3 were analyzed by HTSD. Figure 15 displays the HTSD curves for the bitumen *time zero* sample, the extract samples collected in the “*a*” vials, and the *vessel residue* from Run 3.

Table 13. Recovery mass percentages of hydrocarbons at various distillation temperature ranges from extract, *vessel residue*, and *time zero* samples collected in Run 3 (whole bitumen in SC-CO₂ only).

Sample	RAS #	Recovery Mass Percentage (wt%)			
		177 – 343°C	343 – 524°C	524 – 735°C	> 735°C
<i>1a</i>	E241659	56	42	2	0*
<i>2a</i>	E241661	54	44	2	0*
<i>3a</i>	E241663	51	48	1	0*
<i>4a</i>	E241665	53	45	2	0*
<i>5a</i>	E241667	52	44	4	0*
<i>Vessel Residue</i>	E241675	8	32	43	17
<i>Time Zero</i>	E241676	13	32	40	15

* Normalized to 100 wt% at 735°C

Using the information provided in Figure 15, Table 13 details the recovery mass percentages of the hydrocarbons that are distilled at temperature ranges of 177 to 343°C, 343 to 524°C, and + 524°C for the extracts collected in vials *1a* to *5a*, the *vessel residue* sample, and the *time zero* whole bitumen material. As shown in Table 13, almost all of the hydrocarbons found in the extracts (≥ 96 wt%) collected in vials *1a* to *5a* were distilled at lower to moderate temperatures of 177 to 524°C, while only a very small percentage of the hydrocarbons (≤ 2 wt%) found in the extracts from Run 3 were distilled at temperatures ranging between 524 to 735°C. Based on this analysis, it can be speculated that the extracts sampled in vials *1a* to *5a* during Run 3 are predominately light to moderate-weighted hydrocarbons, while a very small amount of heavy hydrocarbons are found in the extracts collected.

Based on Figure 15 and Table 13, the recovery mass percentages and distillation temperature ranges for the *vessel residue* sample is similar to the *time zero* whole bitumen material. This is largely expected since in theory when the initial solubility measurements are performed, the bitumen to CO₂ ratio is infinite such that the dissolution of the bitumen in the SC-CO₂ should not alter the original composition of the bitumen in the SFE system. What is seen in Figure 15 and Table 13 can further suggest that the hydrocarbon composition from these two samples are alike.

Based on the data from Figure 15, the *time zero* sample first begins distillation at 220°C. By the time a distillation temperature of 735°C is reached, approximately 85 wt% of its

hydrocarbons have been distilled out. Due to the limitations of the HTSD instrument utilized, a distillation temperature of higher than 735°C cannot be achieved, and therefore the remaining 15 wt% of the bitumen material with boiling points of over 735°C are not distilled. The *vessel residue* analyzed from Run 3 begins distillation at a temperature of 245°C and by the time a distillation temperature of 735°C is reached, approximately 83 wt% of the hydrocarbon materials from the vessel residue have been distilled.

As mentioned previously, the hydrocarbon contents found in the extracts collected in vials *1a* to *5a* are lighter in composition when compared to the hydrocarbons found in the *time zero* and *vessel residue* samples. As a result, the distillation temperature ranges for the hydrocarbons found in vials *1a* to *5a* are lower than the ones for the *time zero* and *vessel residue* samples (see Figure 15).

The compositional differences between the extracts collected in vials *1a* to *5a* and the *time zero* sample in Run 3 as shown in Table 13 largely demonstrates SC-CO₂'s, and in general, SCFs' partial upgrading potential for bitumen. The upgrading potential of SCFs (e.g. supercritical propane, ethane, and n-pentane) for bitumen have been widely studied in literature throughout the years. Specifically, Rudyk and Spirov (2014) examined the extraction of bitumen using SC-CO₂ and found that the extracted hydrocarbons were lighter and contained lower concentrations of impurities when compared to the original bitumen feed material.

4.2.2 Compositional Analysis of Samples from Whole Bitumen with Toluene Added to SC-CO₂

Photographs of the extracts that were collected during Runs 4, 5, 6, and 7 from the initial solubility measurements with 5 mol% toluene are displayed in Figure 16. Upon further visual observation and comparison of the extracts collected from the four runs performed, the extracts collected from Runs 4, 6, and 7 has a dark yellow/golden colour while the extracts from Run 5 appears to have a much darker brown/red colour. Furthermore, vial *1a* from Run 5 appears to have collected a larger volume of extracts compared to vials *2a*, *3a*, *4a*, and *5a* from the same run.

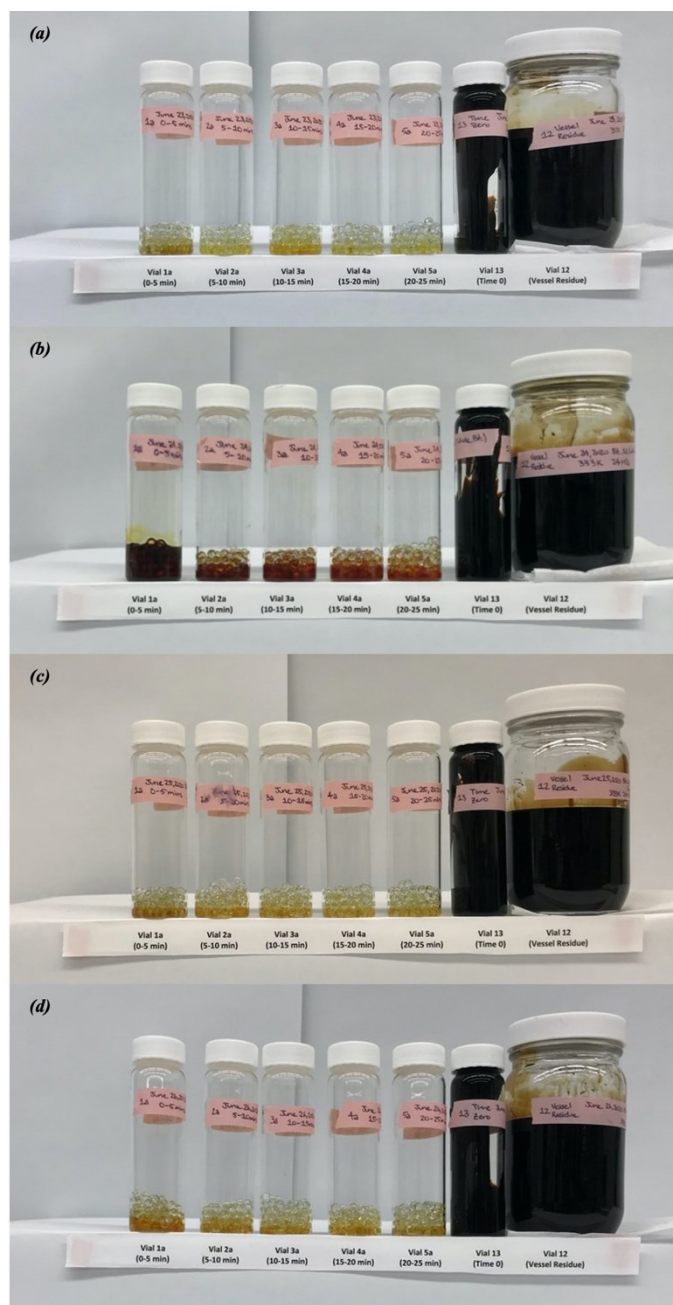


Figure 16. Visual comparison of extracts, starting materials, and vessel residue from initial solubility experiments for whole bitumen with SC-CO₂ added with 5 mol% toluene: (a) Run 4, (b) Run 5, (c) Run 6, and (d) Run 7.

Compared to the extracts collected using SC-CO₂ only from Runs 1 to 3 (whole bitumen no toluene; see Figure 14), the extracts collected with the addition of the 5 mol% toluene in Runs 4, 6, and 7 appeared to be darker in colour as displayed in Figure 16. The darker colour likely

suggests that heavier hydrocarbons were extracted with 5 mol% toluene. This interpretation is closely correlated to the research findings of Al-Sabawi et al. (2011) and Hwang and Ortiz (2000), where heavier hydrocarbons and larger concentrations of metal and heteroatomic impurities were collected when modifiers were added to the SCF. From Figure 16, the extracts collected with the addition of the 5 mol% toluene in Runs 4, 6, and 7 also appears to be slightly larger in volume compared to the extracts collected when only SC-CO₂ was used in Runs 1 to 3. This observation is further verified in Table 10; larger masses of extracts were collected when 5 mol% of toluene was added to SC-CO₂ as compared to when only SC-CO₂ was used.

Based on earlier discussions in Section 4.1.2, it was noted that the data collected from Run 5 was omitted due to the malfunctioning of the ISCO pumps during the experiment which resulted in a lower pressure being maintained in the extraction vessel during the static period. The incorrect pressure that was maintained at 20 MPa compared to the targeted 24 MPa that should have been sustained for the SC-CO₂ during the static period for Run 5 altered the density behaviour of the SC-CO₂ from 0.776 g/mL (24 MPa, 333 K) to 0.724 g/mL (20 MPa, 333 K). Although the pressure was immediately corrected back to 24 MPa once it was noticed and was maintained consistently at 24 MPa throughout the dynamic collection period of the run, the impact of sustaining a lowered pressure during the static period can affect the initial solubility of the bitumen sample in the SC-CO₂ during the static period. Recalling from Chapter 2, Guiliano et al. (2000) and Al-Marzouqi et al. (2009) both examined the changes in solubility behaviour as a function of SCF density and determined that as pressure decreased, the density and solubility of a SCF would typically decrease as well. The darker colours of the extracts collected in the sampling vials from Run 5 can be likely correlated to the incorrect pressure that was maintained during the static period that resulted in the altering of the SC-CO₂ density characteristic.

Based on the HTSD for Run 6 (see Figure 17) that was performed with whole bitumen using SC-CO₂ added with 5 mol% toluene at 24 MPa and 333 K, ≥ 90 wt% of the total hydrocarbons collected in vials *1a* to *5a* were distilled at lower to moderate temperatures of 177 to 524°C, with 52 to 54 wt% of these hydrocarbons being distilled at temperatures ranging between 343 to 524°C. Furthermore, ≤ 8 wt% of the total hydrocarbons collected in vials *1a* to *5a* were distilled at temperatures beyond 524°C. Based on this analysis, it can be speculated that the extracts collected in vials *1a* to *5a* from Run 6 are predominantly light to moderately

weighted hydrocarbons, while a very small amount of heavy hydrocarbons are found in the extracts.

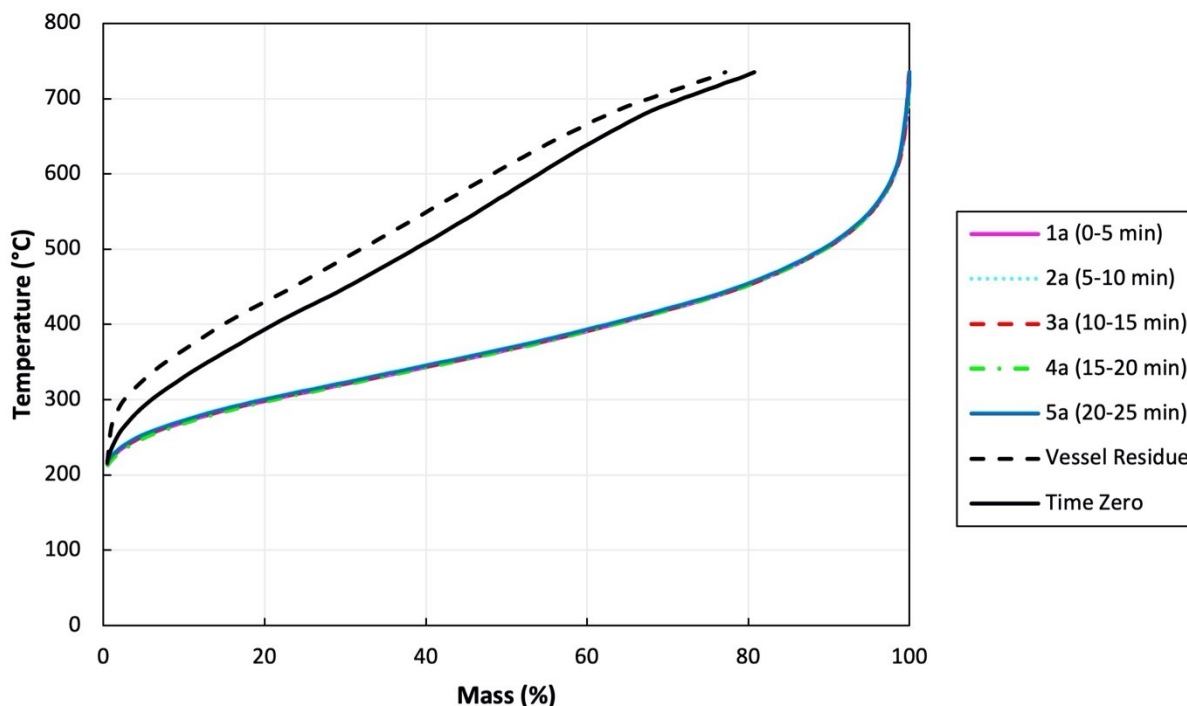


Figure 17. HTSD curves for samples from Run 6 (whole bitumen in SC-CO₂ at 333 K, 24 MPa with 5 mol% toluene addition).

Table 14. Recovery mass percentages of hydrocarbons at various distillation temperature ranges from extract, *vessel residue*, and *time zero* samples collected from Run 6 (whole bitumen in SC-CO₂ modified with 5 mol% toluene).

Sample	RAS #	Recovery Mass Percentage (wt%)			
		177 – 343°C	343 – 524°C	524 – 735°C	> 735°C
<i>1a</i>	E241713	40	52	8	0*
<i>2a</i>	E241715	39	54	7	0*
<i>3a</i>	E241717	39	53	8	0*
<i>4a</i>	E241719	40	52	8	0*
<i>5a</i>	E241721	39	53	8	0*
<i>Vessel Residue</i>	E241729	7	29	41	23
<i>Time Zero</i>	E241730	12	30	39	19

* Normalized to 100 wt% at 735°C

Compared to the extracts collected in vials *1a* to *5a* from Run 3 when only SC-CO₂ was used, extracts collected in Run 6 contained less light-weighted hydrocarbons with distillation temperatures ranging between 177 to 343°C (from ~ 50 wt% in Run 3 to ~ 40 wt% in Run 6), more moderately-weighted hydrocarbons with distillation temperatures ranging between 343 to 524°C (from ~ 40 wt% in Run 3 to ~ 53 wt% in Run 6), and more heavy hydrocarbons with distillation temperatures greater than 524°C (from ~ 3 wt% in Run 3 to ~ 8 wt% in Run 6). Overall, the hydrocarbon composition of the extracts collected from Run 6 saw a slight shift towards heavier hydrocarbons when 5 mol% toluene was added to the SC-CO₂. The addition of the toluene modifier improves the solubility of the SC-CO₂ with heavier hydrocarbons. This observation corresponds closely to the findings of Al-Sabawi et al. (2011) and Hwang and Ortiz (2000) where it was determined that when modifiers are added to SCFs, heavier hydrocarbons were able to be extracted.

Based on Figure 17 and Table 14, the recovery mass percentages and distillation temperature ranges for the *vessel residue* sample is similar to the *time zero* whole bitumen sample. This similarity between the two samples is largely expected. Based on the HTSD curves shown in Figure 17, the *time zero* sample begins distillation at 218°C. By the time a distillation temperature of 735°C is reached, approximately 81 wt% of the hydrocarbons have been distilled. Due to limitations of the HTSD instrument, a distillation temperature of higher than 735°C cannot be achieved, and therefore the remaining 19 wt% of the bitumen material with boiling points of over 735°C are not distilled. The *vessel residue* analyzed from Run 6 begins distillation at a temperature of 216°C and by the time a distillation temperature of 735°C is reached, approximately 77 wt% of the hydrocarbon components from the *vessel residue* sample have been distilled. Based on Table 14, the slight mass percentage differences seen between the *vessel residue* and the *time zero* samples from Run 6 are more noticeable in the 177 to 343°C and +524°C temperature ranges. It has been indicated by Syncrude that the HTSD method utilized lacks accuracy when analyzing extremely light and heavy hydrocarbons. Therefore, the slight mass percentage differences noticed in the 177 to 343°C and +524°C temperature ranges may be attributed to the inaccuracies of the analytical method.

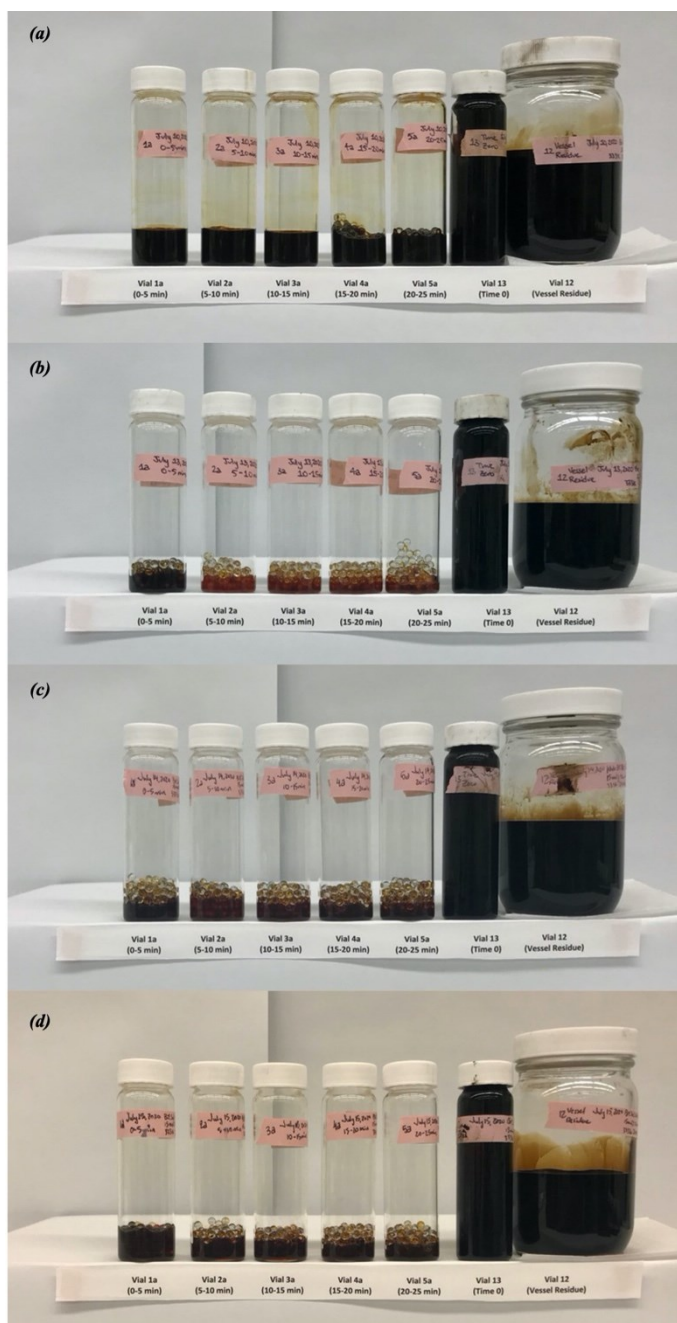


Figure 18. Visual comparison of extracts, starting materials, and vessel residue from initial solubility experiments for whole bitumen with SC-CO₂ added with 15 mol% toluene: (a) Run 8, (b) Run 9, (c) Run 10, and (d) Run 11.

Photographs of the extracts collected during Runs 8, 9, 10, and 11 from initial solubility measurements with 15 mol% toluene addition are displayed in Figure 18. As seen in Figure 18b, c, and d, dark brown/red colours are observed in the extracts collected from Runs 9 to 11; the

extracts collected from Run 8 (Figure 18a) display a much darker red, brown to black colour compared to the extracts collected from the other runs performed with whole bitumen when 15 mol% toluene was used. The darker coloured extracts collected from Run 8 in vials *1a* to *5a* visually appear to be largely similar to the *time zero* sample in terms of colour (i.e. dark brown and black) and viscosity. The visual similarities between the extracts collected in vials *1a* to *5a* and the *time zero* material in Run 8 further support the earlier speculations discussed in Section 4.1.2 suggesting that because of the exceedingly high flow rates that were achieved during the early periods of Run 8, some of the bitumen starting material may have been driven out from the vessel and into the outlet collection lines, and finally into the sampling vials during the dynamic collection process. However, a better understanding of the composition of the hydrocarbons collected in vials *1a* to *5a* during Run 8 can be provided once the HTSD analysis for the extracts is performed.

Overall, the sampled extracts collected from whole bitumen initial solubility experiments using 15 mol% toluene added to the SC-CO₂ provided the darkest extracts out of all three of the toluene conditions examined in this research study. The darker colours observed in the extracts collected with 15 mol% toluene can be likely attributed to the increase weight percentage of heavier hydrocarbons found in the extracts as higher concentrations of toluene is added as a modifier to the SC-CO₂. This observation closely correlates to the established findings from studies conducted by Al-Sabawi et al. (2011), Rudyk et al. (2014), Al-Marzouqi et al. (2009), and Hwang and Ortiz (2000) where higher concentrations of heavier hydrocarbons were extracted when increasing concentrations of modifiers were added to the SCF.

Select extract samples collected in vials *1a*, *2a*, *3a*, *4a*, *5a*, the *time zero* sample, and the *vessel residue* sample from Run 11 was analyzed by HTSD. Figure 19 displays the HTSD curves for the bitumen *time zero* sample, the extract samples collected in the “*a*” vials, and the *vessel residue* from Run 11.

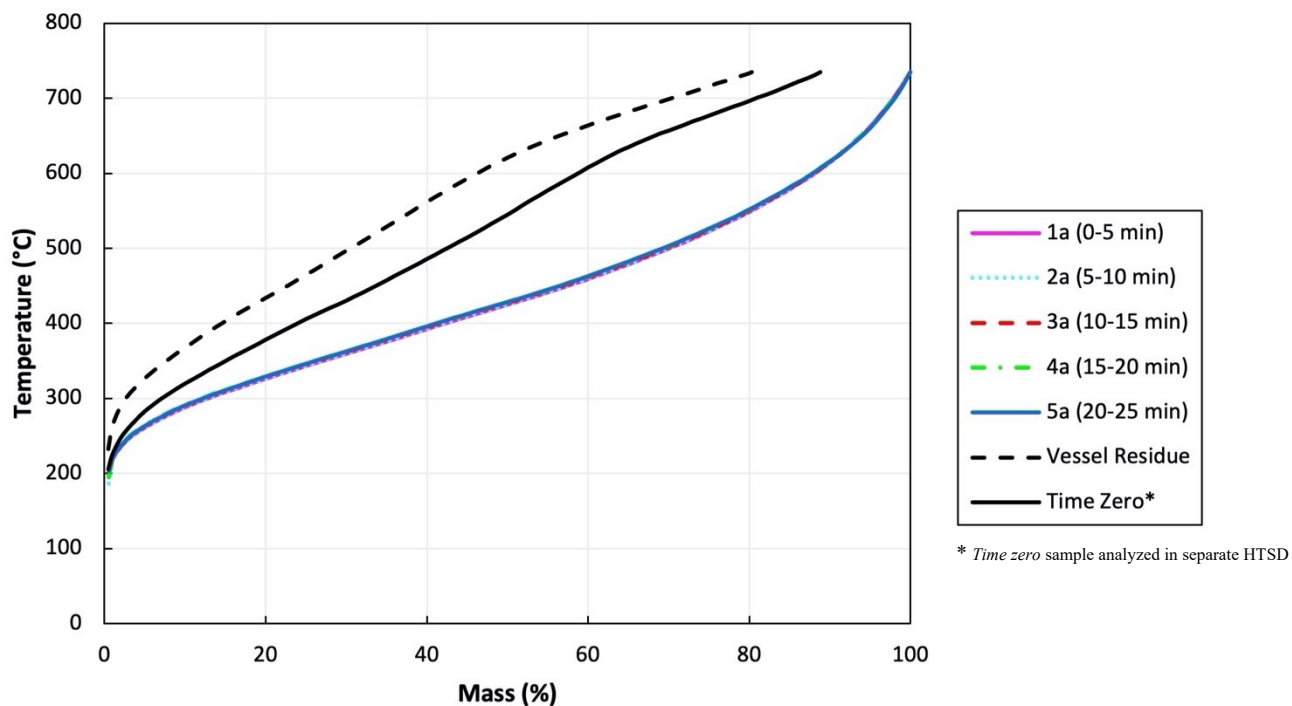


Figure 19. HTSD curves for samples from Run 11 (whole bitumen in SC-CO₂ at 333 K, 24 MPa with 15 mol% toluene addition)

Using the HTSD information provided in Figure 19, Table 15 details the recovery mass percentages of the hydrocarbons that are distilled out at temperature ranges of 177 to 343°C, 343 to 524°C, and +524°C for the extracts collected in vials *1a* to *5a*, the *vessel residue* sample, and the *time zero* whole bitumen material. Based on Table 15, around 51 wt% of the total hydrocarbons found in the extracts collected in vials *1a* to *5a* from Run 11 distills at temperatures ranging between 343 to 524°C, around 25 wt% of the hydrocarbons distills at temperatures between 177 to 343°C, and the remaining 25 wt% distills at temperatures beyond 524°C. Based on this analysis, it can be approximated that most of the extracts sampled in vials *1a* to *5a* during Run 11 are predominantly moderate-weighted hydrocarbons, while light and heavy hydrocarbons are almost equally found in the sampled extracts.

Table 15. Recovery mass percentages of hydrocarbons at various distillation temperature ranges from extract, *vessel residue*, and *time zero* samples collected from Run 11 (whole bitumen in SC-CO₂ modified with 15 mol% toluene).

Sample	RAS #	Recovery Mass Percentage (wt%)			
		177 – 343°C	343 – 524°C	524 – 735°C	> 735°C
<i>1a</i>	E220227	24	51	25	0**
<i>2a</i>	E220228	25	51	24	0**
<i>3a</i>	E220229	24	51	25	0**
<i>4a</i>	E220230	23	52	25	0**
<i>5a</i>	E220231	23	51	26	0**
<i>Vessel Residue</i>	E220232	7	27	46	20
<i>Time Zero</i> *	34807	14	33	42	11

* *Time zero sample analyzed in separate HTSD*

** *Normalized to 100 wt% at 735°C*

Compared to the hydrocarbons found in the extracts sampled in vials *1a* to *5a* from Run 6, the extracts from Run 11 contains a larger mass percentage of heavy to extremely heavy hydrocarbons (from ~ 8 wt% in Run 6 to ~ 25 wt% in Run 11) that distills at the +524°C temperature range. Furthermore, compared to Run 6, the extracts collected from Run 11 also contained less light-weighted hydrocarbons with distillation temperatures ranging between 177 to 343°C (from ~ 40 wt% in Run 6 to ~ 24 wt% in Run 11). However, the mass percentages of moderately weighted hydrocarbons found in the extracts between Runs 6 and 11 remained relatively unchanged (~ 50 wt%). Overall, the hydrocarbon composition of the extracts collected from Run 11 saw a slight shift with the collection of a higher mass percentage of heavier hydrocarbons when toluene added to the SC-CO₂ increased from 5 to 15 mol%. As discussed previously, the addition of the toluene modifier can help to improve the solubilization of heavier hydrocarbons into the SC-CO₂. With increasing concentrations of toluene added to the SC-CO₂, this can further improve the solubility of the SC-CO₂ to allow more of the heavier hydrocarbons found in whole bitumen to be dissolved.

Based on the provided data in Figure 19 and Table 15, the recovery mass percentages and distillation temperature ranges for the *vessel residue* sample is similar to the *time zero* whole bitumen material. This similarity is largely expected. Based on the HTSD from Figure 19, the *time zero* sample first begins distillation at 206°C. By the time a distillation temperature of 735°C is achieved, approximately 89 wt% of its hydrocarbons have been distilled out. Due to

limitations of the HTSD instrument, a distillation temperature of higher than 735°C cannot be achieved, and therefore the remaining 11 wt% of the bitumen material with boiling points of over 735°C are not distilled. The *vessel residue* sample from Run 11 begins distillation at a temperature of 233°C and by the time a distillation temperature of 735°C is reached, approximately 80 wt% of the hydrocarbon materials from the *vessel residue* have been distilled out. Based on Table 15, the slight mass percentage differences seen between the *vessel residue* and the *time zero* samples from Run 11 are more noticeable in the 177 to 343°C and +524°C temperature ranges. It has been indicated by Syncrude that the HTSD method utilized lacks accuracy when analyzing extremely light and heavy hydrocarbons. Therefore, the slight mass percentage differences noticed in the 177 to 343°C and +524°C temperature ranges may be attributed to the inaccuracies of the analytical method.

Because the HTSD of the *time zero* sample shown in Figure 19 was not performed at the same time as the *vessel residue* and extracts collected in the “a” vials from Run 11, there is a large difference in the mass percentage end points between the *vessel residue* and *time zero* curves. This difference can be largely attributed to calibration differences and instrumentation variations (e.g. change in column used for HTSD analysis) during the HTSD analyses performed on separate days.

4.2.3 Compositional Analysis of Samples from Bitumen Cuts with SC-CO₂ only

Photographs of the extracts that were collected from Runs 12, 13, and 14 (LGO no toluene) are displayed in Figure 20. It was noticed that, visually, the *time zero* LGO sample was less viscous in nature and has a slightly lighter brown/dark golden colour compared to the *time zero* whole bitumen sample. From Figure 20, the extracts collected in the *1a* to *5a* vials from Runs 12, 13, and 14 displays a much brighter yellow/golden colour compared to the extracts collected from Runs 1 to 3 (whole bitumen no toluene). Furthermore, larger volumes of extracts were also collected during Runs 12 to 14 compared to the extracts collected during Runs 1 to 3. Recalling from Figure 13 and Table 12, the LGO starting material is much lighter in composition than whole bitumen; in fact, LGO is the lightest out of all four whole bitumen and bitumen cut samples that is examined in this research study. Due to the lighter hydrocarbon composition found in LGO, the initial solubilities measured from Runs 12 to 14 was also larger than the solubilities measured during Runs 1 to 3 with whole bitumen (see Table 10 and Table 11). Based

on Table 10 and Table 11, Runs 12 and 14 also collected larger hydrocarbon masses when compared to Runs 1 to 3, despite utilizing a similar amount of CO₂ during the runs. This is further demonstrated by the larger amount of extracts seen to be collected in the sampling vials from Runs 12 to 14 as shown in Figure 20. The larger amount of extracts collected during Runs 12 to 14 can be correlated to the predominantly lighter hydrocarbon composition found in the LGO material. Since lighter hydrocarbons are more soluble with SC-CO₂ when compared to heavier hydrocarbons, this can further explain why more extracts were collected from LGO during Runs 12 to 14 than whole bitumen during Runs 1 to 3. Issues of carry-over were not observed from the extracts collected in Runs 12 to 14.

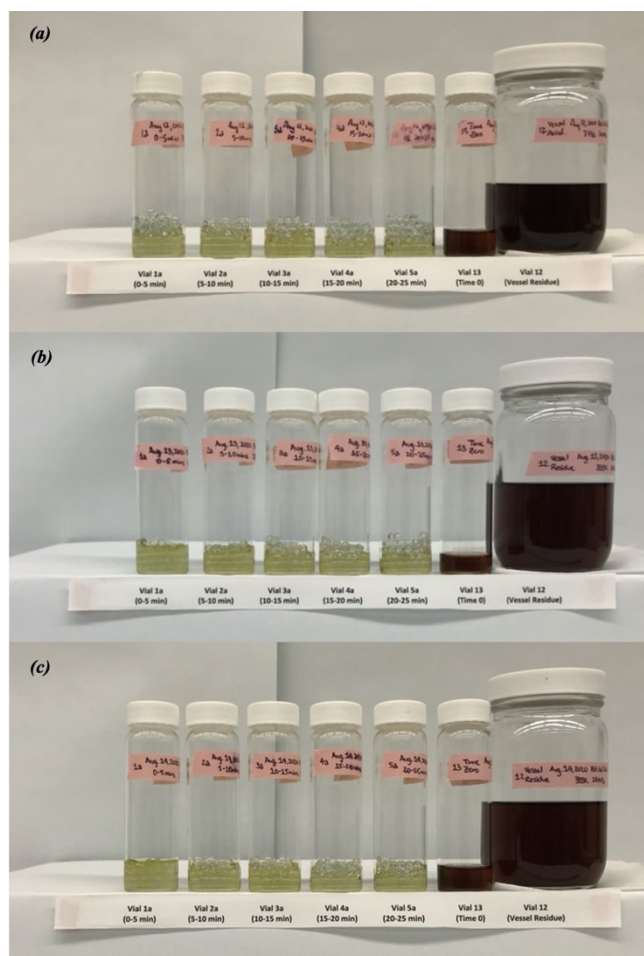


Figure 20. Visual comparison of extracts, starting materials, and vessel residue from initial solubility experiments for LGO with SC-CO₂ only: (a) Run 12, (b) Run 13, and (c) Run 14.

Samples collected in vials *1a*, *2a*, *3a*, *4a*, *5a*, the *time zero* sample, and the *vessel residue* material from Run 13 were analyzed by HTSD. Figure 21 displays the HTSD curves for the LGO *time zero* sample, the extract samples collected in the “*a*” vials, and the *vessel residue* from Run 13. The HTSD curve for whole bitumen is provided for comparison purposes.

Using the information provided in Figure 21, Table 16 details the recovery mass percentages of the hydrocarbons that are distilled out at temperature ranges of 177 to 343°C, 343 to 524°C, and +524°C for the extracts collected in vials *1a* to *5a*, the *vessel residue* sample, and the *time zero* LGO material. As shown in Table 16, almost all of the hydrocarbons found in the extracts (≥ 99 wt%) collected in vials *1a* to *5a* were distilled at lower to moderate temperatures ranging between 177 to 524°C, with a majority of these hydrocarbons (~ 80 wt%) being distilled at temperatures between 177 to 343°C. Only a very small amount of hydrocarbons (≤ 1 wt%) found in the extracts from Run 13 were distilled at temperatures beyond 524°C. Based on this analysis, it can be speculated that the extracts sampled in vials *1a* to *5a* during Run 13 are made up of mostly light hydrocarbons (~ 80 wt%), with some moderately-weight hydrocarbons (~ 20 wt%), and a very small amount of heavy to extremely heavy hydrocarbons (≤ 1 wt%).

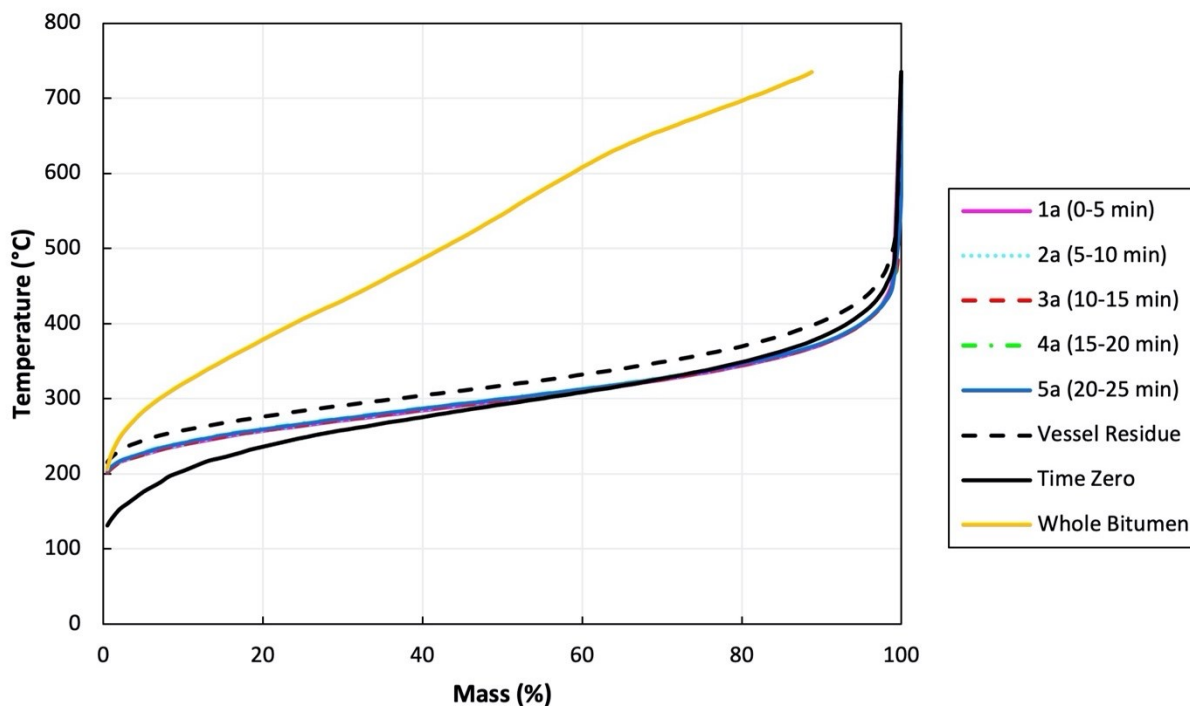


Figure 21. HTSD curves for samples from Run 13 (LGO in SC-CO₂ at 333 K, 24 MPa with no toluene addition).

Table 16. Recovery mass percentages of hydrocarbons at various distillation temperature ranges from extract, vessel residue, and time zero samples collected from Run 13 (LGO in SC-CO₂ only).

Sample	RAS #	Recovery Mass Percentage (wt%)		
		177 – 343°C	343 – 524°C	+524°C
<i>1a</i>	E200686	79	20	1
<i>2a</i>	E200687	79	20	1
<i>3a</i>	E200688	79	21	0
<i>4a</i>	E200689	78	21	1
<i>5a</i>	E200690	78	21	1
<i>Vessel Residue</i>	E200691	66	33	1
<i>Time Zero</i>	E200692	74 *	22	1

* Approximately 3 wt% of hydrocarbons were distilled at temperatures from 131 to 171°C

Based on the HTSD provided in Figure 21 and the information presented in Table 16, the hydrocarbon composition of the extracts collected in vials *1a* to *5a* appears to be similar to the

time zero LGO starting material. The compositional similarities between the extracts and the starting material can be attributed to the lighter hydrocarbon composition of the LGO sample. Since LGO's composition is largely made up of light to moderately weighted hydrocarbons, most of these hydrocarbons are easily soluble with SC-CO₂ and can be readily extracted. As a result, the extracts collected during the dynamic sampling process would have hydrocarbon compositions that closely resemble the LGO starting material.

From the HTSD provided in Figure 21, it can be seen that the extracts collected in the “a” vials from Run 13 mostly began its distillation at temperatures around 204°C, while the distillation of the *time zero* material began at temperatures of around 131°C instead. This difference may indicate that hydrocarbons between the distillation temperature range of 131 to 204°C were not effectively analyzed or perhaps even collected in the “a” vials. It is possible that these light hydrocarbons may have been extracted but were ineffectively collected in the collection vials and were carried out with the CO₂ and were released into the fume hood. Furthermore, it has been indicated by Syncrude that the HTSD method utilized lacks accuracy when analyzing extremely light and heavy hydrocarbons. Therefore, the distillation temperature gap from 131 to 204°C observed in Figure 21 between the “a” vial curves and the *time zero* curve can be likely correlated to one or both of these aforementioned factors.

Based on the HTSD from Figure 21, the *time zero* sample first begins distillation at 131°C. By the time a distillation temperature of 735°C is achieved, almost all of the hydrocarbons have been distilled. The *vessel residue* analyzed for Run 13 begins distillation at a temperature of 216°C and by the time a distillation temperature of 735°C is reached, approximately all of the hydrocarbons from the *vessel residue* have been distilled. Based on Table 16, a slight mass percentage difference is seen between the *vessel residue* and the *time zero* samples in the 177 to 343°C temperature range. It has been indicated by Syncrude that the HTSD method utilized lacks accuracy when analyzing extremely light hydrocarbons. Therefore, the slight mass percentage differences noticed in the 177 to 343°C temperature range may be attributed to the inaccuracies of the analytical method.

Photographs of the extracts that were collected from Runs 19, 20, and 21 (HGO no toluene) are displayed in Figure 22. The HGO *time zero* material appeared to be slightly more viscous than the LGO starting material but was slightly less viscous than the whole bitumen starting material. Comparing Figure 22 and Figure 20, it can be seen that the “a” vials from Runs

19 to 21 collected a much smaller extract sample size than experiments with LGO; this mass difference between the extracts collected is further verified in Table 10 and Table 11. The colours of the extracts in the “a” vials from Runs 19 to 21 (HGO) and from Runs 1 to 3 (whole bitumen) both displayed a similar yellow/light golden colour.

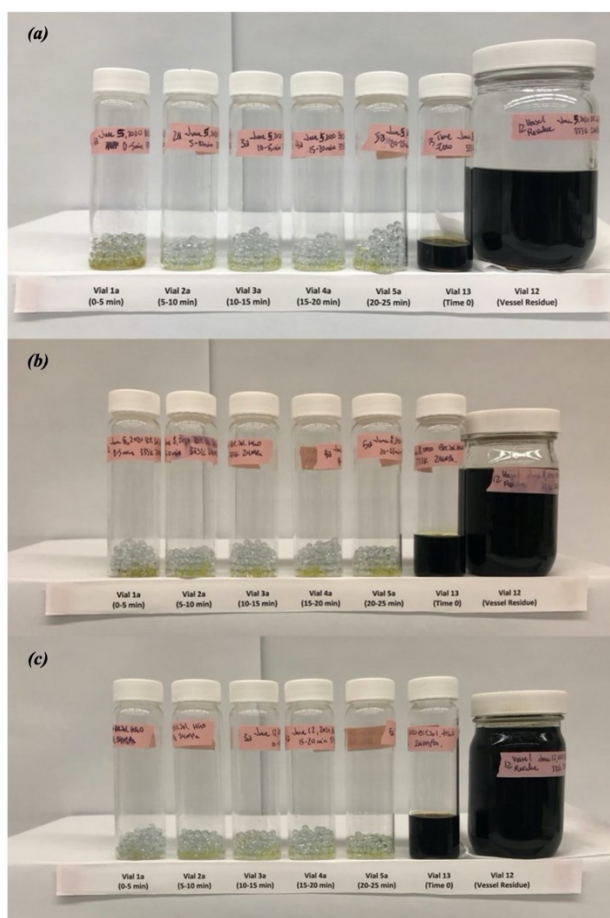


Figure 22. Visual comparison of extracts, starting materials, and vessel residue from initial solubility experiments for HGO with SC-CO₂ with no toluene added: (a) Run 19, (b) Run 20, and (c) Run 21.

Select extract samples collected in vials *1a*, *2a*, *3a*, *4a*, *5a*, the *time zero*, and the *vessel residue* samples from Run 20 were analyzed by HTSD. Figure 23 displays the HTSD curves for the bitumen *time zero* sample, the extract samples collected in the “a” vials, and the *vessel residue* from Run 20. The HTSD curve for whole bitumen is provided for comparison purposes.

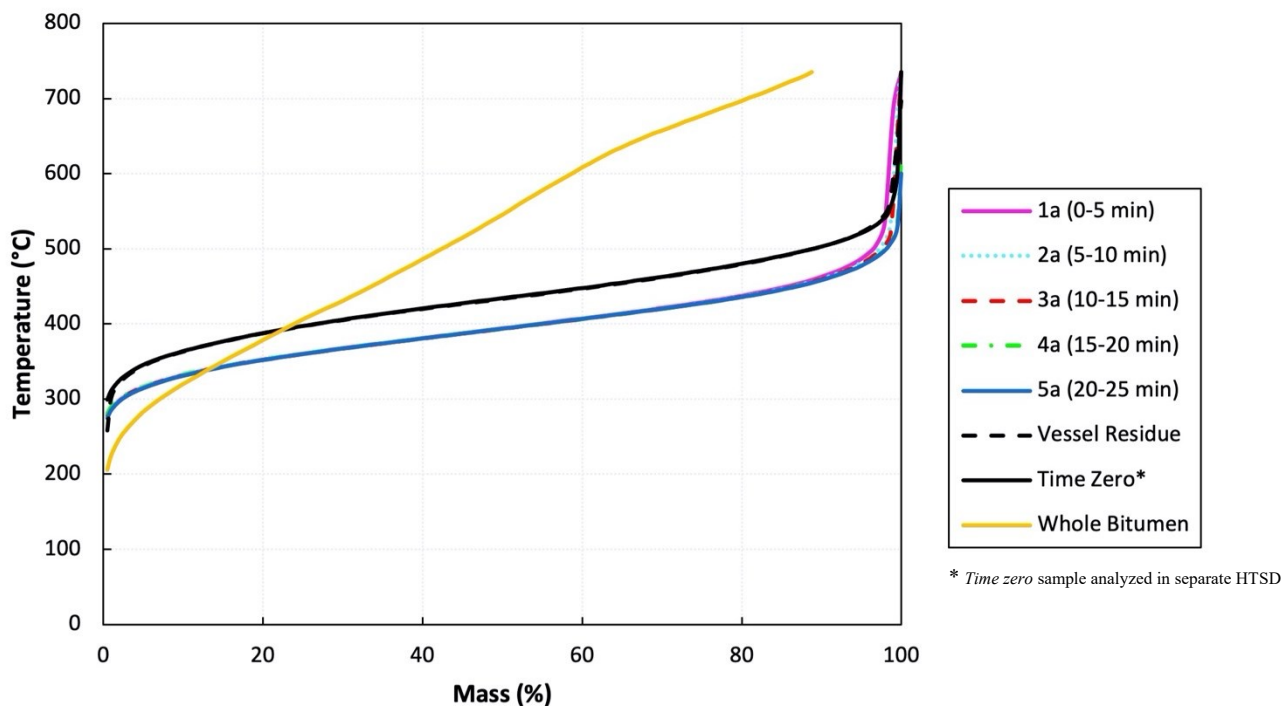


Figure 23. HTSD curves for samples from Run 20 (HGO in SC-CO₂ at 333 K, 24 MPa with no toluene addition).

Using the information provided in Figure 23, Table 17 details the recovery mass percentages of the hydrocarbons that are roughly distilled at temperature ranges of 177 to 343°C, 343 to 524°C, and +524°C for the extracts collected in vials *1a* to *5a*, the *vessel residue* sample, and the *time zero* HGO material. As shown in Table 17, almost all of the hydrocarbons found in the extracts (≥ 98 wt%) collected in vials *1a* to *5a* were distilled at lower to moderate temperatures ranging between 177 to 524°C. Specifically, of the 98 wt% of hydrocarbons distilled at this temperature range, most of the hydrocarbons (~ 84 wt%) were distilled at temperatures between 343 to 524°C. The remaining 1 to 2 wt% of the hydrocarbons found in the extracts were distilled at temperatures beyond 524°C. Based on this analysis from Table 17, it can be speculated that the extracts sampled in vials *1a* to *5a* during Run 20 predominantly consist of light to moderate-weighted hydrocarbons, with a majority of these hydrocarbons being more moderately weighted. Table 17 can further suggest that only a very small amount of heavy to extremely heavy hydrocarbons are found in the extracts collected in vials *1a* to *5a*.

Based on Figure 23 and Table 17, the recovery mass percentages and distillation temperature ranges for the *vessel residue* sample are similar to the *time zero* HGO material. This is largely expected since in theory when initial solubility measurements are performed, the bitumen to CO₂ ratio is infinite such that the dissolution of the bitumen in the SC-CO₂ should not alter the original composition of the bitumen in the SFE system.

Table 17. Recovery mass percentages of hydrocarbons at various distillation temperature ranges from extract, *vessel residue*, and *time zero* samples collected from Run 20 (HGO in SC-CO₂ only).

Sample	RAS #	Recovery Mass Percentage (wt%)		
		177 – 343°C	343 – 524°C	+524°C
1a	E200909	15	83	2
2a	E200911	14	84	2
3a	E200913	14	84	2
4a	E200915	15	84	1
5a	E200917	15	84	1
<i>Vessel Residue</i>	E200925	5	90	5
<i>Time Zero</i> *	E226483_37HVGO	4	91	5

* *Time zero sample analyzed in separate HTSD*

From the HTSD provided in Figure 23, it can be observed that the *time zero* HGO sample first begins distillation at 301°C. By the time a distillation temperature of 735°C is reached, approximately 95 wt% of its hydrocarbons have been distilled out. Due to the limitations of the HTSD instrument utilized, a distillation temperature of higher than 735°C cannot be achieved, and therefore, the remaining 5 wt% of the HGO material with boiling temperatures greater than 735°C are not distilled. The *vessel residue* analyzed for Run 20 begins distillation at a temperature of 258°C and by the time a distillation temperature of 735°C is achieved, almost all of the hydrocarbons from the *vessel residue* material have been distilled out.

Photographs of the extracts that were collected from Runs 29, 30, and 31 (resid no toluene) are displayed in Figure 24. At ambient conditions, the resid *time zero* sample exhibits glass-like solid and brittle properties; this made the handling and transfer of the starting sample into the extraction vessel extremely difficult. Through heating the resid material to a temperature

of around 120°C, the resid became softer and more malleable instead and could be more easily handled and transferred into the extraction vessel.

Based on the observations noted during the experiment and from the images provided in Figure 24, the “*a*” vials from Runs 29 to 31 did not seem to collect any visually noticeable amount of hydrocarbon extracts during their three 25-minute dynamic collection periods. As previously discussed, resid is the heaviest of the three bitumen cuts examined in this research study and contains a high concentration of heavy hydrocarbon compounds (such as asphaltenes and other impurities) that are largely insoluble in SC-CO₂. This correlates to the observations made during the experiments and with Figure 24 where a significantly smaller (or not visually observable) amount of extracts were collected in the “*a*” vials during Runs 29 to 31.

Furthermore, the lack of mixing performed during the static and dynamic collection periods in Runs 29 to 31 may have also impacted the ability to accurately measure the initial solubility of resid in SC-CO₂. Although glass beads were mixed into the resid starting material so that a larger surface area of the sample could be created and a longer static period of 6 hours was also provided so that the SC-CO₂ could have a longer time to equilibrate with the resid material, these experimental modifications did not appear to have been sufficient to result in any visible amount of material being collected in the collection vials.

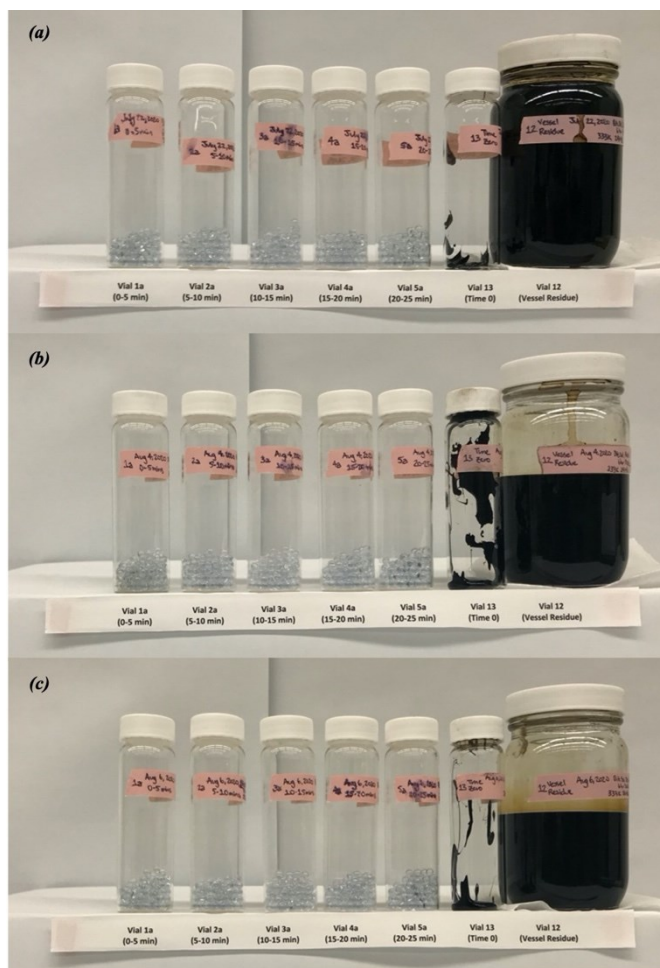


Figure 24. Visual comparison of extracts, starting materials, and vessel residue from initial solubility experiments for resid with SC-CO₂ with no toluene addition: (a) Run 29, (b) Run 30, and (c) Run 31.

Due to the insufficient amount of extracts collected in the “a” vials from Runs 29 to 31, HTSD could not be performed on these samples. Therefore, only the HTSD for the *time zero* and *vessel residue* samples from Run 31 are shown in Figure 25. A HTSD curve for whole bitumen is provided in Figure 25 for comparison purposes.

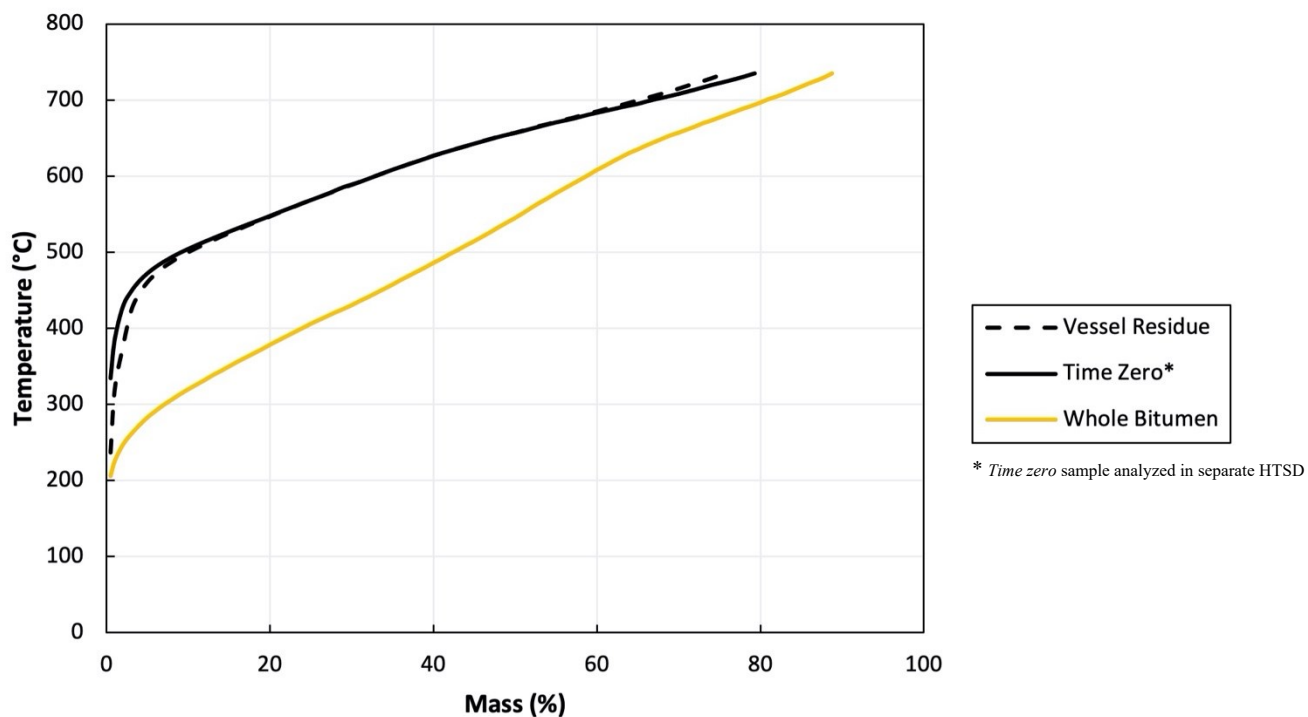


Figure 25. HTSD curves for the vessel residue and time zero samples from Run 31 (resid in SC-CO₂ at 333 K, 24 MPa with no toluene addition).

Using the information provided in Figure 25, Table 18 details the recovery mass percentages of the hydrocarbons that are distilled out at temperature ranges of 177 to 343°C, 343 to 524°C, and greater than 524°C for the *vessel residue* and *time zero* samples collected during Run 31. As shown in both Figure 25 and Table 18, the hydrocarbon compositions between the *vessel residue* and *time zero* sample appears to be similar. The compositional similarities between the two samples are expected. In theory when initial solubility measurements are performed, the bitumen to CO₂ ratio is infinite such that the dissolution of the bitumen in the SC-CO₂ should not alter the original composition of the bitumen in the SFE system. It should be noted that the HTSD for the *time zero* sample was performed on a different date than the *vessel residue* sample.

Table 18. Recovery mass percentages of hydrocarbons at various distillation temperature ranges from the *vessel residue* and *time zero* samples collected in Run 31 (Resid in SC-CO₂ only).

Sample	RAS #	Recovery Mass Percentage (wt%)			
		177 – 343°C	343 – 524°C	524 – 735°C	> 735°C
<i>Vessel Residue</i>	E200685	1	14	61	24
<i>Time Zero</i> *	21127	1	14	65	21

* *Time zero sample analyzed in separate HTSD*

Based on the HTSD from Figure 25, the *time zero* sample first begins distillation at 334°C. By the time a distillation temperature of 735°C is achieved, approximately 80 wt% of its hydrocarbons have been distilled out. Due to the limitations of the HTSD instrument utilized, a distillation temperature of greater than 735°C cannot be achieved, and therefore the remaining 20 wt% of the resid material with boiling points of over 735°C are not distilled. From this analysis, it can be observed that the resid *time zero* material has a higher distillation temperature than the other bitumen cuts of LGO and HGO and the resid material contains very little light hydrocarbons as compared to LGO or even HGO. Furthermore, the resid *time zero* sample also has a slightly lower mass percentage of 80 wt% that distills by 735°C when compared to the other bitumen cuts. Similar to the *time zero* sample, the *vessel residue* from Run 31 begins distillation at a temperature of 237°C and by the time a distillation temperature of 735°C is reached, approximately 76 wt% of the hydrocarbons from the *vessel residue* have been distilled out. Given the high percentage of heavy hydrocarbons that are not very soluble with SC-CO₂, this can explain the low initial solubilities measured for Runs 29 to 31.

4.2.4 Compositional Analysis of Samples from Bitumen Cuts with Toluene Added to SC-CO₂

Photographs of the extracts that were collected from Runs 15, 16, 17, and 18 performed with LGO using 5 mol% toluene are displayed in Figure 26. The extracts collected in the “a” vials from Runs 15 to 18 appeared to have a darker yellow/gold-brown colour as compared to the bright yellow/light golden colours seen in the extracts from Runs 12 to 14 (LGO no toluene). In fact, the colours of the extracts collected in the “a” vials from Runs 15 to 18 largely resembled the colour of the *time zero* LGO sample. As previously mentioned in Section 4.1.3, it was this observation that caused the speculation that the LGO starting material was being carried over out

of the extraction vessel and deposited into the sampling vials during the dynamic collection period. Initially, it was hypothesized that during the dynamic collection period, the volume of the LGO sample in the extraction vessel was being expanded so much that it caused the starting sample material to overflow out of the vessel. To examine if volume expansion was causing the carry-over issue, the LGO starting sample mass was reduced from 50 g in Run 15 to 25 g in Runs 16, 17, and 18 so that the LGO sample occupies a smaller volume inside the extraction vessel to prevent it from overflowing when its volume expands. In Figure 26, it can also be seen that the extract volumes collected in the “a” vials from Run 15 were slightly larger than the volume of extracts sampled in the “a” vials during Runs 16, 17, and 18. This noticeable difference in extract volume is correlated to the reduction of the LGO starting sample mass. Despite the changes made to the starting sample mass, no significant observable differences to the colour and consistency of the extracts collected in the “a” vials from Runs 16 to 18 were noticed when compared to the extracts collected during Run 15 and the LGO *time zero* sample. Based on these observations, it can largely indicate that the volume expansion of the LGO starting material unlikely caused the carry-over issue. A density inversion of the bitumen and CO₂-rich phases can also be a likely factor causing the bitumen sample in the extraction vessel to be carried out into the sampling vials. However, due to the limitations of the SFE apparatus (lack of a view cell) that was available for this research study, it cannot be confirmed if a density inversion occurred between the LGO sample and SC-CO₂ phases during the dynamic collection period.

Select extract samples collected in vials *1a*, *2a*, *3a*, *4a*, *5a*, the *time zero* sample, and the *vessel residue* sample from Run 16 were analyzed by HTSD. Figure 27 displays the HTSD curves for the LGO *time zero* sample, the extract samples collected in the “a” vials, and the *vessel residue* from Run 16. A HTSD curve for whole bitumen is included in Figure 27 for comparison purposes.

Using the information provided in Figure 27, Table 19 details the recovery mass percentages of the hydrocarbons that are distilled out at temperature ranges of 177 to 343°C, 343 to 524°C, and +524°C for the extracts collected in vials *1a* to *5a*, the *vessel residue* sample, and the *time zero* LGO material. As shown in Table 19, a majority of the hydrocarbons found in the extracts (≥ 99 wt%) collected in vials *1a* to *5a* were distilled at lower to moderate temperatures roughly ranging between 177 to 524°C, where a large portion of these hydrocarbons (~ 74 wt%) were specifically distilled at lower temperatures ranging between 177 to 343°C.

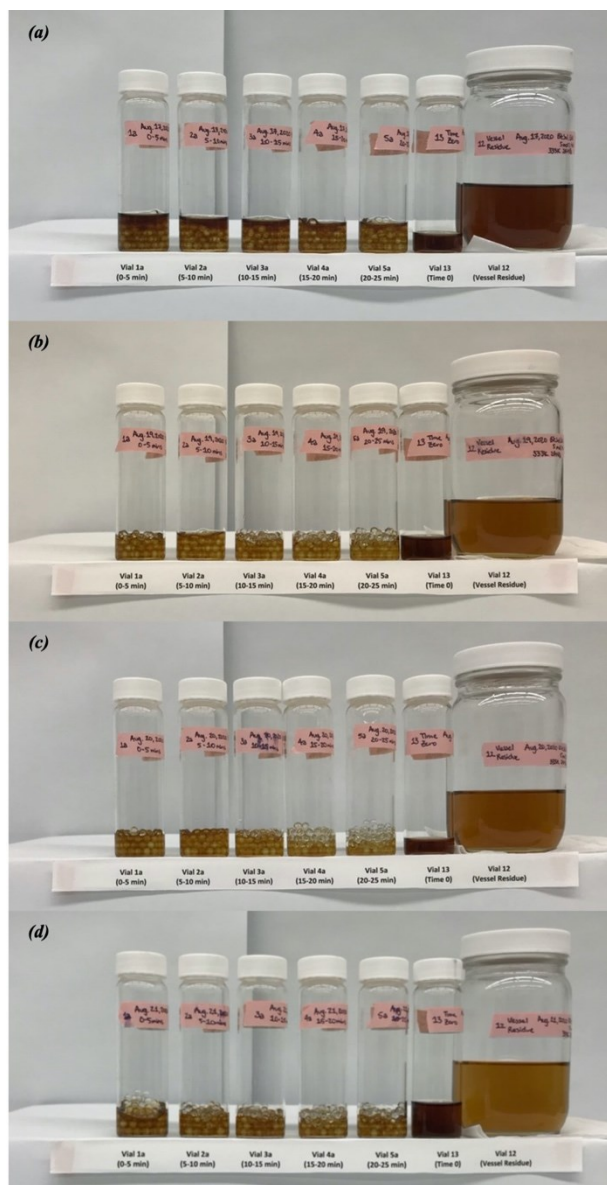


Figure 26. Visual comparison of extracts, starting materials, and vessel residue from initial solubility experiments for LGO with SC-CO₂ added with 5 mol% toluene: (a) Run 15, (b) Run 16, (c) Run 17, and (d) Run 18.

A very small percentage of the hydrocarbons (≤ 1 wt%) found in the extracts collected in vials *1a* to *5a* during Run 16 were distilled at temperatures beyond 524°C. Based on the analysis performed in Table 19, it can be speculated that the extracts sampled in vials *1a* to *5a* during Run 16 are made up of mostly light hydrocarbons (~ 74 wt%), with some moderately-weight

hydrocarbons (~ 25 wt%), and very few (if any) heavy to extremely heavy hydrocarbons (≤ 1 wt%).

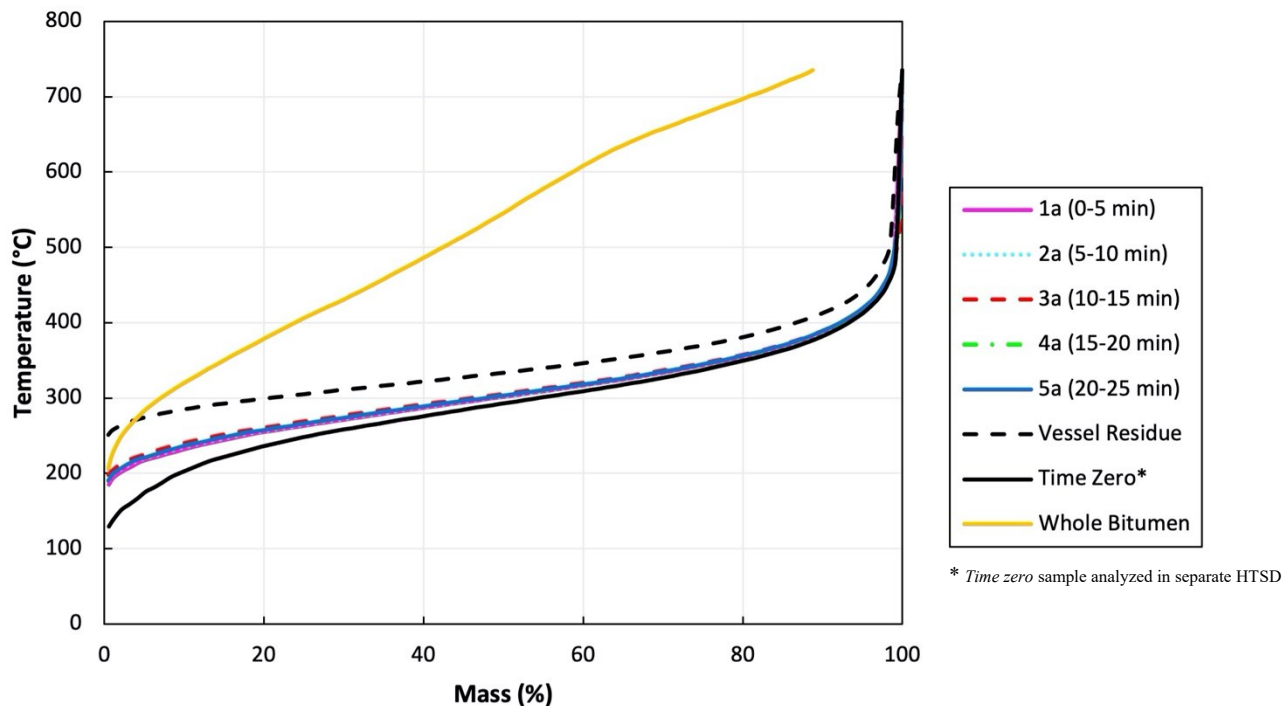


Figure 27. HTSD curves for samples from Run 16 (LGO in SC-CO₂ at 333 K, 24 MPa with 5 mol% toluene addition)

Table 19. Recovery mass percentage of hydrocarbons at various distillation temperature ranges from extract, *vessel residue*, and *time zero* samples collected from Run 16 (LGO in SC-CO₂ modified with 5 mol% toluene).

Sample	RAS #	Recovery Mass Percentage (wt%)		
		177 – 343°C	343 – 524°C	+524°C
1a	E243002	74	25	1
2a	E243003	74	26	0
3a	E243004	73	26	1
4a	E243005	74	25	1
5a	E243006	74	26	0
<i>Vessel Residue</i>	E243001	58	41	1
<i>Time Zero*</i>	E203140-N	77	22	1

* Time zero sample analyzed in separate HTSD

Based on the HTSD provided in Figure 27 and the information presented in Table 19, the hydrocarbon composition of the extracts collected in vials *1a* to *5a* appears to be similar to the *time zero* LGO starting material. The compositional similarities between the extracts and the starting material can be attributed to the lighter hydrocarbon composition of the LGO sample. Since LGO's composition is largely made up of light to moderately weighted hydrocarbons, most of these hydrocarbons are easily soluble with SC-CO₂ and can be readily extracted. When comparing the HTSD curves from Run 13 (LGO with no toluene) to Run 16 (LGO with 5 mol% toluene), the effects of toluene addition on the hydrocarbon composition of the extracts can be seen. When toluene was added at a 5 mol% concentration to the SC-CO₂ in Run 16, a larger mass percentage (~ 26 wt%) of moderately weighted hydrocarbons with distillation temperatures ranging between 343 to 524°C were collected as compared to the 21 wt% of the similar hydrocarbons that were collected when no toluene was added to the SC-CO₂ (Run 13). Although this mass percentage increase may be arguably negligible, it can further demonstrate that the effects of adding a toluene modifier to increase the solubility of the heavier hydrocarbons with SC-CO₂ is not as pronounced in LGO due to its overall lighter hydrocarbon composition.

From the HTSD provided in Figure 27, it can be seen that the extracts collected in the “*a*” vials from Run 16 mostly began its distillation at temperatures around 190°C, while the distillation of the *time zero* material began at temperatures of around 129°C instead. With this difference, this can indicate that hydrocarbons between the distillation temperature range of 129 to 190°C were not effectively analyzed or perhaps even collected in the “*a*” vials. It is possible that these light hydrocarbons may have been extracted but were ineffectively collected in the collection vials and were carried out with the CO₂ and was released into the fume hood. Furthermore, it has been indicated by Syncrude that the HTSD method utilized lacks accuracy when analyzing extremely light and heavy hydrocarbons. Therefore, the distillation temperature gap from 129 to 190°C observed in Figure 27 between the “*a*” vial curves and the *time zero* curve can be likely correlated to one or both of these aforementioned reasons.

Based on the HTSD from Figure 27, the *time zero* sample first begins distillation at 129°C. By the time a distillation temperature of 735°C is reached, almost all of the hydrocarbons have been distilled out. The *vessel residue* analyzed for Run 16 begins distillation at a temperature of 251°C and by the time a distillation temperature of 735°C is reached, approximately all of the hydrocarbons from the *vessel residue* was distilled out. Based on Table

19, a slight mass percentage difference is seen between the *vessel residue* and the *time zero* samples from Run 16 in the 177 to 343°C temperature range. It has been indicated by Syncrude that the HTSD method utilized lacks accuracy when analyzing extremely light hydrocarbons. Therefore, the slight mass percentage differences noticed in the 177 to 343°C temperature range may be attributed to the inaccuracies of the analytical method.

With some visual and analytical evidence suggesting that the LGO starting material was likely being directly carried over from the extraction vessel and into the collection vials during Runs 15 to 18, it would be theoretically expected that the hydrocarbon compositions between the extracts collected in the “a” vials, the *vessel residue* sample, and the *time zero* material to be compositionally identical to each other. However, based on the HTSD from Figure 27 and the data from Table 19, this is not the case. Assuming that carry-over did occur during Runs 15 to 18, a likely explanation for the compositional dissimilarities between these samples can be attributed to the aforementioned factors of (1) the loss of lighter hydrocarbons in the extracts due to volatilization during the dynamic sampling process, and (2) the inaccuracies of HTSD when analyzing detecting extremely light and/or extremely heavy hydrocarbons from samples.

Photographs of the extracts that were collected from Runs 22, 23, 24, and 25 performed with HGO using SC-CO₂ added with 5 mol% toluene are displayed in Figure 28. It can be observed that the extracts collected in the “a” vials from Run 22 has a slightly lighter yellow/golden colour and contains a somewhat smaller volume of extracts when compared to the contents in the other “a” vials from Runs 23 to 25. This noticeable difference in colour and volume seen in the “a” vials from Run 22 contributed to the slightly lower initial solubility that was measured during Run 22. The extracts collected in the “a” vials from Run 25 displayed a much darker yellow/golden colour compared to the extracts collected from the other runs performed with HGO in SC-CO₂ added with 5 mol% toluene. This contributed to the higher initial solubility measured in Run 25. From visually comparing the extracts collected in Runs 19 to 21 (HGO in SC-CO₂ only) and in Runs 22 to 25 (HGO in SC-CO₂ with 5 mol% toluene), the extracts collected from Runs 22 to 25 appear to have a larger mass and display a much darker yellow/golden colour. The visual differences observed between the two sets of runs can preliminarily indicate that the toluene modifier added at concentrations of 5 mol% had enhanced the solubilization of SC-CO₂ with heavier hydrocarbon components found in the HGO material.

Select extract samples collected in vials 1a, 2a, 3a, 4a, 5a, the *time zero* sample, and the *vessel residue* sample from Run 23 performed with HGO and 5mol% toluene added to the SC-CO₂ were analyzed by HTSD. Figure 29 displays the HTSD curves for the bitumen *time zero* sample, the extract samples collected in the “a” vials, and the *vessel residue* from Run 23. Again, the whole bitumen curve is provided for comparison purposes.

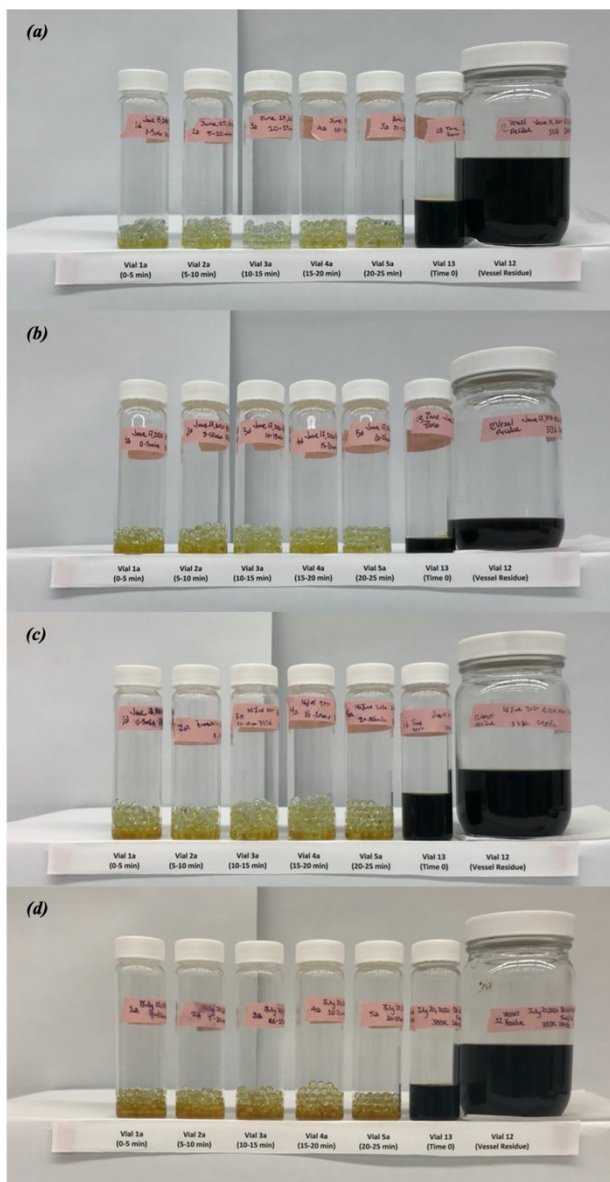


Figure 28. Visual comparison of extracts, starting materials, and vessel residue from initial solubility experiments for HGO with SC-CO₂ added with 5 mol% toluene: (a) Run 22, (b) Run 23, (c) Run 24, and (d) Run 25.

Using the information provided in Figure 29, Table 20 details the recovery mass percentages of the hydrocarbons that are distilled out at temperature ranges of 177 to 343°C, 343 to 524°C, and +524°C for extracts collected in vials *1a* to *5a*, the *vessel residue* sample, and the *time zero* HGO material. As shown in Table 20, almost all of the hydrocarbons found in the extracts (~ 98 wt%) collected in vials *1a* to *5a* were distilled at lower to moderate temperatures of 177 to 524°C. Specifically, a majority of these extracts (~ 89 wt%) were distilled at temperatures ranging between 343 to 524°C. Only a very small mass percentage (~ 2 wt%) of the extracts found in vials *1a* to *5a* had distillation temperatures of greater than 524°C. Based on this analysis, it can be speculated that the extracts collected in vials *1a* to *5a* during Run 23 contains predominantly moderate-weighted hydrocarbons, with some light hydrocarbons, and very few heavy hydrocarbons.

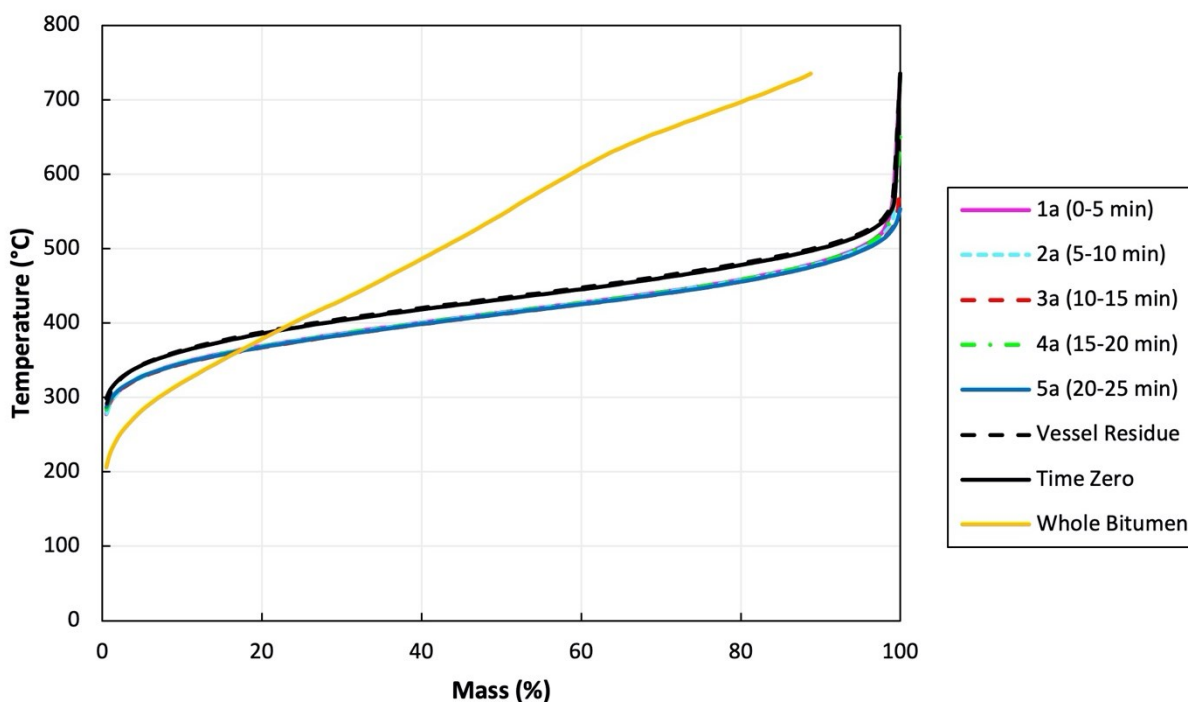


Figure 29. HTSD curves for samples from Run 23 (HGO in SC-CO₂ at 333 K, 24 MPa with 5 mol% toluene addition).

Table 20. Recovery mass percentages of hydrocarbons at various distillation temperature ranges from extract, *vessel residue*, and *time zero* samples collected from Run 23 (HGO in SC-CO₂ modified with 5 mol% toluene).

Sample	RAS #	Recovery Mass Percentage (wt%)		
		177 – 343°C	343 – 524°C	+524°C
<i>1a</i>	E220255	9	89	2
<i>2a</i>	E220257	9	89	2
<i>3a</i>	E220259	9	89	2
<i>4a</i>	E220261	9	89	2
<i>5a</i>	E220263	9	89	2
<i>Vessel Residue</i>	E220271	4	92	4
<i>Time Zero</i>	E220272	5	91	4

Compared to the extracts collected in vials *1a* to *5a* from Run 20 (HGO with SC-CO₂ only; see Table 17) when only SC-CO₂ was used, extracts collected in Run 23 contained less light-weight hydrocarbons with distillation temperatures ranging between 177 to 343°C (from ~15 wt% in Run 20 to ~9 wt% in Run 23), more moderately-weighted hydrocarbons with distillation temperatures ranging between 343 to 524°C (from ~84 wt% in Run 20 to ~89 wt% in Run 23), and around the same amount of heavy hydrocarbons with distillation temperatures beyond 524°C. Overall, the hydrocarbon composition of the extracts collected from Run 23 saw a minor shift towards extracting more heavier hydrocarbons from the HGO starting material when 5 mol% of toluene was added to the SC-CO₂. The addition of a toluene modifier has been known to improve the solubility behaviour of the SC-CO₂ so that heavier hydrocarbons can be more easily dissolved with the SCF. This observation corresponds closely to the findings of Al-Sabawi et al. (2011) and Hwang and Ortiz (2000) where it was determined that when modifiers are added to SCFs, heavier hydrocarbons were able to be extracted as a result.

Based on Figure 29 and Table 20, the recovery mass percentages and distillation temperature ranges for the *vessel residue* sample is similar to the *time zero* HGO material. This is largely expected since in theory when initial solubility measurements are performed, the bitumen to CO₂ ratio is infinite such that the dissolution of the bitumen in the SC-CO₂ should not alter the original composition of the bitumen in the SFE system. What is seen in Figure 29 and Table 20 can further suggest that the hydrocarbon compositions from these two samples are alike.

Based on Figure 29, the *time zero* sample from Run 23 first begins distillation at 298°C. By the time a distillation temperature of 735°C is reached, approximately 98 wt% of its hydrocarbons have been distilled out. Due to the limitations of the HTSD instrument utilized, a distillation temperature of beyond 735°C cannot be reached, and therefore the remaining 2 wt% of the HGO material with boiling points greater than 735°C are not distilled. The *vessel residue* from Run 23 begins distillation at a temperature of 292°C and by the time a distillation temperature of 735°C is reached, approximately 96 wt% of the hydrocarbon materials from the *vessel residue* have been distilled.

Photographs of the extracts that were collected from Runs 26, 27, and 28 performed with HGO with 15 mol% toluene added to the SC-CO₂ are displayed in Figure 30. Unlike the extracts collected in the “a” vials from Runs 22 to 25 (HGO with 5 mol% toluene) that displayed a darker yellow/golden colour, the extracts collected in the “a” vials from Runs 26 to 28 had a darker brown to black colour that largely resembled the HGO *time zero* material. As previously mentioned in Section 4.1.4, it was due to this observation where it was roughly speculated that the HGO starting material was being carried over out of the extraction vessel and deposited into the sampling vials during the dynamic collection period. The volume expansion of the HGO sample in the extraction vessel was once again examined to see if it was the cause to the carry-over issue seen. To do so, the HGO starting sample mass was reduced from 50 g in Run 26 to 25 g in Run 27, and further to 10 g in Run 28 so that the HGO sample occupies a smaller volume inside the extraction vessel to prevent it from overflowing when its volume expands. In Figure 30, it can be noticed that the extract volumes collected in the “a” vials in Runs 26, 27, and 28 were observably different. This noticeable difference in extract volume is correlated to the reductions of the HGO starting sample mass. Despite the changes made to the starting sample mass, no significant observable changes to the colour, consistency, and composition of the extracts collected in the “a” vials from Runs 27 and 28 were noticed when compared to the extracts collected during Run 26 and with the HGO *time zero sample*. Based on these observations, it can largely indicate that the volume expansion of the HGO starting material unlikely resulted in the carry-over issue. A density inversion of the bitumen and CO₂-rich phases may be a likely factor causing the HGO sample to be carried out of the vessel. Because of the technical limitations of the SFE system (lack of a view cell) used in this research study, the factor of a density inversion occurring between the LGO and CO₂ phases cannot be determined.

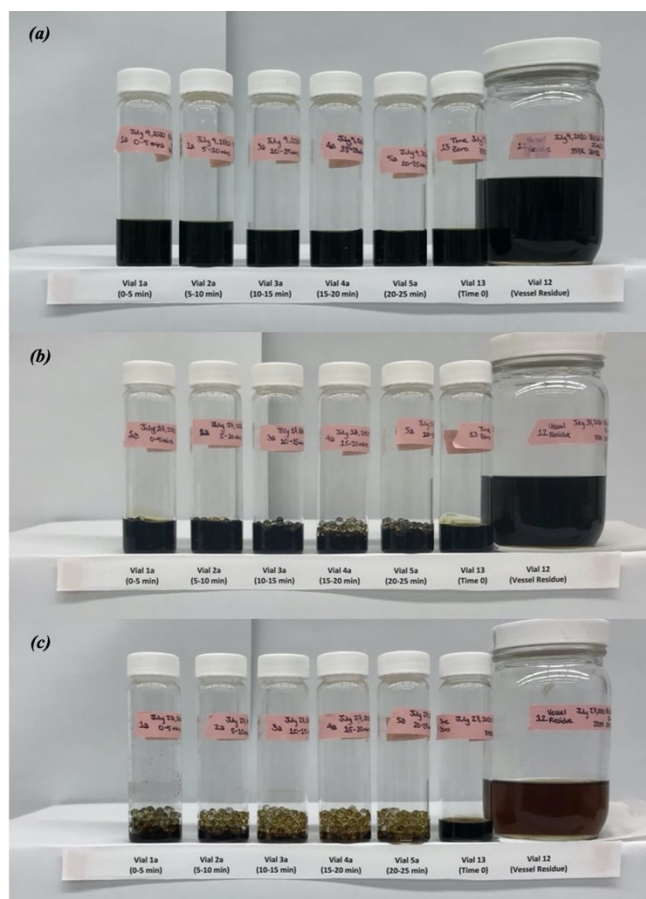


Figure 30. Visual comparison of extracts, starting materials, and vessel residue from initial solubility experiments for HGO with SC-CO₂ added with 15 mol% toluene: (a) Run 26, (b) Run 27, (c) Run 28.

Select extract samples collected in vials *1a*, *2a*, *3a*, *4a*, *5a*, the *time zero* sample, and the *vessel residue* sample from Run 26 were analyzed by HTSD. Figure 31 displays the HTSD curves for the HGO *time zero* sample, the extract samples collected in the “*a*” vials, and the *vessel residue* from Run 26. The HTSD curve for whole bitumen is provided for comparison purposes.

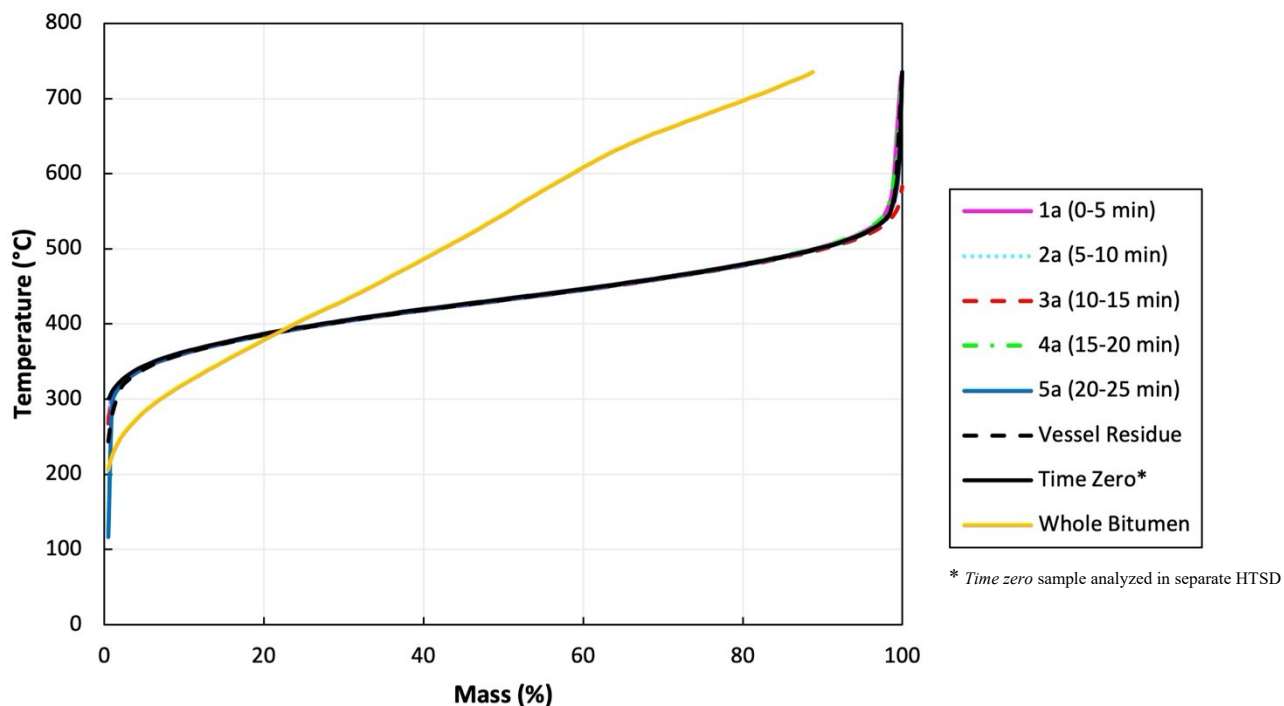


Figure 31. HTSD curve for samples from Run 26 (HGO in SC-CO₂ at 333 K, 24 MPa with 15 mol% toluene addition).

Using the information provided in Figure 31, Table 21 details the recovery mass percentages of the hydrocarbons that are distilled out at temperature ranges of 177 to 343°C, 343 to 524°C, and +524°C for the extracts collected in vials *1a* to *5a*, the *vessel residue* sample, and the *time zero* HGO material. As shown in Table 21, a majority of the hydrocarbons found in the extracts (~ 91 wt%) collected in vials *1a* to *5a* were distilled at moderate temperatures ranging roughly between 343 to 524°C. Only 5 and 4 wt% of the hydrocarbons found in the extracts collected were distilled at temperature ranges of 177 to 343°C and +524°C, respectively. Based on the analysis provided in Table 21, it can be approximated that the extracts collected in vials *1a* to *5a* during Run 26 are made up of mostly moderate weight hydrocarbons, with some light and heavy hydrocarbons as well.

Table 21. Recovery mass percentages of hydrocarbons at various distillation temperature ranges from extract, *vessel residue*, and *time zero* samples collected from Run 26 (HGO in SC-CO₂ modified with 15 mol% toluene).

Sample	RAS #	Recovery Mass Percentage (wt%)		
		177 – 343°C	343 – 524°C	+524°C
<i>1a</i>	E200869	5	91	4
<i>2a</i>	E200870	5	91	4
<i>3a</i>	E200871	5	91	4
<i>4a</i>	E200872	5	90	5
<i>5a</i>	E200873	5	91	4
<i>Vessel Residue</i>	E200874	6	90	4
<i>Time Zero</i> *	E226483 37HVGO	4	91	5

* *Time zero sample analyzed in separate HTSD*

Based on Figure 31 and Table 21, it can be observed that the distillation temperature distributions and recovery mass percentages of the extracts collected in vials *1a* to *5a*, the *vessel residue* sample, and the *time zero* material from Run 26 are all similar. Recalling from earlier discussions, it was strongly suggested that during Runs 26 to 28, the HGO starting material was being directly carried over from the extraction vessel and into the collection vials without being effectively dissolved with the SC-CO₂ first. These speculations were preliminarily supported by the colour and viscosity similarities observed between the extracts collected in Runs 26 to 28 and the HGO starting material (see Figure 30). Furthermore, it was noted in Section 4.1.4 that as the HGO starting sample mass was reduced from 50 g in Run 26 to 25 g in Run 27 and 10 g in Run 28, their respective initial solubilities measured from Runs 26, 27, and 28 were also proportionally reduced as well. This further indicates that a reliable initial solubility may not have been accurately measured for HGO when toluene is added to the SC-CO₂ at 15 mol%. The compositional similarities seen between the extracts and the HGO *time zero* material can further support the possibility that the HGO starting material was being carried over from the extraction vessel and being deposited into the collection vials.

Based on the HTSD from Figure 31, the *time zero* sample first begins distillation at 301°C. By the time a distillation temperature of 735°C is achieved, approximately 94 wt% of its hydrocarbons have been distilled out. Due to limitations of the HTSD instrument utilized, a distillation temperature of higher than 735°C cannot be achieved, and therefore the remaining 6

wt% of the HGO material with boiling temperatures beyond 735°C are not distilled. The *vessel residue* analyzed for Run 26 begins distillation at a temperature of 244°C and by the time a distillation temperature of 735°C is reached, approximately all of the hydrocarbons from the *vessel residue* was distilled out. It should be further noted that the HGO *time zero* material was analyzed on a different day than the *vessel residue* and extracts collected from the “a” vials; this may explain the dissimilarities between the *time zero*, the *vessel residue*, and the extract HTSD curves. Additionally, the analytical inaccuracies of HTSD in detecting extremely heavy hydrocarbons as noted previously can also be a valid factor contributing to the dissimilarities seen in the tail-end of the three sets of HTSD curves.

Photographs of the extracts that were collected from Runs 32, 33, and 34 are displayed in Figure 32 (resid 5 mol% toluene). Unlike Runs 29 to 31 (resid with no toluene addition) where little to no extracts were collected in the “a” vials, Runs 32 to 34 were able to collect a small amount of extracts in the “a” vials that were dark yellow/golden in colour. By comparing the extracts collected from Runs 29 to 31 (resid with no toluene addition) and 32 to 34 (resid with 5 mol% toluene), the results suggest that the 5 mol% of toluene added to the SC-CO₂ was able to largely improve the solubilization of SC-CO₂ with extremely heavy hydrocarbons. As a result of its improved solubility, the heavier hydrocarbons found in resid that were initially insoluble with SC-CO₂ alone during Runs 29 to 31 became more soluble in the SC-CO₂ modified with toluene at a concentration of 5 mol% in Runs 32 to 34. The dark extracts seen in the “a” vials from Runs 32 to 34 can also further suggest that much heavier hydrocarbons were resultantly collected in comparison to the other bitumen cuts that were examined at similar toluene concentrations. Compared to the extracts collected from LGO and HGO when 5 mol% toluene was added to the SC-CO₂, the contents collected during Runs 32 to 34 as shown in Figure 32 had a much smaller mass (see Table 11).

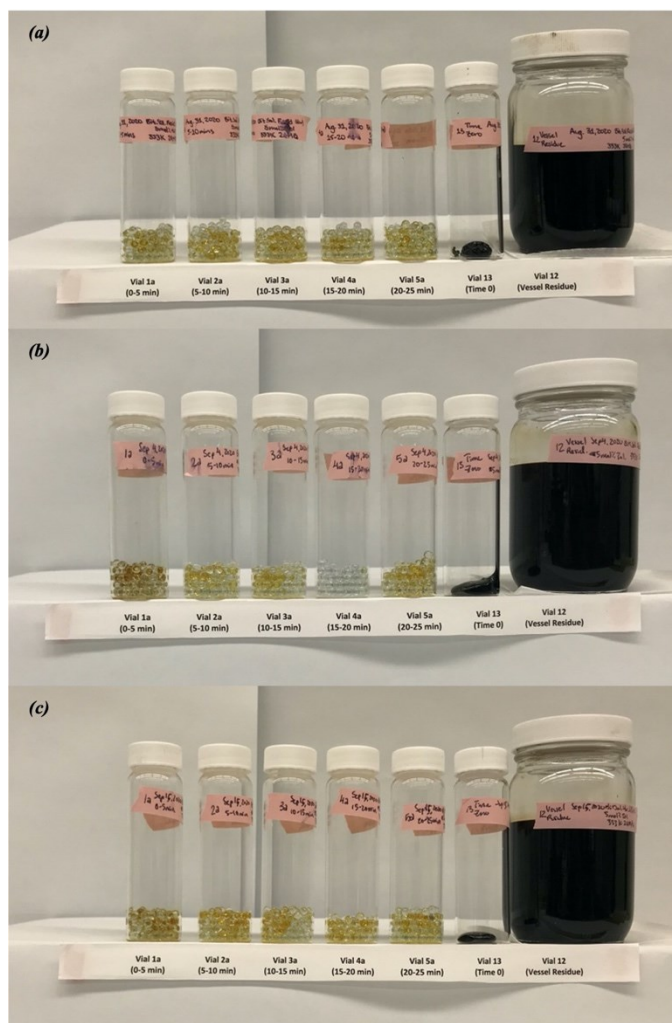


Figure 32. Visual comparison of extracts, starting materials, and vessel residue from initial solubility experiments for resid with SC-CO₂ added with 5 mol% toluene: (a) Run 32, (b) Run 33, and (c) Run 34.

Select extract samples collected in vials *1a*, *2a*, *3a*, *4a*, *5a*, the *time zero* sample, and the *vessel residue* sample from Run 34 were analyzed by HTSD. Figure 33 displays the HTSD curves for the resid *time zero* sample, the extract samples collected in the “a” vials, and the *vessel residue* sample from Run 34. The HTSD curve for whole bitumen is provided for comparison purposes.

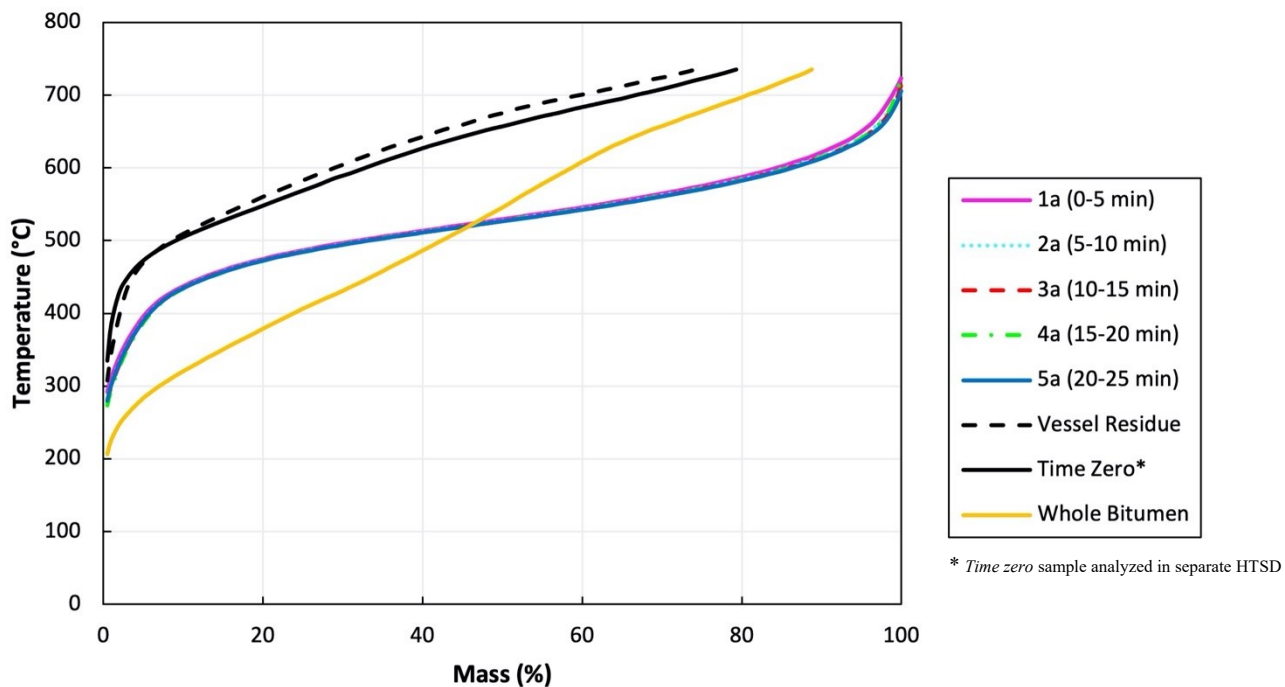


Figure 33. HTSD curves for samples from Run 34 (resid in SC-CO₂ at 333 K, 24 MPa with 5 mol% toluene addition).

Using the information provided in Figure 33, Table 22 details the recovery mass percentages of the hydrocarbons that are distilled at temperature ranges of 177 to 343°C, 343 to 524°C, and +524°C for the extracts collected in vials *1a* to *5a*, the *vessel residue* sample, and the *time zero* resid material. As shown in Table 22, almost all of the hydrocarbons found in the extracts (~ 98 wt%) collected in vials *1a* to *5a* were distilled at moderate to high temperatures of 343°C and beyond. Specifically, almost half (~ 50 wt%) of the hydrocarbons found in the extracts collected from Run 34 have distillation temperatures of greater than 524°C. Only a very small mass percentage (~ 2 wt%) of light hydrocarbons are found in the extracts collected.

Table 22. Recovery mass percentages of hydrocarbons at various distillation temperature ranges from extract, *vessel residue*, and *time zero* samples collected from Run 34 (Resid in SC-CO₂ modified with 5 mol% toluene).

Sample	RAS #	Recovery Mass Percentage (wt%)			
		177 – 343°C	343 – 524°C	524 – 735°C	> 735°C
<i>1a</i>	E200881	2	45	53	0**
<i>2a</i>	E200882	2	45	53	0**
<i>3a</i>	E200883	2	46	52	0**
<i>4a</i>	E200884	2	45	53	0**
<i>5a</i>	E200885	2	46	52	0**
<i>Vessel Residue</i>	E200886	1	12	61	26
<i>Time Zero</i> *	21127	1	14	65	21

* *Time zero sample analyzed in separate HTSD*

** *Normalized to 100 wt% at 735°C*

Based on Figure 33 and Table 22, the recovery mass percentages and distillation temperature ranges for the *vessel residue* sample is similar to the *time zero* resid material. This is largely expected since in theory when initial solubility measurements are performed, the bitumen to CO₂ ratio is infinite such that the dissolution of the bitumen in the SC-CO₂ should not alter the original composition of the bitumen in the SFE system. What is seen in Figure 33 and Table 22 can further suggest that the hydrocarbon compositions from these two samples are alike.

Using the data provided in Figure 33, it can be determined that the *time zero* sample first begins distillation at 335°C. By the time a distillation temperature of 735°C is reached, approximately 80 wt% of its hydrocarbons have been distilled. Due to the limitations of the HTSD instrument utilized, a distillation temperature of higher than 735°C cannot be achieved, and therefore the remaining 20 wt% of the bitumen material with boiling points of over 735°C are not distilled. The *vessel residue* analyzed from Run 34 begins distillation at a temperature of 308°C and by the time a distillation temperature of 735°C is reached, approximately 74 wt% of the hydrocarbon materials from the *vessel residue* have been distilled. The lower recovery mass percentage that was distilled at 735°C and the higher starting distillation temperature can further demonstrate the much heavier hydrocarbon composition that is seen in resid compared to the other bitumen cuts that were examined in this research study. It should be noted that the HTSD analysis of the *time zero* sample was performed on a different date than the “a” vial and *vessel*

residue samples and may explain some differences seen between the *time zero* and *vessel residue* curves.

Photographs of the extracts that were collected from Runs 35, 36, and 37 performed with resid using 15 mol% toluene are displayed in Figure 34. The extracts collected in the “a” vials from Runs 35 to 37 displays a brown/dark red colour and has an oily viscosity; this is distinctively different than the black/dark brown colour of the resid starting material. Compared with the extracts collected during Runs 32 to 34 (resid with 5 mol% toluene addition) and from Runs 29 to 31 (resid with no toluene addition), the extracts sampled during Runs 35 to 37 are darker in colour. The darker colours of these extracts collected can further indicate that heavier hydrocarbons were effectively dissolved with the SC-CO₂ added with 15 mol% of toluene during Runs 35 to 37.

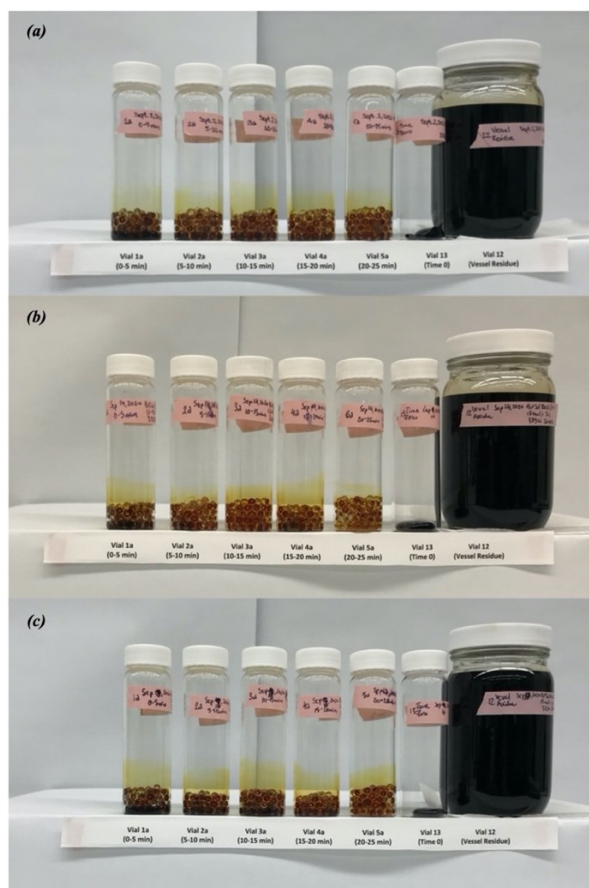


Figure 34. Visual comparison of extracts, starting materials, and vessel residue from initial solubility experiments for resid with SC-CO₂ added with 15 mol% toluene: (a) Run 35, (b) Run 36, and (c) Run 37.

By increasing the toluene concentration from 5 to 15 mol%, the solubilization of the SC-CO₂ was further enhanced so that the heavier hydrocarbons that were initially insoluble with the SC-CO₂ modified with only 5 mol% of toluene would become much more soluble with the SC-CO₂ that was now modified with 15 mol% toluene instead.

Select extract samples collected in vials *1a*, *2a*, *3a*, *4a*, *5a*, the *time zero* sample, and the *vessel residue* sample from Run 35 were analyzed by HTSD. Figure 35 displays the HTSD curves for the resid *time zero* sample, the extract samples collected in the “*a*” vials, and the *vessel residue* from Run 35. The HTSD curve for whole bitumen is provided for comparison purposes.

Using the information provided in Figure 35, Table 23 details the recovery mass percentages of the hydrocarbons that are distilled out at temperature ranges of 177 to 343°C, 343 to 524°C, and +524°C for the extracts collected in vials *1a* to *5a*, the *vessel residue* sample, and the *time zero* resid material. As shown in Table 23, a majority of the hydrocarbons found in the extracts (≥ 98 wt%) collected in vials *1a* to *5a* from Run 35 were distilled at temperatures roughly ranging between 343°C to beyond 524°C. Specifically, around 72 wt% of these extracts were distilled out at higher temperatures of beyond 524°C, while only a very small amount (~ 1 wt%) of the remaining extracts were distilled at lower temperatures of 177 to 343°C. Based on the analysis performed in Table 23, it can be speculated that the extracts collected in vials *1a* to *5a* from Run 35 are made up of mostly heavy to extremely heavy hydrocarbons (~ 72 wt%), some moderate weight hydrocarbons (~ 27 wt%), and very few (or if any) light hydrocarbons (~1 wt%).

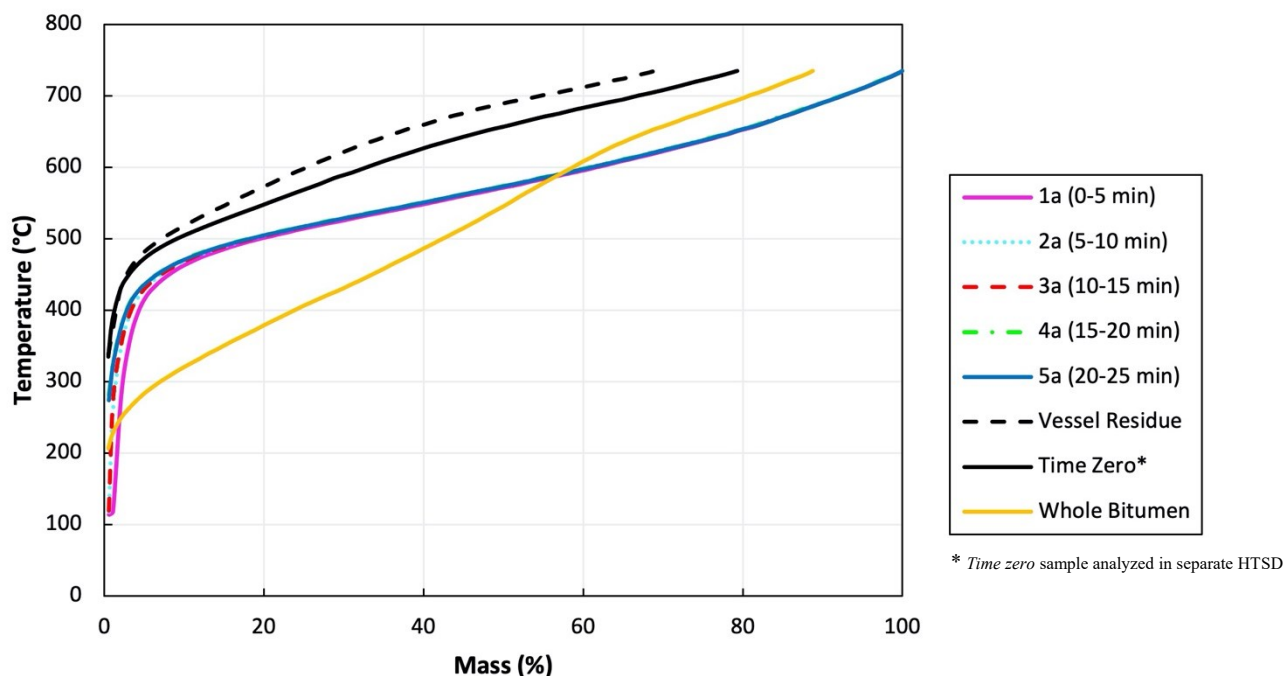


Figure 35. HTSD curves for samples from Run 35 (resid in SC-CO₂ at 333 K, 24 MPa with 15 mol% toluene addition).

Table 23. Recovery mass percentages of hydrocarbons at various distillation temperature ranges from *extract*, *vessel residue*, and *time zero* samples collected from Run 35 (Resid in SC-CO₂ modified with 15 mol% toluene).

Sample	RAS #	Recovery Mass Percentage (wt%)			
		177 – 343°C	343 – 524°C	524 – 735°C	> 735°C
<i>1a</i>	E200875	2	27	71	0**
<i>2a</i>	E200876	1	27	72	0**
<i>3a</i>	E200877	1	27	72	0**
<i>4a</i>	E200878	1	26	73	0**
<i>5a</i>	E200879	1	27	72	0**
<i>Vessel Residue</i>	E200880	1	10	58	31
<i>Time Zero*</i>	21127	1	14	65	21

* *Time zero sample analyzed in separate HTSD*

** *Normalized to 100 wt% at 735°C*

Compared to the extracts collected in vials *1a* to *5a* from Run 34 when only 5 mol% of toluene was added to the SC-CO₂, the extracts collected during Run 35 contains less moderately

weight hydrocarbons with distillation temperatures ranging between 343 to 524°C (from ~ 45 wt% in Run 34 to ~ 27 wt% in Run 35), more heavy hydrocarbons with distillation temperatures beyond 524°C (from ~ 53 wt% in Run 34 to ~72 wt% in Run 35), and a relatively small amount (1 to 2 wt%) of light hydrocarbons. Overall, the hydrocarbon composition of the extracts sampled during Run 35 saw an increase in the mass percentage of heavier hydrocarbons that were collected and a decrease in the mass percentage of moderately weight hydrocarbons that were sampled when compared to the extracts from Run 34. This shift in hydrocarbon composition between the two runs can be largely attributed to the toluene concentration increase from 5 to 15 mol% that was added to the SC-CO₂. With the added toluene concentration, the solubilization of the SC-CO₂ with the heavier hydrocarbons that were initially insoluble with SC-CO₂ that was only modified by 5 mol% of toluene became much more soluble when 15 mol% of toluene was added to the SCF instead. This closely corresponds with the findings of Al-Sabawi et al. (2011) and Hwang and Ortiz (2000) where it was determined that when modifiers are added to SCFs, heavier hydrocarbons were able to be extracted as a result.

Based on Figure 35 and Table 23, the recovery mass percentages and distillation temperature ranges for the *vessel residue* sample is similar to the *time zero* resid material. This is largely expected since in theory when initial solubility measurements are performed, the bitumen to CO₂ ratio is infinite such that the dissolution of the bitumen in the SC-CO₂ should not alter the original composition of the bitumen in the SFE system. What is seen in Figure 35 and Table 23 can suggest that the hydrocarbon compositions from these two samples are similar.

Based on the HTSD from Figure 35, the *time zero* sample first begins distillation at 335°C. By the time a distillation temperature of 735°C is reached, approximately 80 wt% of its hydrocarbons have been distilled out. Due to limitations of the HTSD instrument utilized, a distillation temperature of greater than 735°C cannot be reached, and therefore the remaining 20 wt% of the resid material with boiling points of over 735°C are not distilled. The *vessel residue* analyzed from Run 35 begins distillation at a temperature of 338°C and by the time a distillation temperature of 735°C is reached, only 69 wt% of the hydrocarbon materials from the *vessel residue* have been distilled out. Based on Table 23, the minor mass percentage differences seen between the *vessel residue* and the *time zero* samples from Run 35 are more noticeable in the 177 to 343°C and +524°C temperature ranges. It has been indicated by Syncrude that the HTSD method utilized lacks accuracy when analyzing extremely light and heavy hydrocarbons.

Therefore, the slight mass percentage differences noticed in the 177 to 343°C and +524°C temperature ranges may be attributed to the inaccuracies of the analytical method. It should be noted that the HTSD analysis of the *time zero* sample was performed on a different date than the “a” vial and *vessel residue* samples.

CHAPTER 5: CONCLUSIONS AND RECOMMENDATIONS

5.1 Conclusions

The research study performed for this thesis measured the initial solubilities of whole bitumen and the bitumen cuts of LGO, HGO, and resid with SC-CO₂ modified with toluene (0, 5, and 15 mol%). The initial solubility measurements were performed at a pressure of 24 MPa and a temperature of 333 K (density of SC-CO₂ was maintained at 0.78 g/mL). Additionally, the research study further analyzed the hydrocarbons that were dissolved with SC-CO₂ by HTSD analysis for all experiments conducted.

The research study performed has answered the objectives established in Chapter 1:

1. The average initial solubility measured for whole bitumen at a SC-CO₂ density of 0.78 g/mL with no toluene added was 1.3×10^{-2} g/g. The average initial solubilities measured for the bitumen cuts of LGO, HGO, and resid at a SC-CO₂ density of 0.78 g/mL with no toluene modifier added were 8.7×10^{-2} , 1.1×10^{-2} , and 5.9×10^{-4} g/g, respectively. Of the three bitumen cuts examined, LGO had the highest average initial solubility at the given experimental conditions when no toluene was added, while resid measured the lowest average initial solubility.
2. The average initial solubility measured for whole bitumen at a SC-CO₂ density of 0.78 g/mL with 5 mol% of toluene added was 3.5×10^{-2} g/g. When 15 mol% of toluene was added, the initial solubility measured for whole bitumen increased to 1.1×10^{-1} g/g. The average initial solubilities measured for the bitumen cuts of HGO and resid at a SC-CO₂ density of 0.78 g/mL with 5 mol% of toluene added were 4.5×10^{-2} and 5.6×10^{-3} g/g, respectively. Due to limitations of the SFE system used in this research study, the initial solubilities for LGO with SC-CO₂ modified with toluene at 5 mol% could not be reliably measured. When the toluene concentration was increased to 15 mol%, the average initial solubility measured for resid was increased to 2.4×10^{-2} g/g. Due to technical limitations of the SFE system utilized in this study, the initial solubilities for HGO with SC-CO₂ modified with toluene at 15 mol% were unreliably measured. In general, higher initial solubilities were measured in the whole bitumen and selected

bitumen cut samples when the toluene concentrations added to the SC-CO₂ were increased.

3. Extracts obtained from initial solubility experiments with SC-CO₂ only for whole bitumen and bitumen cuts of LGO and HGO contained light hydrocarbons. No extracts were successfully analyzed for initial solubility experiments with SC-CO₂ only and resid. When SC-CO₂ was modified with increasingly higher concentrations of toluene, extracts obtained from initial solubility experiments with whole bitumen and the bitumen cuts of LGO, HGO, and resid generally contained heavier hydrocarbons.

5.2 Recommendations

Recommendations pertaining to the research conducted in this thesis includes:

1. Utilization of a view cell to better visualize how the bitumen-rich phase of LGO and HGO behaves with SC-CO₂ at the experimental conditions of 333 K and 24 MPa. Specifically, a better understanding of the LGO and HGO behaviour with SC-CO₂ modified with 5 and 15 mol% toluene would be of interest to examine.
2. Measuring the initial solubilities of a larger number of bitumen cuts that are distilled from whole bitumen at narrower temperature ranges. Measuring the initial solubilities of more bitumen cuts can provide a more comprehensive characterization of the complex bitumen mixture.
3. Investigating the initial solubilities of bitumen cuts at additional pressure and temperature conditions and using different modifiers.

REFERENCES

- Abu-Khader, M.M, and Speight, J.G. 2007. Influence of high asphaltene feedstocks on processing. *Oil and Gas Science and Technology*, **62**(5): 715-722.
- Abusaid, A., Fear, C., McRoberts, E., and Wells, S. 2011. An update to the construction of the Suncor oil sands tailings Pond 5 cover. *In Proceedings Tailings and Mine Waste 2011*, Vancouver, BC., 6-9 November 2011. Tailings and Mine Waste Conference.
- Akgerman, A. 1997. Supercritical fluids in environmental remediation and pollution prevention. *In Supercritical fluid: Extraction and pollution prevention. Edited by M.A. Abraham and A.K. Sunol*. American Chemical Society, Washington, DC. pp. 208-231.
- Alberta Energy Regulator (AER). 2019. Tailings. Available from <https://www.aer.ca/providing-information/by-topic/tailings> [accessed 15 June 2019].
- Alberta Geological Survey (AGS). 2017. Mountain Building and the Alberta Basin. Available from <https://ags.aer.ca/activities/mountain-building-and-the-alberta-basin.htm> [accessed 15 June 2019].
- Alberta Innovates. 2017. Solvent Assisted and Solvent-Based Extraction for Surface Mined Oil Sands: Workshop 2, Solvent Leadership Series. Available from <https://albertainnovates.ca/wp-content/uploads/2019/03/Solvent-Leadership-Series-Workshop-2.pdf> [accessed 27 June 2019].
- Allawzi, M., Al-Otoom, A., Allaboun, H., Ajlouni, A., and Al Nseirat, F. 2011. CO₂ supercritical fluid extraction of Jordanian oil shale utilizing different co-solvents. *Fuel Processing Technology*, **92**: 2016-2023.

- Allen, E.W. 2008. Process water treatment in Canada's oil sands industry: I: Target pollutants and treatment objectives. *Journal of Environmental Engineering and Science*, **7**(2): 123-138.
- Al-Marzouqi, A.H., Zekri, A.Y., Jobe, B., and Dowaidar, A. 2007. Supercritical fluid extraction for the determination of optimum oil recovery conditions. *Journal of Petroleum Science and Engineering*, **55**(1-2): 37-47.
- Al-Marzouqi, A.H., Zekri, A.Y., Azzam, A.A., and Dowaidar, A. 2009. Hydrocarbon recovery from porous media using supercritical fluid extraction. *Journal of Porous Media*, **12**(6): 489-500.
- Al-Sabawi, M., Seth, D., and de Bruijn, T. 2011. Effect of modifiers in n-pentane on the supercritical extraction of Athabasca bitumen. *Fuel Processing Technology*, **92**(10): 1929-1938.
- Alvarez, J., and Han, S. 2013. Current overview of cyclic steam injection process. *Journal of Petroleum Science Research*, **2**(3): 116-127.
- American Society for Testing Materials (ASTM) International. 2011. Standard test method for boiling point distribution of samples with residues such as crude oils and atmospheric and vacuum residues by high temperature gas chromatography (D7169). American Society for Testing Materials International, West Conshohocken, P.A.
- Arai, Y., Sako, T., and Takebayashi, Y. 2002. Supercritical Fluids: Molecular Interactions, Physical Properties, and New Applications. *In Materials Processing*. Springer Series: Springer – Verlag Berlin Heidelberg, New York, NY.
- Aristizábal, J.J.G., and Vargas, J.L.G. 2005. Modeling segregated insitu combustion processes through a vertical displacement model applied to a Colombian field. *Ciencia Tecnología y Futuro*, **3**(1): 111-126.

- Australian Government. 2018. Ethyl acetate. Available from <http://www.npi.gov.au/resource/ethyl-acetate> [accessed 8 July 2019].
- Autoclave Engineers. 2002. Engineering data book for bolted closure assembly. Autoclave Engineers, Division of Snap-tite Inc., Erie, PA.
- Bacon, R. and Tordo, S. 2005. Crude Oil Price Differentials and Differences in Oil Qualities: A Statistical Analysis, Joint UNDP/World Bank Energy Sector Management Assistance Program (ESMAP). Available from https://www.esmap.org/sites/default/files/esmap-files/08105.Technical%20Paper_Crude%20Oil%20Price%20Differentials%20and%20Differences%20in%20Oil%20Qualities%20A%20Statistical%20Analysis.pdf [accessed 21 May 2019].
- Banerjee, D.K. 2012. Oil sands, heavy oil and bitumen: from recovery to refinery. PennWell Corporation, Tulsa, Oklahoma.
- Bian, X., Du, Z., and Tang, Y. 2011. An improved density-based model for the solubility of some compounds in supercritical carbon dioxide. *Thermochimica Acta*, **519**(1-2): 16-21.
- Brunner, G. 1994. Gas Extraction: An Introduction to Fundamentals of Supercritical Fluids and the Application to Separation Processes, Vol. 4. Springer-Verlag Berlin Heidelberg, New York, NY.
- Brunner, G. 2005. Supercritical fluids: Technology and application to food processing. *Journal of Food Engineering*, **67**(1-2): 21-33.
- Cabrera, S.C.M. 2008. Characterization of Oil Sands Tailings Using Low Field Nuclear Magnetic Resonance (NMR) Technique. M.Sc. thesis, Department of Chemical and Petroleum Engineering, University of Calgary, Calgary, AB.

- Canada's Oil Sands Innovation Alliance (COSIA). n.d.a. Carbon dioxide amended tailings. Available from <https://www.cosia.ca/initiatives/tailings/projects/carbon-dioxide-amended-tailings> [accessed 3 January 2021].
- Canada's Oil Sands Innovation Alliance (COSIA). n.d.b. Tailings centrifugation. Available from <https://www.cosia.ca/initiatives/tailings/projects/tailings-centrifuge> [accessed 3 January 2021].
- Canadian Association of Petroleum Producers (CAPP). 2018. Oil Sands. Available from <https://www.capp.ca/canadian-oil-and-natural-gas/oil-sands> [accessed 5 June 2019].
- Canadian Association of Petroleum Producers (CAPP). 2020. Uses for Oil. Available from <https://www.capp.ca/oil/uses-for-oil/> [accessed 22 November 2020].
- Cansell, F., and Rey, S. 1998. Thermodynamic aspects of supercritical fluids processing: Applications of polymers and waste treatment. *Revue de L'Institut Français du Pétrole*, **53**(1): 71-98.
- Cant, D.J., and Stockmal, G.S. 1989. The Alberta foreland basin: relationship between stratigraphy and Cordilleran terrane-accretion events. *Canadian Journal of Earth Sciences*, **26**(10): 1964-1975.
- Chalaturnyk, R.J., Scott, J.D., and Özü, B. 2002. Management of oil sands tailings. *Petroleum Science and Technology*, **20**(9-10): 1025-1046.
- Chandra, A., and Nair, M.G. 1997. Supercritical fluid carbon dioxide extraction of α - and β -Carotene from carrot (*Daucus carota* L.). *Photochemical Analysis*, **8**(5): 244-246.
- Chow, D.L., Nasr, T.N., Chow, R.S., and Sawatzky, R.P. 2008. Recovery techniques for Canada's heavy oil and bitumen resources. *Journal of Canadian Petroleum Technology*, **47**(5): 12-17.

- Chrastil, J. 1982. Solubility of solids and liquids in supercritical gases. *The Journal of Physical Chemistry*, **86**(15): 3016-3021.
- Chung, K.H., Xu, C., Hu, Y., and Wang, R. 1997. Supercritical fluid extraction reveals resid properties. *Oil and Gas Journal*, **95**(3): 66-69.
- Clark, K.A., and Pasternack, D.S. 1932. Hot water separation of bitumen from Alberta bituminous sand. *Industrial and Engineering Chemistry*, **24**(12): 1410-1416.
- Clemente, J. 2015. Three Reasons Oil Will Continue to Run the World. Available from <https://www.forbes.com/sites/judeclemente/2015/04/19/three-reasons-oil-will-continue-to-run-the-world/?sh=6000aaf643f9> [accessed 5 September 2020].
- Cossey, H.L. 2018. Extraction of Hydrocarbons from Bitumen and Bitumen-containing Process and Process Waste Streams Using Supercritical Carbon Dioxide. M.Sc. thesis, Department of Civil and Environmental Engineering, University of Alberta, Edmonton, AB.
- Cossey, H.L., Guigard, S.E., Underwood, E., Stiver, W.H., McMillan, J., and Bhattacharya, S. 2019. Supercritical fluid extraction of bitumen using chemically modified carbon dioxide. *The Journal of Supercritical Fluids*, **154**: 104599.
- Curtis, C., Kopper, R., Decoster, E., Guzman-Garcia, A., Huggins, C., Knauer, L., Minner, M., Kupsch, N., Linares, L.M., Rough, H., and Waite, M. 2002. Heavy-oil reservoirs. *Oilfield Review*, **14**(3): 30-51.
- DeCelles, P.G., and Giles, K.A. 1996. Foreland basin systems. *Basin Research*, **8**(2): 105-123.
- De Marco, I., Riemma, S., and Iannone, R. 2017. Supercritical carbon dioxide decaffeination process: A life cycle assessment study. *Chemical Engineering Transactions*, **57**: 1699-1704.

- Denney, D. 1997. Steam-assisted gravity-drainage and Vapex process reservoir screening. *Journal of Petroleum Technology*, **49**(10): 1122-1124.
- Deo, M.D., Hwang, J., and Hanson, F.V. 1992. Supercritical fluid extraction of a crude oil, bitumen-derived liquid and bitumen by carbon dioxide and propane. *Fuel*, **71**(12): 1519-1526.
- De Zordi, N., Cortesi, A., Kikic, I., Moneghini, M., and Solinas, D. 2014. Pharmaceutical and Nutraceutical Applications of Supercritical Carbon Dioxide. *In Handbook on Supercritical Fluids: Fundamentals, Properties and Applications. Edited by J. Osborne.* Nova Science Publishers, Hauppauge, NY. pp. 79-103.
- Eastick, R.R., Svrcek, W.Y., and Mehrotra, A.K. 1992. Phase behavior of CO₂-bitumen fractions. *The Canadian Journal of Chemical Engineering*, **70**(1): 159-164.
- El-Haj, R., Lohi, A., and Upreti, S.R. 2009. Experimental determination of butane dispersion in vapor extraction of heavy oil and bitumen. *Journal of Petroleum Science and Engineering*, **67**(2009): 41-47.
- Eschard, R., and Huc, A.Y. 2008. Habitat of biodegraded heavy oils: Industrial implications. *Oil and Gas Science and Technology*, **63**(5): 587-607.
- Færgestad, I. 2016. Heavy Oil, Schlumberger. Available from https://pdfs.semanticscholar.org/d9a7/4d08759ff3529b65906639e371745efae5f7.pdf?_ga=2.39070691.196985900.1563385044-72539752.1561514157 [accessed 23 May 2019].
- Fang, Y. 2010. Extraction of Hydrocarbons from Oil Sand Using Supercritical Carbon Dioxide. M.Sc. thesis, Department of Civil and Environmental Engineering, University of Alberta, Edmonton, AB.

- García-Casas, I., Montes, A., Valor, D., Pereyra, C., and Martínez de la Ossa, E.J. 2018. Impregnation of mesoporous silica with mangiferin using supercritical CO₂. *Journal of Supercritical Fluids*, **140**: 129-136.
- Geranmayeh, A., Mowla, A., Rajaei, H., Esmailzadeh, F., and Kaljahi, J.F. 2012. Extraction of hydrocarbons from contaminated soil of Pazanan II production unit by supercritical carbon dioxide. *The Journal of Supercritical Fluids*, **72**: 298-304.
- Gordon, D. 2012. *Understanding Unconventional Oil*. Carnegie Endowment for International Peace. Available from <https://carnegieendowment.org/2012/05/03/understanding-unconventional-oil-pub-48007> [accessed 20 May 2019].
- Government of Alberta. 2017. *Oil Sands Facts and Stats*. Available from <https://open.alberta.ca/dataset/b6f2d99e-30f8-4194-b7eb-76039e9be4d2/resource/063e27cc-b6d1-4dae-8356-44e27304ef78/download/fsoilsands.pdf> [accessed 4 June 2019].
- Government of Alberta. 2019a. *The Formation of Oil Sands*. Available from <http://www.history.alberta.ca/energyheritage/sands/origins/the-geology-of-the-oil-sands/the-formation-of-oil-sands.aspx> [accessed 5 June 2019].
- Government of Alberta. 2019b. *Economic Dashboard: Oil Production*. Available from <https://economicdashboard.alberta.ca/OilProduction#typeGraphPie> [accessed 6 June 2019].
- Government of Alberta. 2019c. *The Location of Oil Sands*. Available from <http://history.alberta.ca/energyheritage/sands/origins/the-geology-of-the-oil-sands/the-location-of-oil-sands.aspx> [accessed 6 June 2019].

- Government of Alberta. 2019d. The Composition of Oil Sands. Available from <http://history.alberta.ca/energyheritage/sands/origins/the-geology-of-the-oil-sands/the-composition-of-oil-sands.aspx> [accessed 6 June 2019].
- Government of Alberta. 2020. High-Pressure Injection Wounds. Available from <https://myhealth.alberta.ca/Health/Pages/conditions.aspx?hwid=tm6523> [accessed 13 January 2020].
- Government of British Columbia. 2019. Conventional versus Unconventional Oil and Gas. Available from <https://www2.gov.bc.ca/gov/content/industry/natural-gas-oil/petroleum-geoscience/pet-geol-conv-uncon> [accessed 6 June 2019].
- Government of Canada. 2020. Crude Oil Facts. Available from <https://www.nrcan.gc.ca/science-data/data-analysis/energy-data-analysis/energy-facts/crude-oil-facts/20064#L8> [accessed 14 September 2020].
- Gray, M.R. 2001. Tutorial on Upgrading of Oilsands Bitumen. Available from <https://sites.ualberta.ca/~gray/Library/Tutorials/Upgrading/> [accessed 23 June 2019].
- Gray, M.R. 2015. Upgrading oilsands bitumen and heavy oil. The University of Alberta Press, Edmonton, Alberta.
- Guiliano, M., Boukir, A., Doumenq, P., Mille, G., Crampon, C., Badens, E., and Charbit, G. 2000. Supercritical fluid extraction of Bal 150 crude oil asphaltenes. *Energy and Fuels*, **14**(1): 89-94.
- Gupta, R.B., and Shim, J.J. 2007. Solubility in Supercritical Carbon Dioxide. CRC Press, Taylor Francis Group, Boca Raton, FL.
- Haghighat, P., and Maini, B.B. 2010. Role of asphaltene precipitation in VAPEX process. *Journal of Canadian Petroleum Technology*, **49**(3): 14-21.

- Halliburton. 2018. What Makes Heavy Oil “Heavy”. Available from <https://www.halliburton.com/en-US/ps/solutions/heavy-oil/what-makes-heavy-oil-heavy.html> [accessed 1 June 2019].
- He, L., Li, X., Wu, G., Lin, F., and Sui, H. 2013. Distribution of saturates, aromatics resins, and asphaltenes fractions in the bituminous layer of Athabasca oil sands. *Energy and Fuels*, **27**(8): 4677-4683.
- Head, I.M., Jones, D.M., and Larter, S.R. 2003. Biological activity in the deep subsurface and the origin of heavy oil. *Nature*, **426**(6964): 344-352.
- Heins, W., and Peterson, D. 2003. Use of evaporation for heavy oil produced water treatment. *In* Proceedings of the Canadian International Petroleum Conference, Calgary, AB., 10-12 June 2003. Canadian International Petroleum Conference.
- Herrero, M., Cifuentes, A., and Ibañez, E. 2006. Sub – and supercritical fluid extraction of functional ingredients from different natural sources: Plants, food-by-products, algae and microalgae – A review. *Food Chemistry*, **98**(1): 136-148.
- Holly, C., Mader, M., Soni, S., and Toor, J. 2016. Oil Sands Production Profile: 2004-2014. Alberta Energy, Energy Technical Services, Resources Development Policy Division, Edmonton, AB.
- Huang, S.H., and Radosz, M. 1990. Phase behavior of reservoir fluids II: Supercritical carbon dioxide and bitumen fractions. *Fluid Phase Equilibria*, **60**(1-2): 81-98.
- Husky Energy. 2011. Oil Sands Water De-oiling: Challenges and Innovation. Available from <https://huskyenergy.com/downloads/InvestorRelations/Presentations/Oil-Sands-Water-De-Oiling-2011.pdf> [accessed 20 June 2019].

- Hwang, R.J., and Ortiz, J. 1998. Effect of CO₂ flood on geochemistry of McElroy oil. *Organic Geochemistry*, **29**(1-3): 485-503.
- Hwang, R.J., and Ortiz, J. 2000. Mitigation of asphaltics deposition during CO₂ flood by enhancing CO₂ solvency with chemical modifiers. *Organic Geochemistry*, **31**: 1451-1462.
- Hyndman, A.W., and Luhning, R.W. 1991. Recovery and upgrading of bitumen and heavy oil in Canada. *Journal of Canadian Petroleum Technology*, **30**(2): 61-71.
- Ikebe, H., Yokohata, H., Sakurai, M., and Morita, T. 2010. Method of produced water treatment, method of water reuse, and systems for these methods. US 2010/0264068 A1.
- International Energy Agency (IEA). 2011. World Energy Outlook 2011. Available from <https://www.iea.org/reports/world-energy-outlook-2011> [accessed 21 May 2019].
- Jaremko, D. 2017. MEG seeks to expand eMVAPEx oilsands propane-injection plant. Available from <https://www.jwnenergy.com/article/2017/3/27/meg-seeks-expand-emvapex-oilsands-propane-injectio/> [accessed 27 June 2019].
- Jones, C.H., Farmer, G.L., Sageman, B., and Zhong, S. 2011. Hydrodynamic mechanism for the Laramide orogeny. *Geosphere*, **7**(1): 183-201.
- Kariznovi, M., Nourozieh, H., and Abedi, J. 2010. Bitumen characterization and pseudocomponents determination for equation of state modeling. *Energy Fuels*, **24**(1): 624-633.
- Kasperski, K.L. 1992. A review of properties and treatment of oil sands tailings. *AOSTRA Journal of Research*, **8**(1): 11-53.

- Kasperski, K.L., and Mikula, R.J. 2011. Waste streams of mined oil sands: Characteristics and remediation, *Elements*, **7**(6): 387-392.
- Khaw, K.Y., Parat, M.O., Shaw, P.N., and Falconer, J.R. 2017. Solvent supercritical fluid technologies to extract bioactive compounds from natural sources: A review. *Molecules*, **22**(7): 1186-1208.
- King, J.W., Eller, F.J., Snyder, J.M., Johnson, J.H., McKeith, F.K., and Stites, C.R. 1996. Extraction of fat from ground beef for nutrients analysis using analytical supercritical fluid extraction. *Journal of Agricultural and Food Chemistry*, **44**(9): 2700-2704.
- Knox, D.E. 2005. Solubilities in supercritical fluids. *Pure and Applied Chemistry*, **77**(3): 513-530.
- Koots, J.A., and Speight, J.G. 1975. Relation of petroleum resins to asphaltenes. *Fuel*, **54**(3): 179-184.
- Kulkarni, M.M., and Rao, D.N. 2004. Analysis of the novel Toe-To-Heel Air Injection (THAI) process using simple analytical models. *In Proceedings of the AIChE Annual Meeting*, Austin, TX., 7-12 November 2004. Louisiana State University, Baton Rouge, LA, pp. 3779-3800.
- Kumar, R., Mahalingam, H., and Tiwari, K.K. 2014. Selection of solvent in supercritical antisolvent process. *APCBEE Procedia*, **9**: 181-186.
- La, H., and Guigard, S.E. 2015. Extraction of hydrocarbons from Athabasca oil sand slurry using supercritical carbon dioxide. *The Journal of Supercritical Fluids*, **100**(1): 146-154.
- Laitinen, A., Michaux, A., and Aaltonen, O. 1994. Soil cleaning by carbon dioxide extraction: A review. *Environmental Technology*, **15**(8): 715-727.

- Li, N., Yan, B., and Xiao, X.-M. 2015. A review of laboratory-scale research on upgrading heavy oil in supercritical water. *Energies*, **8**(8): 8962-8989.
- Lin, Y., Smart, N.G., and Wai, C.M. 1995. Supercritical fluid extraction and chromatography of metal chelates and organometallic compounds. *TrAC Trends in Analytical Chemistry*, **14**(3): 123-133.
- Low, G.K.C., and Duffy, G.J. 1995. Supercritical fluid extraction of petroleum hydrocarbons from contaminated soils. *Trends in Analytical Chemistry*, **14**: 218-225.
- Magomedov, R.N., Pripakhaylo, A.V., and Maryutina, T.A. 2017. Solvent demetalization of heavy petroleum feedstock using supercritical carbon dioxide with modifiers. *The Journal of Supercritical Fluids*, **119**: 150-158.
- Manivannan, G., and Sawan, S.P. 1998. The Supercritical State. *In Supercritical Fluid Cleaning – Fundamentals, Technology, and Applications. Edited by J. McHardy and S.P. Sawan.* Noyes Publications, Westwood, NJ. pp. 1-21.
- McHugh, M.A., and Krukonis, V.J. 1994. *Supercritical Fluid Extraction: Principles and Practice*, 2nd ed. Butterworth – Heinemann: Newton, MA.
- Mohamed, R.S., Neves, G.B.M., and Kieckbusch, T.G. 1998. Reduction in cholesterol and fractionation of butter oil using supercritical CO₂ with adsorption on alumina. *International Journal of Food Science and Technology*, **33**(5): 445-454.
- Mokrys, I.J., and Butler, R.M. 1993. In-situ upgrading of heavy oils and bitumen by propane deasphalting: The Vapex process. *In Proceedings of the Production Operations Symposium, Oklahoma City, OK., 21-23 March 1993.* University of Calgary, Calgary, Alberta, pp. 409-424.

- Morgan, G. 2016. Changing the way crude is extracted from the oilsands is a daunting task but this entrepreneur believes his solution works. Financial Post. Available from <https://financialpost.com/entrepreneur/fp-startups/change-the-way-crude-is-extracted-from-the-oilsands-is-daunting-task-but-this-entrepreneur-believes-his-solution-works> [accessed 24 June 2019].
- Morselli, L., Setti, L., Iannuccilli, A., Maly, S., Dinelli, G., and Quattroni, G. 1999. Supercritical fluid extraction for the determination of petroleum hydrocarbons in soil. *Journal of Chromatography A*, **845**(1-2): 357-363.
- Mossop, G.D. 1980. Geology of the Athabasca oil sands. *Science*, **207**(4427): 145-152.
- Moussa, T. 2019. Performance and economic analysis of SAGD and VAPEX recovery processes. *Arabian Journal for Science and Engineering*, **2019**(44): 6139-6153.
- Nagpal, V., and Guigard, S.E. 2005. Remediation of flare pit soils using supercritical fluid extraction. *Journal of Environmental Engineering and Science*, **4**(5): 307-318.
- Nasr, T.N., and Ayodele, O.R. 2005. Thermal techniques for the recovery of heavy oil and bitumen. *In Proceedings of the SPE International Improved Oil Recovery Conference in Asia Pacific, Kuala Lumpur, Malaysia, 5-6 December 2005. Society of Petroleum Engineers*, pp. 87-101.
- Palmer, M.V., and Ting, S.S.T. 1995. Applications for supercritical-fluid technology in food processing. *Food Chemistry*, **52**(4): 345-352.
- Phelps, C.L., Smart, N.G., and Wai, C.M. 1996. Past, present and possible future applications of supercritical fluid extraction technology. *Journal of Chemical Education*, **73**(12): 1163-1168.

National Aeronautics and Space Administration (NASA). 2019. Folding a Mountain, NASA Earth Observatory. Available from <https://earthobservatory.nasa.gov/images/145002/folding-a-mountain> [accessed 1 June 2019].

National Energy Board (NEB). 2000. Canada's Oil Sands: A Supply and Market Outlook to 2015. Available from the National Energy Board of Canada, Calgary, AB. Cat. No. – NE23-89/2000E.

National Institute of Standards and Technology (NIST). 2018. Thermophysical Properties of Fluid Systems. Available from <https://webbook.nist.gov/chemistry/fluid/> [accessed 10 October 2020].

Natural Resources Canada (NRCAN). 2018. Refining Economics. Available from <https://www.nrcan.gc.ca/energy/energy-sources-distribution/refinery-economics/4561> [accessed 21 May 2019].

Natural Resources Canada (NRCAN). 2019a. What are the oil sands? Available from <https://www.nrcan.gc.ca/our-natural-resources/energy-sources-distribution/clean-fossil-fuels/what-are-oil-sands/18089> [accessed 6 June 2019].

Natural Resources Canada (NRCAN). 2019b. 7 facts on the oil sands and the environment. Available from <https://www.nrcan.gc.ca/our-natural-resources/energy-sources-distribution/clean-fossil-fuels/7-facts-oil-sands-and-environment/18091> [accessed 13 June 2019].

Oil Sands Magazine. 2019a. Surface Mining Techniques Used in the Oil Sands. Available from <https://www.oilsandsmagazine.com/technical/mining/surface-mining> [accessed 10 June 2019].

- Oil Sands Magazine. 2019b. Primary Separation Cells. Available from <https://www.oilsandsmagazine.com/technical/mining/extraction/psc-primary-separation-cell> [accessed 12 June 2019].
- Oil Sands Magazine. 2020. Bitumen Upgrading Explained. Available from <https://www.oilsandsmagazine.com/technical/bitumen-upgrading> [accessed 12 July 2020].
- Palmer, M.V., and Ting, S.S.T. 1995. Applications for supercritical-fluid technology in food processing. *Food Chemistry*, **52**(4): 345-352.
- Paszkievicz, L. 2012. Extra Heavy Oils in the World Energy Supply. Total S.A. Available from <http://www.oilproduction.net/files/extra-heavy-oils-in-the-world-energy-supply.pdf> [accessed 24 May 2019].
- Pembina Institute. 2017. Statements of concern on tailings ponds solutions. Available from <https://www.pembina.org/pub/statements-of-concern-on-tailings-ponds-solutions> [accessed 15 June 2019].
- Petroleum Services Association of Canada (PSAC). 2019. Conventional vs. Unconventional Resources. Available from <https://oilandgasinfo.ca/patchworks/conventional-vs-unconventional-resources/> [accessed 20 May 2019].
- Phelps, C.L., Smart, N.G., and Wai, C.M. 1996. Past, present and possible future applications of supercritical fluid extraction technology. *Journal of Chemical Education*, **73**(12): 1163-1168.
- Pitchaiah, K.C., Lamba, N., Deepitha, J., Mohapatra, P.K., Madras, G., and Sivaraman, N. 2019. Experimental measurements and correlation of the solubility of N,N-dialkylamides in supercritical carbon dioxide. *The Journal of Supercritical Fluids*, **143**: 162-170.

- Plotka-Wasyłka, J., Rutkowska, M., Owczarek, K., Tobiszewski, M., and Namieśnik, J. 2017. Extraction with environmentally friendly solvents. *Trends in Analytical Chemistry*, **91**: 12-25.
- Quagraine, E.K., Headley, J.V., and Peterson, H.G. 2005. Is biodegradation of bitumen a source of recalcitrant naphthenic acid mixtures in oil sands tailing pond waters? *Journal of Environmental Science and Health*, **40**(3): 671-684.
- Quinlan, P.J., and Tam, K.C. 2015. Water treatment technologies for the remediation of naphthenic acids in oil sands process-affected water. *Chemical Engineering Journal*, **279**: 696-714.
- Rao, F., and Liu, Q. 2013. Froth treatment in Athabasca oil sands bitumen recovery process: A review. *Energy and Fuels*, **27**(12): 7199-7207.
- Raynie, D.E. 1997. Meeting the natural products challenge with supercritical fluids. *In* *Supercritical fluids: Extraction and pollution prevention*. Edited by M.A. Abraham and A.K. Sunol. American Chemical Society, Washington, DC. pp. 68-75.
- Romaniuk, N., Mehranfar, M., Selani, H., Ozum, B., Tate, M.J., and Scott, J.D. 2015. Residual bitumen recovery from oil sand tailings with lime. *Tailings and Mine Waste Conference*, Vancouver, BC, 25-28 October 2015.
- Roodpeyma, M. 2017. Development, Modelling and Control of a Continuous Pilot Scale Supercritical Fluid Extraction Process. Ph.D. thesis, Department of Civil and Environmental Engineering, University of Alberta, Edmonton, AB.
- Rose, J.L., Svreck, W.Y., and Minnery, W.D. 2000. Fractionation of Peace River bitumen using supercritical ethane and carbon dioxide. *Industrial and Engineering Chemistry Research*, **39**(10): 3875-3883.

- Rudyk, S., and Spirov, P. 2014. Upgrading and extraction of bitumen from Nigerian tar sand by supercritical carbon dioxide. *Applied Energy*, **113**: 1397-1404.
- Rudyk, S., Spirov, P., Al-Hajri, R., Vakili-Nezhaad, G. 2017. Supercritical carbon dioxide extraction of oil sand enhanced by water and alcohols as co-solvents. *Journal of CO₂ Utilization*, **17**: 90-98.
- Rudyk, S., Spirov, P., and Hussain, S. 2014. Effect of co-solvents on SC-CO₂ extraction of crude oil by consistency test. *The Journal of Supercritical Fluids*, **91**: 15-23.
- Rudzinski, W.E., and Aminabhavi, T.M. 2000. A review on extraction and identification of crude and related products using supercritical fluid technology. *Energy and Fuels*, **14**(2): 464-475.
- Saldaña, M.D.A., Negpal, V., and Guigard, S.E. 2005. Remediation of contaminated soils using supercritical fluid extraction: A review (1994-2004). *Environmental Technology*, **26**(9): 1013-1032.
- Santos, R.G., Loh, W., Bannwart, A.C., and Trevisan, O.V. 2014. An overview of heavy oil properties and its recovery and transportation methods. *Brazilian Journal of Chemical Engineering*, **31**(3): 571-590.
- Schlumberger. 2019a. Oilfield Glossary: API gravity. Available from https://www.glossary.oilfield.slb.com/en/Terms/a/api_gravity.aspx [accessed 21 May 2019].
- Schlumberger. 2019b. Oilfield Glossary: In situ combustion. Available from https://www.glossary.oilfield.slb.com/en/Terms/i/in_situ_combustion.aspx [accessed 22 June 2019].

- Schlumberger. 2019c. Oilfield Glossary: Fire flooding. Available from https://www.glossary.oilfield.slb.com/Terms/f/fire_flooding.aspx [accessed 22 June 2019].
- Schlumberger. 2019d. Oilfield Glossary: Toe to heel air injection. Available from https://www.glossary.oilfield.slb.com/en/Terms/t/toe_to_heel_air_injection.aspx [accessed 23 June 2019].
- Scott, A.C., MacKinnon, M.D., and Fedorack, P.M. 2005. Naphthenic acids in Athabasca oil sands tailings waters are less biodegradable than commercial naphthenic acids. *Environmental Science and Technology*, **39**: 8388-8394.
- Singhal, A.K., Das, S.K., Leggitt, S.M., Kasraie, M., and Ito, Y. 1996. Screening of reservoirs for exploitation by application of Steam Assisted Gravity Drainage/Vapex processes. *In* Proceedings of the 1996 2nd International Conference on Horizontal Well Technology, Calgary, AB., 18-20 November 1996. Society of Petroleum Engineering, pp. 867-876.
- Sodeifian, G., Sajadian, S.A., Razmimanesh, F., and Ardestani, N.S. 2018. A comprehensive comparison among four different approaches for predicting the solubility of pharmaceutical solid compounds in supercritical carbon dioxide. *Korean Journal of Chemical Engineering*, **35**(10): 2097-2116.
- Speight, J.G. 2004. Petroleum asphaltenes – Part 1: Asphaltenes, resins and the structure of petroleum. *Oil and Gas Science and Technology*, **59**(5): 467-477.
- Speight, J.G. 2006. *The Chemistry and Technology of Petroleum*, 4th ed. CRC Press, Taylor & Francis Group, Boca Raton, FL.
- Starr, J., and Bulmer, J.T. 1979. Syncrude analytical methods for oil sands and bitumen processing. Alberta Oil Sands Technology and Research Authority, Edmonton, AB.

- Stubbs, J.M., and Siepmann, J.I. 2004. Binary phase behavior and aggregation of dilute methanol in supercritical carbon dioxide: A Monte Carlo simulation study. *The Journal of Chemical Physics*, **121**(3): 1525-1534.
- Su, C.S., and Chen, Y.P. 2007. Correlation for the solubilities of pharmaceutical compounds in supercritical carbon dioxide. *Fluid Phase Equilibria*, **254**(1-2): 167-173.
- Subramanian, M., and Hanson, F.V. 1998. Supercritical fluid extraction of bitumens from Utah oil sands. *Fuel Processing Technology*, **55**(1): 35-53.
- Sun, M., and Temelli, F. 2006. Supercritical carbon dioxide extractions of carotenoids from carrot using canola oil as a continuous co-solvent. *Journal of Supercritical Fluids*, **37**(3): 397-408.
- Taberero, A., Martín del Valle, E.M., Galán, M.A. 2012. Supercritical fluids for pharmaceutical particle engineering: Methods, basic fundamentals and modelling. *Chemical Engineering and Processing: Process Intensification*, **60**: 9-25.
- Tom, J.W., Lim, G.B., Debenedetti, P.G., and Prud'homme, R.K. 1993. Applications of Supercritical Fluids in the Controlled Release of Drugs. *In Supercritical Fluid Engineering Science: Fundamentals and Applications*. Edited by E. Kiran and J.F. Brennecke. American Chemical Society, Washington, DC. pp. 238-257.
- Underwood, E.M., Guigard, S.E., Stiver, W.H., McMillan, J., and Bhattacharya, S. 2018. The effect of temperature, pressure and modifier on the initial solubility of waste stream bitumen in supercritical carbon dioxide. *In Proceedings 12th International Symposium on Supercritical Fluids*, Antibes-Juan-Les-Pins, France, 22-25 April 2018. International Society for Advancement of Supercritical Fluids.
- United Kingdom Oil and Gas Investments (UKOG). 2020. Why oil is important. Available from <https://www.ukogplc.com/page.php?pID=74#:~:text=Oil%3A%20lifeblood%20of%20the>

- %20industrialised,people%20all%20over%20the%20world. [accessed 22 November 2020].
- United States Energy Information Administration (USEIA). 2012a. Crude oil distillation and the definition of refinery capacity. Available from <https://www.eia.gov/todayinenergy/detail.php?id=6970> [accessed 19 April 2020].
- United States Energy Information Administration (USEIA). 2012b. Vacuum distillation is a key part of the petroleum refining process. Available from <https://www.eia.gov/todayinenergy/detail.php?id=9130> [accessed 20 April 2020].
- United States Environmental Protection Agency (USEPA). 2017. Fact Sheet: Methylene Chloride or Dichloromethane (DCM). Available from https://www.epa.gov/sites/production/files/2017-04/documents/fact_sheet_methylene_chloride_or_dichloromethane_dcm.pdf [accessed 8 July 2019].
- United States Geological Survey (USGS). 2003. Heavy Oil and Natural Bitumen – Strategic Petroleum Resources. Available from <https://pubs.usgs.gov/fs/fs070-03/fs070-03.html> [accessed 23 May 2019].
- United States Geological Survey (USGS). 2009. An Estimate of Recoverable Heavy Oil Resources of the Orinoco Belt Venezuela. Available from <https://pubs.usgs.gov/fs/2009/3028/pdf/FS09-3028.pdf> [accessed 2 June 2019].
- University of Alberta. 2005. Biography of Karl Clark. Available from <http://archives.library.ualberta.ca/FindingAids/KClark/kclark.html> [accessed 10 June 2019].
- Upreti, S.R., Lohi, A., Kapadia, R.A., and El-Haj, R. 2007. Vapor extraction of heavy oil and bitumen: A review. *Energy and Fuels*, **21**(3): 1562-1574.

- Vittoratos, E., Scott, G.R., and Beattie, C.I. 1990. Cold Lake cyclic steam stimulation: A multiwell process. *SPE Reservoir Engineering*, **5**(1): 19-24.
- Wai, C.M., Gopalan, A.S., and Jacobs, H.K. 2003. An Introduction to Separations and Processes Using Supercritical Carbon Dioxide. *In Supercritical Carbon Dioxide: Separations and Processes*. A.S. Gopalan. American Chemical Society, Washington, DC. pp. 2-8.
- Wenger, L.M., Davis, C.L., and Isaksen, G.H. 2002. Multiple controls on petroleum biodegradation and impact on oil quality. *SPE Reservoir Evaluation and Engineering*, **5**(5): 375-383.
- Wu, W., Ke, J., and Poliakoff, M. 2006. Phase boundaries of CO₂ + toluene, CO₂ + acetone, and CO₂ + ethanol at high temperatures and high pressures. *Journal of Chemical and Engineering Data*, **51**: 1398-1403.
- Xia, T.X., and Greaves, M. 2006. In situ upgrading of Athabasca Tar Sand bitumen using THAI. *Chemical Engineering Research and Design*, **84**(9A): 856-864.
- Xia, T.X., Greaves, M., and Turta, A.T. 2002. Injector-/producer-well combinations in toe-to-heel air injection. *Journal of Petroleum Technology*, **54**(6): 53-54.
- Xia, T.X., Greaves, M., Turta, A.T., and Ayasse, C. 2003. THAI – A ‘short-distance displacement’ in-situ combustion process for the recovery and upgrading of heavy oil. *Chemical Engineering Research and Design*, **81**(3): 295-304.
- Yan, T., Xu, J., Wang, L., Liu, Y., Yang, C., and Fang, T. 2015. A review of upgrading heavy oils with supercritical fluids. *RSC Advances*, **5**(92): 75129-75140.
- Yao, J., Li, G., and Wu, J. 2018. Application of In-situ combustion for heavy oil production in China: A review. *Journal of Oil, Gas and Petrochemical Science*, **1**(3): 69-72.

- Yeoh, H.S., Chong, G.H., Azahan, N.M., Rahman, R.A., and Choong, T.S.Y. 2013. Solubility measurement method and mathematical modeling in supercritical fluids. *Engineering Journal*, **17**(3): 67-78.
- Yoon, S., Bhatt, S.D., Lee, W., Lee, H.Y., Jeong, S.Y., Baeg, J.-O., and Lee, C.W. 2009. Separation and characterization of bitumen from Athabasca oil sand. *Korean Journal of Chemical Engineering*, **26**(1): 64-71.
- Yu, J.M., Huang, S.H., and Radosz, M. 1989. Phase behavior of reservoir fluids: Supercritical carbon dioxide and Cold Lake bitumen. *Fluid Phase Equilibria*, **53**: 429-438.
- Zhou, S., Huang, H., and Liu, Y. 2008. Biodegradation and origin of oil sands in the western Canada sedimentary basin. *Petroleum Science*, **5**(2): 87-94.
- Zhu, R., Liu, Q., Xu, Z., Masliyah, J.H., and Khan, A. 2011. Role of dissolving carbon dioxide in densification of oil sands tailings. *Energy and Fuels*, **25**(5): 2049-2057.
- Ziegler, J.W., Dorsey, J.G., Chester, T.L., and Innis, D.P. 1995. Estimation of liquid-vapor critical loci for CO₂-solvent mixtures using a peak-shape method. *Analytical Chemistry*, **67**: 456-461.
- Zosel, K. 1963. Extractions of caffeine with supercritical CO₂. DE 1493190 A1.

APPENDIX A: PROPERTIES OF THE FEED MATERIAL

APPENDIX A: PROPERTIES OF WHOLE BITUMEN

The results from the SARA analysis performed on the Athabasca whole bitumen sample provided by Syncrude are listed in Table A1. The whole bitumen sample was then distilled to produce the bitumen cuts of LGO, HGO, and resid. Table A2 provides some of the other properties that are characterized for the whole bitumen sample. Information from both Tables A1 and A2 were provided by Syncrude.

Table A1. Results from the SARA analysis performed on the Syncrude whole bitumen sample.

Components	(wt%)
Saturates	22.5
Aromatics	34.5
Resins	25.4
Asphaltenes	17.5

Table A2. Other properties characterized for the Syncrude whole bitumen sample.

Properties	Whole Bitumen
Density (g/cm ³)	0.9875 (at 333 K)
Viscosity (cSt)	217.34 (at 372 K)
Sulphur (ppm)	4.79 x 10 ⁴
Nitrogen (ppm)	4.93 x 10 ³
Solids (wt%)	0.3

APPENDIX B: LabVIEW™ DATA RECORDINGS

APPENDIX B: SAMPLE OF LabVIEW™ DATA RECORDING

A one-minute data recording generated by the LabVIEW™ program is shown in Table B1. The table includes information such as the scan number of each data recording entry, the time in seconds that the recording was made at, the pressure (psi) and temperature (°C) recorded at that reading, the flow rates (mL min⁻¹) measured from the ISCO Pumps A and B, and the pressures (psi) of Pumps A and B. The data recording shown in Table B1 is taken from the initial solubility measurement for LGO with SC-CO₂ only that was performed on August 13, 2020. For this experiment, the ISCO pumps were set at a pressure of 3480 psi, while a flow rate of approximately 2 to 4 mL min⁻¹ was maintained. Because the ISCO pumps were operated in tandem of each other, only one pump was used at a time as indicated by the operational flow rates recorded from Pump A. Pump B was on stand-by to take over when Pump A was depleted and required to be refilled. The pressure measured by the LabVIEW™ program was performed by a pressure transducer that is installed on a tubing connection before the extraction vessel. As shown in Table B1, the pressures recorded are roughly 83 psi lower than the 3480 psi pre-set pressure. With the experimental conditions being substantially higher than the critical point of CO₂, the slightly lower pressure conditions maintained during the run would not have affected the supercritical nature of the CO₂.

Table B1. One minute of the system's operational data recorded by the LabVIEW™ program.

Scan #	Time (s)	Pressure (psi)	Temperature (°C)	Pump Flow (mL min ⁻¹)		Pump Pressure (psi)	
				A	B	A	B
1419	14200.07	3395.999	60.16617	3.939	0	3480	3480
1420	14210.07	3396.339	60.13709	3.893	0.036	3480	3480
1421	14220.07	3396.394	60.14871	3.65	0.096	3480	3480
1422	14230.07	3396.411	60.07898	3.566	0	3480	3480
1423	14240.07	3395.899	60.13128	3.851	0	3480	3480
1424	14250.07	3395.864	60.15453	3.699	0.008	3480	3480
1425	14260.07	3396.309	60.1778	3.84	0	3480	3480

**APPENDIX C: INITIAL SOLUBILITY MEASUREMENT
PROCEDURE**

APPENDIX C: INITIAL SOLUBILITY MEASUREMENT PROCEDURE

Part 1: System Preparation

1. Ensure the coolant level in the refrigerated circulating bath is filled to the appropriate level before turning it on for the coolant fluid to be circulated through the ISCO syringe pump jackets.
2. Check to ensure the refrigerated circulating bath is programmed to the designated temperature (2°C) setting.
3. Empty both of the hot water baths (one used for circulating hot water into the vessel heating jacket and/or heating the CO₂ and modifier inlet lines; the other bath is utilized for submerging the metering and outlet valves in hot water).
4. Run the hot water tap until the water is sufficiently warm, then fill both of the water baths with the hot water. By doing so, this can allow the water baths to reach their required temperatures at a faster rate.
 - a. Switch on the circulating bath when it is filled to the appropriate level with water (replenishing the bath with hot water maybe required throughout the extraction process due to water loss caused by evaporation), ensure the circulating bath is set to a heating temperature of 67°C (the water bath pre-set temperature is amplified to account for heat loss so a true vessel temperature of 60°C can be approximately achieved). A Styrofoam covering is placed over the circulating bath to minimize evaporation.
 - b. Switch on the hot water bath when the metering and outlet valves are fully submerged with hot water. Ensure the hot water bath is set to a heating temperature of 60°C.
5. Check to ensure that the inlet, outlet, metering, Hamilton® syringe pump, and Gilson pump valves are fully closed.
6. Turn on the designated laboratory computer and initiate the LabVIEW™ software. Begin logging a new run on the program by saving the file into a designated folder using an applicable file name.
7. Label an appropriate number of vials designated for the collection and cleaning processes. Typically, 11 vials are required during the 25-minute collection process (*1a*,

- 1b, 2a, 2b, 3a, 3b, 4a, 4b, 5a, 5b, 6 c/o*), 1 vial for the rinsing process (*7 rinse*), 2 vials for the vessel depressurization process (*8 Dep, 9 Dep*), 2 vials for the high pressure cleaning period (*10 Hi-P, 11 Hi-P*), 1 jar for the collection of the vessel residue (*12 Vessel Residue*), and 1 vial for a time-zero sample collection (*13 Time Zero*).
8. A moderate amount of glass beads (4 mm diameter) are added to the collection vials. Weigh and record the masses of all the vials/jars that will be used for the initial solubility measurement process.
 9. Retrieve one to two scoops (approximately 1 to 1.3 kg) of dry ice to be used for the acetone-dry ice bath during the extraction period.
 10. Ensure that the circular Teflon covering is positioned fittingly beneath the vessel lid to minimize bitumen carryover into the outlet line. Adjust accordingly if required.
 11. Fasten the helical impeller securely to the MagneDrive® mixer connection. Visually inspect the helical impeller for any residual bitumen contents; clean with toluene and Kimwipes® if necessary.
 - a. For extractions with resid samples, the helical impeller will not be utilized.
 12. Visually inspect the interior of the vessel cavity to ensure it is clean from any residual bitumen contents; clean with toluene and Kimwipes® if necessary.
 13. Visually inspect the Teflon o-ring that is fitted to the lip of the vessel opening for any surface damages to prevent pressure leakages during the experiment. If damages are observed on the o-ring, replace immediately before continuing. Otherwise, fit the Teflon o-ring back onto the lip of the vessel opening.
 14. Wrap the six vessel-lid bolts using the nickel-embedded Teflon tape. The nickel-embedded Teflon tape can avoid seizing of the bolts when fastened to the vessel during pressurization.
 15. When toluene as a modifier is used:
 - a. Check to ensure the accurate toluene reservoir bottle is filled and attached to the Gilson pump. Switch on the Gilson pump and using the keypad located on the pump control panel, enter the necessary volume amount of toluene required to be added when the vessel is initially pressurized.
 - b. Open the Gilson pump valve and initiate the pump to allow the toluene modifier to be circulated and discharged out from the vessel inlet line – this is known as

priming the pump. When this is completed, stop and turn off the Gilson pump, and close the pump valve.

Part 2: Sample Preparation, Addition, and Equilibration

1. For solubility measurements utilizing whole bitumen, LGO, and HGO samples:
 - a. Tare the analytical balance scale. Weigh and record the mass of an empty glass jar (preferably 120 mL in volume) contained with a metal spatula on the scale. Retrieve the appropriate feed sample from the lab refrigerator and apportion approximately 50 g of the whole bitumen, LGO, or HGO sample into the 120 mL glass jar. Weigh and record the mass of the sample-containing 120 mL glass jar with the metal spatula on the scale.
 - b. For solubility measurements utilizing whole bitumen, LGO, and HGO samples, insert the stainless-steel vessel sleeve into the vessel cavity prior to transferring the sample material into the vessel. Using the weighed spatula, convey the sample contents from the 120 mL jar into the extraction vessel. With most of the sample contents transferred into the vessel, weigh and record the mass of the 120 mL glass jar again with the metal spatula to determine the mass of sample residue remaining in the jar. By subtracting the determined mass of the sample-containing 120 mL glass jar and the metal spatula from earlier with the mass of the 120 mL glass jar, sample residue, and the metal spatula, the total mass of sample transferred into the vessel can be determined.
2. For solubility measurements utilizing the resid sample:
 - a. Retrieve the appropriate feed sample from the lab refrigerator.
 - b. Turn on the gas chromatograph (GC) unit and initiate the oven function using the analog keypad. Pre-heat the GC oven to 120°C. When the temperature of the oven is maintained at a steady level, place the retrieved feed sample into the GC oven. Keep the resid sample in the GC oven for at least 30 minutes. The applied heat from the GC oven can effectively reduce the sample's viscous consistency. Decreasing the viscous consistency of the feed sample allows the sample to be more easily transferred out of its original container. ***Safety Note:*** *Ensure that the container material for the feed sample can be safely heated at such high*

temperatures. Be cautious when taking the heated container in and out of the GC oven. Use proper protective equipment such as oven mitts to prevent direct contact with hot surfaces.

- c. Tare the analytical scale. Weigh and record the mass of an empty glass jar. This will be used to sub-sample the resid material from its original container after it has been heated.
- d. Once the 30-minute heating time is complete, remove the resid sample in its original container from the GC oven. While the resid sample is still in a less viscous state due to the residual heat maintained from the GC oven, quickly sub-sample an appropriate amount of resid material and place it into the pre-weighed empty glass jar that was initially prepared from the previous step.
- e. Tare the analytical scale. Weigh and record the mass of the glass jar contained with the sub-sampled resid material. Subtract this mass from the recorded mass of the empty jar to determine the amount of resid material contained in the jar. Record this mass (and label it on the jar) for documentation purposes.
- f. Place this sub-sampled jar of resid material into the GC oven again to be heated at 120°C for about 30 minutes.
- g. Tare the analytical scale. Weigh and record the mass of an empty weighing dish. Transfer approximately 40 g of the 4 mm glass beads (roughly 480 glass beads) onto the weighing dish. Subtracting the mass of the empty weighing dish, record the exact mass of the glass beads.
- h. Tare the analytical balance scale. Weigh and record the mass of an empty glass jar.
- i. Retrieve the sub-sampled jar of resid material from the GC oven. Transfer approximately 15 g of the resid material into the newly weighed empty glass jar. While only 10 g of resid sample is normally required, the extra amount of sample transferred is to account for the contents lost from transferring the sample in-between glass jars and to the vessel itself. If the resid material becomes extremely viscous and difficult to be handled with, place the resid material (contained in its glass jar) into the GC oven again to be heated to 120°C for a period of time until the material can be more easily handled.

- j. Weigh and record the mass of the resid sample-containing jar with the spatula that was used; subtract the mass of the empty glass jar that was previously recorded to determine the exact mass of the resid sample obtained. Record this exact mass of the resid sample obtained for documentation purposes.
- k. Tare the analytical balance scale. Weigh and record the mass of a 500 mL glass beaker with a clean metal spatula. Using the clean spatula that was weighed, transfer all of the resid sample obtained in the previous step into the 500 mL beaker. Simultaneously, transfer the 480 glass beads into the glass beaker as well.
- l. Mix the contents in the 500 mL glass beaker thoroughly until the glass beads appear to be uniformly coated with the provided resid sample.
- m. Tare the analytical scale. Weigh and record the mass of the jar that previously contained the resid material as well as the spatula that was used during the transferring process.
- n. Tare the analytical scale again. Weigh and record the mass of the contents contained in the 500 mL beaker with the spatula that was used. Subtract this recorded mass of the 500mL beaker contained with its contents by the mass that was recorded in the previous step; this will determine the total mass of resid sample and glass beads transferred into the 500 mL beaker.
- o. At this point, the resid-glass bead mixture is expected to return to its extremely viscous state again due to the cooling effect imposed by the ambient air. Place the 500 mL beaker containing the resid-glass bead mixture into the GC oven heated to 120°C for approximately 10 to 15 minutes so that the mixture can be mobilized more easily.
- p. When the heating process in the GC oven is complete, retrieve the 500 mL beaker out of the oven using the proper protective equipment and place it safely on the lab bench.
- q. With the spatula that was previously used, quickly transfer all/most of the contents from the 500 mL beaker directly into the extraction vessel. The stainless-steel vessel sleeve that is normally inserted to protect the CO₂ inlet line from being entangled with the helical impeller is omitted in this case since no mixing

will be performed during the static and dynamic collection periods for the resid sample.

- r. Once most/all of the contents from the 500 mL beaker has been transferred into the vessel cavity, tare the analytical balance scale. Weigh and record the mass of the emptied 500 mL glass beaker and the spatula that was used. Subtract the previously recorded mass of the 500 mL glass beaker contained with the resid-glass bead mixture and the used spatula with this newly recorded mass of the emptied 500 mL beaker and the used spatula to determine the mass of resid sample transferred into the vessel cavity.
3. Retrieve a small amount of the LGO, HGO, or resid feed sample and collect it into the already labelled *Time Zero* vial; this will be sent for the HTSD analysis. Tare the analytical scale. Weigh and record the mass of the vial contained with the time zero sample.
4. For extractions utilizing whole bitumen, LGO, and HGO samples, ensure that the inserted stainless-steel vessel sleeve is appropriately positioned within the vessel. By doing so, the CO₂ inlet groove cut-out found on the sleeve should be orientated semi-perpendicularly to the two water ports found on the vessel's heating jacket.
5. Position the extraction vessel directly beneath the helical impeller attached to the MagneDrive® assembly and vessel lid. Carefully lift the vessel and simultaneously thread the CO₂ inlet line into the groove cut-out of the stainless-steel sleeve (only applicable when the MagneDrive® mixer assembly is used). Place the lifting jack underneath the vessel and extend the jack until the vessel is lifted to evenly meet with the vessel lid. Ensure the vessel body is completely flush and is tightly sitting up against its lid.
6. Rotate the vessel body accordingly so that the bolt holes on both of the lid and the vessel are accurately positioned. Lock the lid to the vessel by tightening the six bolts that were previously wrapped in nickel-embedded Teflon tape in a star configuration with a torque wrench. The bolts should be torqued in the order of 25 ft-lbs, then 35 ft-lbs, followed by 42 ft-lbs, and lastly at 50 ft-lbs.
7. Fasten the driving belt onto the MagneDrive® motor and mixer drive wheels (only applicable when the MagneDrive® mixer assembly is used).

8. Connect the two water ports on the vessel's heating jacket with the circulating water tubes from the hot water circulating bath.

Part 3: Equilibration Process and Static Period

1. Verify on the LabVIEW™ display that the vessel temperature is indicated at around 5 to 10°C less than the designated experimental temperature (once the vessel is pressurized, the vessel temperature will rapidly increase to 60°C). Ensure that the refrigerated circulator temperature is steadily maintained at 2°C.
2. Ensure that the inlet, outlet, metering, Hamilton® syringe pump, and Gilson pump valves are all fully closed.
3. Open both the air and liquid CO₂ cylinder reservoirs.
4. Power on the ISCO pump controller and verify in the pump controller's setting that the pumps are operating at a baud (Bd) rate of 19.2 K (at a Bd rate of 19.2 K, this ensures the measured flow rate and pressure data are effectively recorded by the LabVIEW™ program). Using the ISCO pump controller, set and refill both of the ISCO syringe pumps if they are not already refilled from the previous run. Once filled, engage both Pumps A and B to be pressurized to the designated pressure level (3480 psi).
5. Allow the pressures in both of the pumps to be equilibrated before proceeding to the next step.
6. Open the inlet valve to allow the extraction vessel to be pressurized to the designated pressure level. Verify on the LabVIEW™ display that the pressure and temperature in the vessel is achieved to the required experimental levels.
7. Ensure that there are no leakages from the vessel. Leakages originating from the vessel and its port connections can be indicated by a pump flow rate of $\geq 0 \text{ mL min}^{-1}$. With the downstream outlet and metering valves closed, the inflowing pressurized CO₂ should be steadily maintained within the vessel without having the ISCO syringe pumps continuously supplying large volumes of CO₂ into the vessel unless a leakage is occurring. If a leak is detected, the vessel is required to be immediately depressurized to allow for the system to be safely cleaned out of its contents. During its depressurization, seek to identify the location of the leak through visual (e.g. icing formation on connection ports or stainless-steel tubing caused by the low temperatures of the liquid CO₂) or

auditory (e.g. hissing noise resulting from the discharge of the high-pressure CO₂ escaping from the system) indications. If leaking continues, the Teflon o-ring should be replaced. **Safety Note:** *Never use fingers, hands, or any body parts to determine the location of a high-pressure gas leakage. The high-pressure release of the gas can result in extremely dangerous puncture wounds into the skin, causing serious injuries, infections, swelling, and tissue damages (Government of Alberta 2020).*

8. When toluene is added as a modifier to SC-CO₂:
 - a. As the vessel is being pressurized, quickly open the valve to the Gilson pump. Using its module controller, initiate the Gilson pump so that the required volume of toluene is added simultaneously into the pressurizing vessel for 1 minute. Since the Gilson pump only has a maximum discharge rate of 25 mL min⁻¹, modifier volumes that are greater than 25 mL can be precedingly added to the vessel prior to its pressurization, and the remaining 25 mL of modifier solution can be added during the pressurization process. Once the 1-minute modifier addition period concludes, stop the Gilson pump and close off its valve to the system.
9. Using the modular controller attached to the MagneDrive® assembly, power on the modular control using the labelled flip switch. Using the up-down arrows on the keypad on the module, adjust the speed of the MagneDrive® motor to 50 RPM (no mixing is required for resid samples), and shift the toggle switch to its “Start” position.
10. The belt driven MagneDrive® motor and mixer should start rotating at the designated speed.
11. Using a stopwatch or timer, initiate the static period for 60 minutes (whole bitumen, LGO, and HGO samples). A static period of 360 minutes is be applied for the resid sample.

Part 4: Dynamic Collection Process

1. Add a moderate volume of acetone into a small plastic container; the volume of acetone added should be sufficient to partially submerge the collection vials that will be used. Slowly add a necessary amount of dry ice into the acetone bath.
2. Roughly administer 20 mL of toluene into each of the *b* collection vials (for vials 1 through 5) and the carryover (*c/o*) vial.

3. Connect the first three sampling vials/jars (in the order of *1a*, *1b*, *6 c/o*) onto the three outlet collection lines starting from the rightmost position. Both *a* and *b* vials will be changed at every 5-minute intervals for a total of 25 minutes of sampling time, while the *c/o* vial will remain attached to the collection line for the whole 25-minute sampling period. Place the *a* and *b* vials into the prepared acetone-dry ice bath, while the *c/o* vial is kept out of the bath at ambient temperature conditions.
4. When toluene is added as a modifier to SC-CO₂:
 - a. Using the module controller on the Gilson pump, adjust the discharging flow rate of the modifier solution to the pre-determined level so that the appropriate modifier flow rate can be supplemented to maintain its required concentration in the SC-CO₂.
 - b. Open the Gilson pump valve.
5. Document the start time as shown by the timer indicated on the LabVIEW™ display window and begin the stopwatch. Open the outlet valve. Then cautiously and slowly open the metering valve to attain a flow rate between 2 to 4 mL min⁻¹ as indicated by the pump controller display.
6. When toluene is added as a modifier to SC-CO₂:
 - a. With the metering and Gilson pump valve opened, initiate the Gilson pump.
7. Time the sampling process for the first set of collection vials/jars (*1a*, *b*) for 5 minutes, while maintaining a steady flow rate between 2 to 4 mL min⁻¹.
8. After the first 5 minutes of sampling is completed, shut-off the outlet valve and pause the stopwatch.
9. When toluene is added as a modifier to SC-CO₂:
 - a. Stop the Gilson pump.
10. Carefully detach the first set of collection vials (*1a*, *b*) from the outlet ports and attach the next set of collection vials (*2a*, *b*) to the system. If necessary, apply an appropriate amount of dry ice to the acetone-dry ice bath to maintain its cooling temperature. Ensure both *a* and *b* vials are partially submerged into the bath.
11. Repeat steps 5 to 10 for the following 5 – 10 (*2a*, *b*), 10 – 15 (*3a*, *b*), 15 – 20 (*4a*, *b*), and 20 – 25 (*5a*, *b*) minute sampling periods. In total, a 25-minute sampling period is achieved.

12. Following the 20 – 25 (*5a, b*) minute sampling period, close the metering and outlet valves and remove all of the sampling vials from the outlet collection ports (including *6 c/o*).
13. When toluene is added as a modifier to SC-CO₂:
 - a. Stop the Gilson pump and close its valve.
14. Attach the rinsing vial (*7 rinse*) to the rightmost outlet collection port on the extraction system.
15. With the outlet valve remained closed, slowly and cautiously open the metering valve so that the portion between the closed outlet valve and the outlet collection ports can be safely depressurized.
16. When that portion of the system is depressurized, completely open the metering valve by turning 4 to 5 full rotations on the valve handle.
17. Once depressurized, open the valve to the Hamilton® syringe pump and turn on the syringe pump module. Using the control keypad on the pump module, select the appropriate size, volume, and speed options for the injection of 25 mL of toluene used to rinse out any remaining bitumen residue from the outlet collection line.
18. When the toluene rinse is complete, stop and turn-off the syringe pump, close off the pump and metering valves, and detach the rinsing vial (*7 rinse*) from the system.
19. The dynamic sampling process is now complete.

Part 5: Post Extraction Analysis

1. Tare the analytical scale. Weigh and record the masses of the contents in each of the vials collected during the sampling process (*vials 1-7*).
2. Place the vials contained with the extracted contents under the air-blowing apparatus in the fume-hood and ensure that each of the air-blowing nozzles are directed to the openings to each of the vials. Turn on the air-blowing apparatus to the designated level and leave the vials to be air dried for 48 hours.
3. At the end of the 48-hour drying period, remove the vials from the air-blowing apparatus.
4. Tare the analytical scale. Weigh and record the masses of each of the vials again.

Part 6: Depressurization

1. Close off the inlet valve and stop both of the ISCO syringe pumps. Using the pump controller, refill both (Pumps A and B) ISCO syringe pumps. When the pumps are refilled, switch off the pump controller. Close the air and liquid CO₂ cylinder reservoirs.
2. Turn off the refrigerated circulating bath and both of the hot water baths (hot water circulating and heating baths).
3. Lower the speed of the MagneDrive® mixer before stopping and turning it off.
4. Starting from the rightmost position, connect the two vials/jars used for depressurization (*8 Dep, 9 Dep*) onto the outlet collection ports.
5. Open the outlet valve. Cautiously open the metering valve so that a slight flow is achieved to gradually depressurize the vessel overnight. During the depressurization of the vessel, maintain the flow rate on the metering valve as low and gradual as possible. If the vessel is rapidly depressurized, the remaining bitumen residue content in the vessel will be likely carried over into the outlet collection line.

Part 7: Vessel Residue Collection and High-Pressure Cleaning

1. Check on the LabVIEW™ program display to ensure that the vessel has been completely depressurized to approximately 18 to 25 psi. If the vessel is still pressurized above the required level, open the metering valve a slightly more to expedite the depressurization process.
2. Turn on the refrigerated circulating bath and program its cooling temperature to 2°C.
3. Drain both of the hot water baths (hot water circulating and heating baths). Run the hot water tap until the water is sufficiently warm, then fill both of the water baths with the hot water. By doing so, this can allow the water baths to reach their required temperatures at a faster rate. Repeat Steps 4a and b from Part 1.
4. Once depressurized, remove the driving belt from the MagneDrive® motor and mixer drive wheels. Use the torque wrench to unscrew, loosen, and remove the six bolts from the vessel lid. Unroll the existing nickel-embedded Teflon tape from the bolts and rewrap it with a new layer of tape. After the vessel is safely depressurized, the current LabVIEW™ program can now be ended by pressing the “*Stop*” key on the program

display. **Safety Note:** *Ensure a protective face shield is worn when detaching the vessel body from its lid.*

5. Detach the circulating tubes connected between the hot water circulating bath and the two water ports on the vessel's heating jacket.
6. Remove the lifting jack from underneath the vessel so that the vessel and its lid can be slowly detached.
7. Visually inspect the conditions of the helical impeller and the underside of the vessel lid. Make notes of their visual conditions and photograph if deemed necessary for documentation purposes.
8. With the vessel still underneath the helical impeller and vessel lid, use a toluene spray bottle and carefully clean off any remaining bitumen residue from the lid and Teflon disc surfaces. The toluene-bitumen mixture is effectively collected into the vessel.
9. Carefully detach the helical impeller from the MagneDrive® mixer and soak it with the toluene-bitumen solution collected into the vessel basin.
10. Remove the vessel from the SFE system and bring it into the fume-hood for cleaning. Using toluene, clean and rinse the interior walls of the vessel, the helical impeller, the Teflon o-ring, and the vessel sleeve. Once these items are clean of any bitumen residue contents, wipe down the pieces using Kimwipes® to be further air-dried. By using the collected toluene from the previous rinsing and cleaning processes to soak the interior of the vessel basin, the remaining solidified bitumen residues found in the vessel can be effectively dislodged and dissolved.
11. Once the vessel and its components have been thoroughly rinsed and cleaned, transfer the rinsed toluene-bitumen mixture collected from the vessel into the already prepared 250 mL vessel residue collection jar (*12 vessel residue*). Using the provided Kimwipes®, dry the interior of the vessel thoroughly.
12. Add approximately 80 mL of toluene into the vessel basin.
13. Visually inspect the Teflon o-ring that is fitted to the lip of the vessel opening for any surface damages to prevent pressure leakages during the high-pressure cleaning process. If damages are observed on the o-ring, replace immediately before continuing. Otherwise, if the o-ring is still deemed usable, fit the Teflon o-ring back onto the lip of the vessel opening.

14. Appropriately insert the stainless-steel vessel sleeve so that the CO₂ inlet groove cut-out on the sleeve is orientated semi-perpendicularly to the two water ports on the vessel's hot water circulating jacket.
15. Attach the helical impeller back onto the MagneDrive® mixer connection. Connect the two water ports on the vessel's heating jacket with the water circulating tubes from the hot water circulating bath.
16. Position the extraction vessel directly beneath the helical impeller attached to the MagneDrive® assembly and vessel lid. Carefully lift the vessel and simultaneously thread the CO₂ inlet line into the groove cut-out of the stainless-steel sleeve. Place the lifting jack underneath the vessel and extend the jack until the vessel is lifted to evenly meet with the vessel lid. Ensure the vessel body is completely flush and is tightly sitting up against its lid.
17. Rotate the vessel body accordingly so that the bolt holes on both of the lid and the vessel are correctly positioned. Lock the lid to the vessel by tightening the six nickel-embedded Teflon tape-wrapped bolts in a star configuration with a torque wrench. The bolts should be torqued in the order of 25 ft-lbs, then 35 ft-lbs, followed by 42 ft-lbs, and lastly at 50 ft-lbs.
18. Fasten the driving belt onto the MagneDrive® motor and mixer drive wheels.
19. On the laboratory computer, initiate the LabVIEW™ software. Begin logging a new run on the program by saving the file into a designated folder using an applicable file name.
20. Verify on the LabVIEW™ display that the vessel temperature is indicated at around 5 to 10°C less than the designated experimental temperature (once the vessel is pressurized, the vessel temperature will rapidly increase to 60°C). Ensure that the refrigerated circulator temperature is steadily maintained at 2°C.
21. Ensure that the inlet, outlet, metering, Hamilton® syringe pump, and Gilson pump valves are all closed.
22. Power on the ISCO pump controller and verify in the pump controller's setting that the pumps are operating at a Bd rate of 19.2 K (at a Bd rate of 19.2 K, this ensures the measured flow rate and pressure data are effectively recorded by the LabVIEW™ program).
23. Open both the air and liquid CO₂ cylinder reservoirs.

24. Using the ISCO pump controller, set and refill both of the ISCO syringe pumps if they are not already refilled from the previous run. Once filled, engage both Pumps A and B to be pressurized to the designated pressure level (3480 psi).
25. Connect the two pre-labelled vials for the high-pressure cleaning period (*10 Hi-P, 11 Hi-P*) onto the outlet collection ports starting on the rightmost position.
26. Allow the pressures in both of the pumps to be equilibrated before proceeding to the next step.
27. Open the inlet valve to allow the vessel to be pressurized to the designated pressure level. Verify on the LabVIEW™ display that the pressure and temperature in the vessel is achieved to the required experimental levels.
28. Ensure that there are no leakages from the vessel. Refer to Step 7 of Part 3 on how to check for leakages.
29. Using the modular controller attached to the MagneDrive® assembly, power on the modular control using the labelled flip switch. Using the up-down arrows on the keypad on the module, adjust the speed of the MagneDrive® motor to 250 rpm, and shift the toggle switch to its “*Start*” position. The belt driven MagneDrive® motor and mixer should start rotating at the designated speed.
30. To thoroughly maximize washing within the vessel assembly, let the system mix for 25 to 30 minutes before initiating the high-pressure cleaning procedure.
31. Open the outlet valve. Then cautiously and slowly open the metering valve to attain a flow rate ranging between 20 to 25 mL min⁻¹ as indicated by the pump controller display. The flow rate attained during the high-pressure clean can be less precise than the one maintained during the extraction process.
32. Time the high-pressure cleaning process for about 10 to 15 minutes, or until 40 to 60 mL of toluene has been discharged out from the outlet ports and collected into the high-pressure cleaning vials. The duration of the high-pressure cleaning process will ultimately depend on the quality of the feed sample that was extracted from – a more viscous feed sample (e.g. resid material) will require a longer high-pressure cleaning time.

33. Close off the inlet valve and stop both of the ISCO syringe pumps. Using the pump controller, refill both (Pumps A and B) ISCO syringe pumps. When the pumps are refilled, switch off the pump controller. Close the air and liquid CO₂ cylinder reservoirs.
34. Turn off the refrigerated circulating bath and both of the hot water baths (hot water circulating and heating baths).
35. Reduce the speed of the MagneDrive® mixer before stopping and turning it off.
36. Keep the outlet and metering valves open so that the vessel can be safely depressurized. Unlike after the extraction process, only toluene remains in the vessel. Therefore, the metering valve in this case can be opened more extensively, allowing the system to be depressurized at a more rapid pace.
37. Check on the LabVIEW™ program display to ensure that the vessel has been completely depressurized to approximately 18 to 25 psi. Once completely depressurized, the current LabVIEW™ program can now be ended by pressing the “*Stop*” key on the program display.
38. Remove the drive belt from the MagneDrive® motor and mixer drive wheels. Use the torque wrench to unscrew, loosen, and remove the six bolts from the vessel lid. Unroll the existing nickel-embedded Teflon tape from the bolts and rewrap it with a new layer of tape. **Safety Note:** *Ensure a protective face shield is worn when detaching the vessel body from its lid.*
39. Detach the circulating tubes connected between the hot water circulating bath and the two water ports on the vessel’s heating jacket.
40. Remove the lifting jack from underneath the vessel so that the vessel and its lid can be slowly detached.
41. Remove the vessel from the SFE system and bring it into the fume-hood. Dispose the remaining toluene solution in the vessel basin into an appropriate chemical waste collection container.

Part 8: Post Cleaning Analysis

1. Tare the analytical scale. Weigh and record the masses of each of the vials used during the depressurization, vessel residue collection, and high-pressure cleaning processes (*vials/jar 8-12*).

2. Place the vials (*vials 8-11*) contained with the collected contents under the air-blowing apparatus in the fume-hood and ensure that each of the air-blowing nozzles are directed to the openings to each of the vials. Turn on the air-blowing apparatus and leave the vials/jars to be dried for 48 hours.
3. At the end of the 48-hour drying period, remove the vials from the air-blowing apparatus.
4. Tare the analytical scale. Weigh and record the masses of each of the vials again.
5. Prior to delivering them to Syncrude to undergo HTSD analysis, photograph all of the dried vials/jars (*vials/jars 1-13*).

APPENDIX D: HYDROCARBON COLLECTION DATA

APPENDIX D: EXAMPLE OF HYDROCARBON COLLECTION DATA SPREADSHEET

Tables D1 and D2 are examples of the data sheets that were used for recording the results from an initial solubility measurement for HGO with 5 mol% toluene added to the SC-CO₂ that was performed on June 17, 2020.

Table D1. Summary of initial solubility measurement conditions and the initial data recorded.

Description	Initial Solubility Measurement HGO with 5 mol% Toluene – 4 mL min ⁻¹						
Run pressure (psi/MPa)	3480	24	Mass of Sample in Vessel (g)	51.1	Static time (mins)	Set 1	60
Run temperature (°C/K)	63.5177	336.67	Co-solvent	Toluene (5 mol%)			
Pump temperature (°C/K)	2	275.15	Volume of co-solvent added during pressurization (mL)	15.383	Sample Jar ID (#)	37-1HVGOR-3807	
Density of CO ₂ at run conditions (g/mL)	0.758	-	Rate of co-solvent feed (mL min ⁻¹)	0.523	Mass jar + spatula (g)	129.8944	
Density of CO ₂ at pump conditions (g/mL)	1.0272	-	-	-	Mass jar + spatula + sample (g)	183.7192	
Mixing speed (rpm)	50	-	-	-	Mass jar + spatula + residue (g)	132.6192	
Comments					Mass sample in vessel (g)	51.1	

Table D2. Experimental data of hydrocarbon masses collected from the initial solubility measurement performed on June 17, 2020.

Vial ID	Sampling Time (mins)	Initial mass (g)	Final Mass (g)	Mass of sample collected (g)	Volume of CO ₂ from pumps (mL)	Mass of CO ₂ (g)
1a (0-5 min)	5	35.8553	36.7340	0.8787	28.3202	29.0905
1b (0-5 min)		27.2990	27.3016	0.0026		
2a (5-10 min)	10	36.6184	37.5225	0.9041	20.2187	20.7686
2b (5-10 min)		27.0853	27.0866	0.0013		
3a (10-15 min)	15	36.8313	37.3906	0.5593	15.1265	15.5379
3b (10-15 min)		27.0066	27.0083	0.0017		
4a (15-20 min)	20	36.1044	36.7949	0.6905	18.5723	19.0775
4b (15-20 min)		26.9819	26.9830	0.0011		
5a (20-25 min)	25	36.3913	36.8675	0.4762	14.2968	14.6857
5b (20-25 min)		27.2864	27.2867	0.0003		
6 (c/o)	-	27.2056	27.2069	0.0013		
7 (rinse)		27.2071	27.5416	0.3345		
			SUM:	3.8516	96.5345	99.1602
8 (dep) ¹	-	27.1941	27.8467	0.6526		
9 (dep) ¹		27.2409	27.3629	0.1220		
10 (Hi-P) ²	-	26.8951	26.9167	0.0216		
11 (Hi-P) ²		26.8999	26.9769	0.0770		
12 (VR) ³	-	164.8932	195.3106	30.4174		
13 (time 0)	-	27.1769	29.8935	2.7166		

¹ Depressurization

² High pressure clean

³ Vessel residue

$$\text{Initial solubility} = \frac{\text{Cumulative mass of sample collected (g)}}{\text{Cumulative mass of CO}_2\text{(g)}} = \frac{3.8516 \text{ g}}{99.1602 \text{ g}} = 0.039 \text{ g/g}$$

**APPENDIX E: HIGH TEMPERATURE SIMULATED
DISTILLATION**

APPENDIX E: HIGH TEMPERATURE SIMULATED DISTILLATION

Note: All HTSD analyses were performed by the staff from Syncrude.

- 1. Retention Time Calibration Standard:** To initiate the retention time calibration standard, carefully transfer around 20 mL of CS₂ into a 50 mL round bottom-shaped flask. Formulate a mixture of paraffins by first weighing out 500 mg of pentane, hexane, heptane, octane, nonane, decane, undecane, dodecane, tridecane, tetradecane, pentadecane, hexadecane, heptadecane, octadecane, nonadecane, eicosane, and tetracontane into a 20 mL vial. In addition to the 500 mg of normal paraffins already supplemented, add another 500 mg of dodecane and 20 mg of tetracontane into the produced paraffins mixture and keep the mixture refrigerated at about 4°C. The composed paraffins mixture will be utilized when preparing for the production of the Polywax 655 retention time calibration mixture. Measure approximately 25 mg of Polywax 655 and about 10 mg of the already-prepared paraffins mixture; place the two weighed-out mixtures into the 50 mL flask contained with 20 mL of CS₂. Stir the combined solution thoroughly within a fume-hood, while providing adequate heating by using an infrared lamp (powered to about 200 W) that is safely positioned in proximity (15 to 20 cm) to the flask. Stir and heat the contents within the flask for approximately 20 minutes, or until the mixture has produced a clear consistency. **Safety Note:** *Be cautious when handling the CS₂-containing mixture to avoid ignition and flammable potentials.* Carefully collect and seal a 2 mL aliquot of the prepared retention time calibration mixture into a 2 mL auto-sampler vial. From the auto-sampler vial, the 2 mL aliquot is injected and utilized during the HTSD process to produce the retention time – boiling point curve.

2. Validation of the System's Performance:

- a. *Column Resolution:* Begin by injecting 0.1 to 0.2 μL of the retention time calibration mixture from the 2 mL auto-sampler vial. Determine the column resolution, R , by using the following equation:

$$R = 2(t_2 - t_1)/(1.699) (W_2 + W_1)$$

where:

R	=	resolution
t_2	=	$n\text{-C}_{50}$ paraffin retention time(s)
t_1	=	$n\text{-C}_{52}$ paraffin retention time(s)
W_2	=	peak width(s) at half height for $n\text{-C}_{50}$
W_1	=	peak width(s) at half height for $n\text{-C}_{52}$

The calculated resolution value from the provided equation should range between 1.8 to 4.0.

- b. *Detector Relative Response Test Mixture:* Prior to conducting any HTSD analyses, the response of the gas chromatographic system operated must be first validated. Since this testing methodology interprets that all hydrocarbon compounds, disregarding their applied retention time, would have identical relative responses, a chemical mixture is formulated to account for the relative response factors. The chemical mixture is prepared by adding eight normal paraffins (decane, tetradecane, octadecane, eicosane, octacosane, dotriacontane, tetracontane, and pentacontane), each weighed at 100 mg into a 50 mL volumetric flask. CS_2 is then added to the 50 mL flask and mixed thoroughly with the paraffinic contents. Once the paraffins are effectively dissolved, carefully collect an aliquot of the CS_2 – paraffinic mixture into a 2 mL injection vial and inject 0.1 to 0.2 μL to the gas chromatograph. The relative response factor of each paraffin in relation to eicosane, F_i , is calculated using the following equation:

$$F_i = \frac{M_i \times P_i \times Ac_{20}}{A_i \times Mc_{20} \times Pc_{20}}$$

where:

F_i	=	relative response factor
M_i	=	paraffin mass in mg
Mc_{20}	=	eicosane mass in mg
A_i	=	peak area of the paraffin
Ac_{20}	=	peak area of the eicosane
P_i	=	purity percentage of the paraffin
Pc_{20}	=	purity percentage of the eicosane

The calculated relative response factor from the provided equation should range between 0.9 to 1.10. A response factor calculated outside of this range can indicate or be related to issues caused by the inlet, non-uniform flow, or potential blockages/interferences to the flame orifice.

3. **Pre-set Initial Oven Temperature:** The initial oven temperature is selected based on the type of sample that is being analyzed. With samples such as vessel residues that have higher initial boiling points (i.e. greater than 100°C), an initial oven temperature set between 35 to 40°C should be utilized. However, if the type of sample being analyzed is unclear, an initial oven temperature of -20°C should be used instead. Note that the temperature rate of the gas chromatographic oven changes by 15°C every minute.
4. **Baseline/Blank Runs:** Before the sequence of samples are analyzed and after any necessary column maintenance activity is done, an equivalent volume of CS₂ that is similar to the volume of sample that will be injected is delivered for a blank run to be made. An effective blank run should successfully produce a stable plateau when the oven is set to the highest temperature, while indications of carry-over or residual sample elution should not occur.
5. **Retention Time Calibration Standard:** Place the 2 mL auto-sampler vial contained with the retention time calibration mixture prepared in Step 1 into the auto sampler to be injected. By using the retention time calibration mixture chromatogram, determine all of the carbons up till C₁₀₀. From the developed chromatogram, a Boiling Point versus Retention Time curve can be plotted. With the retention time calibration mixture added,

the system is now calibrated to analyze carbons ranging from C₅ to C₁₀₀ with a boiling point that ranges between 40 to 735°C. Nearing the end of the analytical procedure, place the 2 mL auto-sampler vial into the system again to verify and ensure that the column's stability is maintained.

6. **Response Factor Standard:** To determine the sample recovery amount, the detector response factor must be first identified. Using Reference Oil 5010, a response factor standard can be prepared to be utilized. To do so, 0.2 to 0.25 g of Reference Oil 5010 is weighed and added to 10 mL of CS₂. The total mass of the Reference Oil and CS₂ mixture is then weighed, recorded, and/or stored at 4°C if the mixture is not used immediately. A 2 mL aliquot is obtained from the prepared mixture and carefully transferred into an auto-sampler vial. The vial is then placed into an auto sampler and injected in duplicates. The response factor of the Reference Oil 5010, *RF*, can then be calculated by using the following equation:

$$RF = \frac{(M_{STD})}{(M_{STD} + M_{SLSTD})} \times \frac{1}{A_{STD}}$$

where:

<i>RF</i>	=	response factor
<i>A_{STD}</i>	=	net area calculated from the Reference Oil 5010 chromatogram, subtracted from baseline and with the solvent peak excluded
<i>M_{SLSTD}</i>	=	mass of the solvent used for the dissolution of the Reference Oil, measured in grams
<i>M_{STD}</i>	=	mass of the Reference Oil 5010 used to prepare the response factor solution, measured in grams

The calculated response factor, *RF*, should not differ by more than over 2%.

7. **Sample Analysis:** Allow the collected extract, time zero, and/or vessel residue samples to be maintained at room temperature before weighing and recording their respective masses. To prepare for the analytical procedure, weigh approximately 0.2 to 0.25 g of each sample and add 10 mL of CS₂. Weigh and record the masses of each of these mixtures, and then carefully collect a 2 mL aliquot of each mixture into auto sampler

vials. Inject each of these samples for analysis. To ensure the issue of carry-over can be effectively detected after each sample is analyzed, blank runs will be further performed.

- 8. *Zeroing of the Reference Oil 5010 and Sample Chromatograms:*** Arrange a batch containing slices of the Reference Oil 5010 chromatogram. Visually inspect each chromatogram from the system to ensure that the first five slices (a slice is equated to a time interval of 0.1 seconds) are free of any sample or solvent elution. Using the areas of the first five slices, calculate its total average value. Then, deduct the calculated average of the first five area slices from each slice of the Reference Oil 5010 chromatogram. Set any negative values that may arise to zero. Using the same calculation approach, the blank baseline and sample chromatograms can be zeroed. By doing so, each zeroed baseline slice is subtracted from their respective zeroed Reference Oil 5010 slice. Similarly, set any negative values that may arise to zero.
- 9. *Determination of the Boiling Point Distribution for Reference Oil 5010:*** Using the corrected slices from Reference Oil 5010, the boiling point distribution is calculated through a Test Method D6352. The calculated boiling points are then comparatively analyzed with the consensus values as reported in Test Method D6352 to ensure that the values calculated are within the specified standards. If the calculated values are deemed beyond the specified range, corrective actions must be taken to resolve any possible chromatographic issues before the sample can be analyzed. Some common possible chromatographic issues can include solvent contamination, errors with sample preparation, inlet or column containing sample residue, the integrity and quality of the baseline utilized, and/or a partially obstructed detector jet.
- 10. *Quenching Correction:*** To account for the reduced FID response resulting from the co-elution of CS₂ and the analyzed sample contents, a quenching correction factor must be applied to the respective time segment when co-elution occurs. To do so, isolate the solvent peak between when the elution of CS₂ initiates and ends. Identify the nearest slices to the beginning and end of the elution from the solvent peak. Using the identified slices, multiply each slice by the quenching factor of 1.930 to correct for the diminished response. Note that the quenching factor should be applied to all relevant chromatograms.

11. Determining the Percent Recovery of the Sample: The percent recovery of the sample, %RC, can be calculated by using the following equation for each of the sample analyzed:

$$\%RC = \frac{(ME)}{\left(\frac{M_{SMP}}{(M_{SMP} + M_{SLSMP})}\right)} \times 100 = \frac{ME \times (M_{SMP} + M_{SLSMP})}{M_{SMP}} \times 100$$

where:

$\%RC$	=	percent recovery of the sample
ME	=	mass of the eluted sample, in grams
M_{SMP}	=	mass of the sample, in grams
M_{SLSMP}	=	mass of the solvent from the solution, in grams

Furthermore, the mass of the eluted sample, ME , can be calculated by using the following equation:

$$ME = (A_{SMP}) \times (RF)$$

where:

ME	=	mass of the eluted sample, in grams
A_{SMP}	=	area of the net sample
RF	=	response factor of Reference Oil 5010

12. Calculating the Boiling Point Distribution: Multiply each slice from the sample chromatogram with the sample percent recovery that was calculated earlier. Then, divide each slice of the sample chromatogram with the sample's total area. Reiterate this calculation process for all of the samples analyzed. Using 1% intervals, determine for each sample the time needed to exactly produce 0.5, 1, 2, 3, 4... percent recoveries. By using the Boiling Point versus Retention Time curve that was developed in Step 5, the retention times determined can be associated to its respective boiling points. Plot the cumulative percent recoveries of each analyzed sample with the corresponding boiling points to yield the required HTSD curve.